Chapter 2
Isotope Fractionation Processes of Selected Elements

The foundations of stable isotope geochemistry were laid in 1947 by Urey's classic paper on the thermodynamic properties of isotopic substances and by Nier's development of the ratio mass spectrometer. Before discussing details of the naturally occurring variations in stable isotope ratios, it is useful to describe some generalities that are pertinent to the field of non-radiogenic isotope geochemistry as a whole.

1. Isotope fractionation is pronounced when the mass differences between the isotopes of a specific element are large relative to the mass of the element. Therefore, isotope fractionations are especially large for the light elements (up to a mass number of about 40). Recent developments in analytical techniques have opened the possibility to detect small variations in elements with much higher mass numbers. The heaviest element for which natural variations have been reported is thallium with isotopes of masses 203 and 205 (Rehkämper and Halliday 1999).
2. All elements that form solid, liquid, and gaseous compounds stable over a wide temperature range are likely to have variations in isotopic composition. Generally, the heavy isotope is concentrated in the solid phase in which it is more tightly bound. Heavier isotopes tend to concentrate in molecules in which they are present in the highest oxidation state.
3. Mass balance effects can cause isotope fractionations because modal proportions of substances can change during a chemical reaction. They are especially important for elements in situations where these coexist in molecules of reduced and oxidized compounds. Conservation of mass in an n component system can be described by

$$\delta_{(\text{system})} = \sum x_i \, \delta_i \tag{2.1}$$

   where "x_i" is the mole fraction of the element in question for each of n phases within the system.
4. Isotopic variations in most biological systems are mostly caused by kinetic effects. During biological reactions (e.g. photosynthesis, bacterial processes) the lighter isotope is very often enriched in the reaction product relative to the substrate. Most of the fractionations in biological reactions generally take place

J. Hoefs, *Stable Isotope Geochemistry,*

during the so-called rate determining step, which is the slowest step. It commonly involves a large reservoir, where the material actually used is small compared to the size of the reservoir.

2.1 Hydrogen

Until 1931 it was assumed that hydrogen consisted of only one isotope. Urey et al. (1932) detected the presence of a second stable isotope, which was called deuterium. (In addition to these two stable isotopes there is a third naturally occuring but radioactive isotope, ^{3}H, tritium, with a half-life of approximately 12.5 years). Rosman and Taylor (1998) gave the following average abundances of the stable hydrogen isotopes:

$$^{1}H : 99.9885\%$$

$$^{2}D : 0.0115\%$$

The isotope geochemistry of hydrogen is particularly interesting, for two reasons:

1. Hydrogen is omnipresent in terrestrial environments occurring in different oxidation states in the forms of H_2O, H_3O^+, OH^-, H_2 and CH_4, even at great depths within the Earth. Therefore, hydrogen is envisaged to play a major role, directly or indirectly, in a wide variety of naturally occurring geological processes.
2. Hydrogen has by far the largest mass difference relative to the mass of the element between its two stable isotopes. Consequently hydrogen exhibits the largest variations in stable isotope ratios of all elements.

The ranges of hydrogen isotope compositions of some geologically important reservoirs are given in Fig. 2.1. It is noteworthy that all rocks on Earth have somewhat similar hydrogen isotope compositions, which is a characteristic feature of hydrogen, but not of the other elements. The reason for this overlap in isotope composition for rocks is likely due to the enormous amounts of water that have been cycled through the outer shell of the Earth.

2.1.1 Preparation Techniques and Mass Spectrometric Measurements

Determination of the D/H ratio of water is performed on H_2-gas. There are two different preparation techniques: (1) equilibration of milliliter-sized samples with gaseous hydrogen gas, followed by mass-spectrometric measurement and back calculation of the D/H of the equilibrated H_2 (Horita 1988). Due to the very large fractionation factor (0.2625 at 25°C) the measured H_2 is very much depleted in D, which complicates the mass-spectrometric measurement. (2) water is converted to hydrogen by passage over hot metals (uranium: Bigeleisen et al. 1952; Friedman 1953;

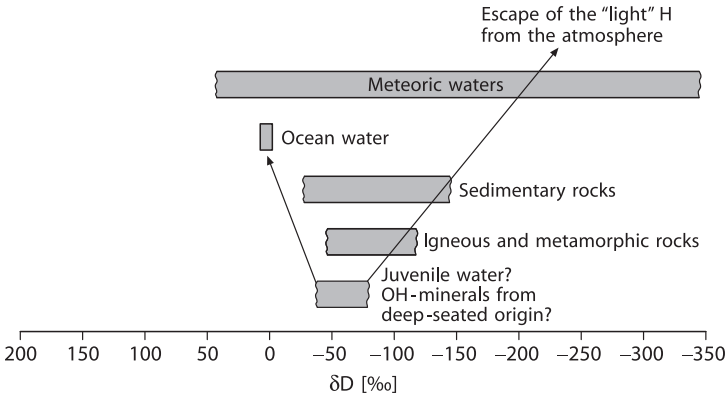

Fig. 2.1 δD ranges of some geologically important reservoirs

Godfrey 1962, zinc: Coleman et al. 1982, chromium: Gehre et al. 1996). This is still the classic method and commonly used.

A difficulty in measuring D/H isotope ratios is that, along with the H_2^+ and HD^+ formation in the ion source, H_3^+ is produced as a by-product of ion-molecule collisions. Therefore, a H_3^+ correction has to be made. The amount of H_3^+ formed is directly proportional to the number of H_2 molecules and H^+ ions. Generally the H_3^+ current measured for hydrogen from ocean water is on the order of 16% of the total mass 3. The relevant procedures for correction have been evaluated by Brand (2002).

Analytical uncertainty for hydrogen isotope measurements is usually in the range ±0.5 to ±5‰ depending on different sample materials, preparation techniques and laboratories.

Burgoyne and Hayes (1998) and Sessions et al. (1999) introduced the continuously flow technique for the D/H measurement of individual organic compounds. The precise measurement of D/H ratios in a He carrier poses a number of analytical problems, related to the tailing from the abundant $^4He^+$ onto the minor HD^+ peak as well as on reactions occurring in the ion source that produce H_3^+. However, these problems have been overcome and precise hydrogen isotope measurements of individual organic compounds are possible.

2.1.2 Standards

There is a range of standards for hydrogen isotopes. The primary reference standard, the zero point of the δ-scale, is V-SMOW, which is virtually identical in isotopic composition with the earlier defined SMOW, being a hypothetical water sample orginally defined by Craig (1961b).

Table 2.1 Hydrogen isotope standards

Standards	Description	δ-value
V-SMOW	Vienna Standard Mean Ocean Water	0
GISP	Greenland Ice Sheet Precipitation	−189.9
V-SLAP	Vienna Standard Light Antarctic Precipitation	−428
NBS-30	Biotite	−65

V-SMOW has a D/H ratio that is higher than most natural samples on Earth, thus δD-values in the literature are generally negative. The other standards, listed in Table 2.1, are generally used to verify the accuracy of sample preparation and mass spectrometry.

2.1.3 Fractionation Processes

The most effective processes in the generation of hydrogen isotope variations in the terrestrial environment are phase transitions of water between vapor, liquid, and ice through evaporation/precipitation and/or boiling/condensation in the atmosphere, at the Earth's surface, and in the upper part of the crust. Differences in H-isotopic composition arise due to vapor pressure differences of water and, to a smaller degree, to differences in freezing points. Because the vapor pressure of HDO is slightly lower than that of H_2O, the concentration of D is lower in the vapor than in the liquid phase. In a simple, but elegant experiment Ingraham and Criss (1998) have monitored the effect of vapor pressure on the rate of isotope exchange between water and vapor, which is shown in Fig. 2.2. Two beakers with isotopically differing waters were juxtaposed in a sealed box to monitor the exchange process at different temperatures (in this case 21 and 52°C). As shown in Fig. 2.12 in the 52°C experiment the isotopic composition of the water changes rapidly and nearly reaches equilibrium in only 27 days.

Horita and Wesolowski (1994) have summarized experimental results for the hydrogen isotope fractionation between liquid water and water vapor in the temperature range 0–350°C (see Fig. 2.3). Hydrogen isotope fractionations decrease rapidly with increasing temperatures and become zero at 220–230°C. Above the crossover temperature, water vapor is more enriched in deuterium than liquid water. Fractionations again approach zero at the critical temperature of water (Fig. 2.3).

From experiments, Lehmann and Siegenthaler (1991) determined the equilibrium H-isotope fractionation between ice and water to be +21.2‰. Under natural conditions, however, ice will not necessarily be formed in isotopic equilibrium with the bulk water, depending mainly on the freezing rate.

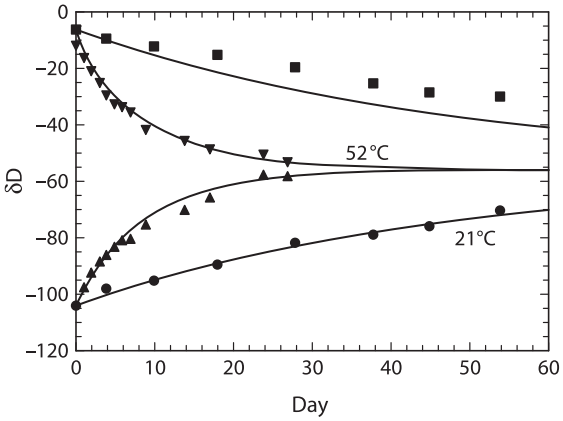

Fig. 2.2 δD values versus time for two beakers that have equal surface areas and equal volumes undergoing isotopic exchange in sealed systems. In both experiments at 21 and 52°C isotope ratios progress toward an average value of −56‰ via exchange with ambient vapour. *Solid curves* are calculated, *points* are experimental data (after Criss, 1999)

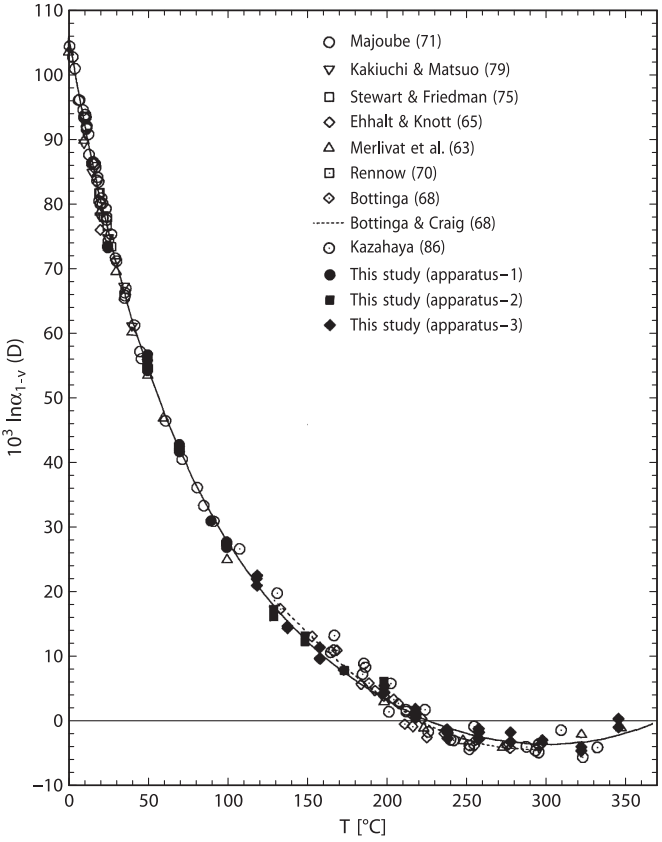

Fig. 2.3 Experimentally determined fractionation factors between liquid water and water vapour from 1 to 350°C (after Horita and Wesolowski, 1994)

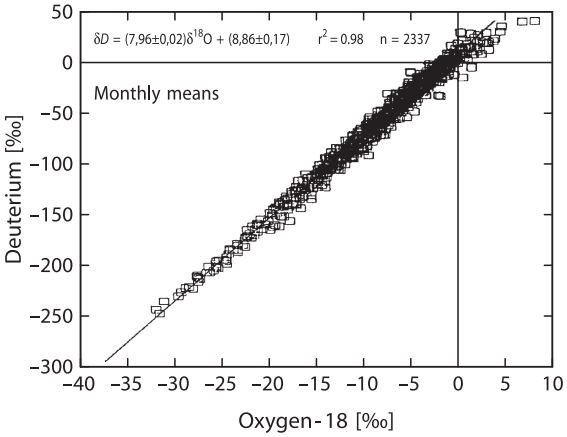

Fig. 2.4 Global relationship between monthly means of δD and $\delta^{18}O$ in precipitation, derived for all stations of the IAEA global network. *Line* indicates the global meteoric water line (MWL) (after Rozanski et al. 1993)

In all processes concerning the evaporation and condensation of water, hydrogen isotopes are fractionated in a similar fashion to those of oxygen isotopes, albeit with a different magnitude, because a corresponding difference in vapor pressures exists between H_2O and HDO in one case and $H_2^{16}O$ and $H_2^{18}O$ in the other.

Therefore, the hydrogen and oxygen isotope distributions are correlated for meteoric waters. Craig (1961a) first defined the generalized relationship:

$$\delta D = 8\delta^{18}O + 10,$$

which describes the interdependence of H- and O-isotope ratios in meteoric waters on a global scale.

This relationship, shown in Fig. 2.4, is described in the literature as the "Global Meteoric Water Line (GMWL)".

Neither the numerical coefficient 8 nor the constant 10, also called the deuterium excess d, are constant in nature. Both may vary depending on the conditions of evaporation, vapor transport and precipitation and, as a result, offer insight into climatic processes. The deuterium excess d is a valuable tool to derive information on relative humidities.

2.1.3.1 Equilibrium Exchange Reactions

D/H fractionations among gases are extraordinarily large, as calculated by Bottinga (1969a) and Richet et al. (1977) and plotted in Fig. 2.5. Even in magmatic systems, fractionation factors are sufficiently large to affect the δD-value of dissolved water in melts during degassing of H_2, H_2S or CH_4. The oxidation of H_2 or CH_4 to H_2O

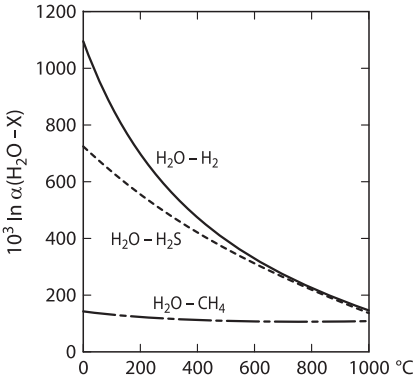

Fig. 2.5 D/H fractionations between H_2O – H_2, H_2O – H_2S and H_2O – CH_4 (from calculated data of Richet et al. 1977)

and CO_2 may also have an effect on the isotopic composition of water dissolved in melts due to the large fractionation factors.

With respect to mineral-water systems, different experimental studies obtained widely different results for the common hydrous minerals with respect to the absolute magnitude and the temperature dependence of D/H fractionations (Suzuoki and Epstein 1976; Graham et al. 1980; Vennemann et al. 1996). Suzuoki and Epstein (1976) first demonstrated the importance of the chemical composition of the octahedral sites in crystal lattices to the mineral H-isotope composition. Subsequently, isotope exchange experiments by Graham et al. (1980, 1984) suggested that the chemical composition of sites other than the octahedral sites can also affect hydrogen isotope compositions. These authors postulate a qualitative relationship between hydrogen-bond distances and hydrogen isotope fractionations: the shorter the hydrogen bond, the more depleted the mineral is in deuterium.

On the basis of theoretical calculations, Driesner (1997) proposed that many of the discrepancies between the experimental studies were due to pressure differences at which the experiments were carried out. Thus for hydrogen, pressure is a variable that must be taken into account in fluid-bearing systems. Later, Horita et al. (1999) presented experimental evidence for a pressure effect between brucite and water.

Chacko et al. (1999) developed an alternative method for the experimental determination of hydrogen isotope fractionation factors. Instead of using powdered minerals as starting materials these authors carried out exchange experiments with large single crystals and then analyzed the exchanged rims with the ion probe. Although the precision of the analytical data is less than that for conventional bulk techniques, the advantage of this technique is that it allows the determination of fractionation factors in experiments in which isotopic exchange occurs by a diffusional process rather than by a combination of diffusion and recrystallization.

In summary, as discussed by Vennemann and O'Neil (1996), discrepancies between published experimental calibrations in individual mineral–water systems are difficult to resolve, which limits the application of D/H fractionations in mineral–water systems to estimate δD-values of coexisting fluids.

2.1.3.2 Kinetic Isotope Effects

Large hydrogen isotope fractionations occur during the conversion of hydrogen from water to organic matter. The magnitude of H isotope fractionations is generally controlled by the biochemical pathways used. Although details of this complex process are still unknown, there is discussion about the quantitative role of kinetic and equilibrium isotope fractionations. Tremendous progress has been achieved through the introduction of the compound specific hydrogen isotope analysis (Sessions et al. 1999; Sauer et al. 2001; Schimmelmann et al. 2006), which allows the δD analysis of individual biochemical compound. Further details are discussed in Sect. 3.10.1.2.

2.1.3.3 Other Fractionation Effects

In salt solutions, isotopic fractionations can occur between water in the "hydration sphere" and free water (Truesdell 1974). The effects of dissolved salts on hydrogen isotope activity ratios in salt solutions can be qualitatively interpreted in terms of interactions between ions and water molecules, which appear to be primarily related to their charge and radius. Hydrogen isotope activity ratios of all salt solutions studied so far are appreciably higher than H-isotope composition ratios. As shown by Horita et al. (1993), the D/H ratio of water vapor in isotope equilibrium with a solution increases as salt is added to the solution. Magnitudes of the hydrogen isotope effects are in the order $CaCl_2 > MgCl_2 > MgSO_4 > KCl \sim NaCl > NaSO_4$ at the same molality.

Isotope effects of this kind are relevant for an understanding of the isotope composition of clay minerals and absorption of water on mineral surfaces. The tendency for clays and shales to act as semipermeable membranes is well known. This effect is also known as "ultrafiltration". Coplen and Hanshaw (1973) postulated that hydrogen isotope fractionations may occur during ultrafiltration in such a way that the residual water is enriched in deuterium due to its preferential adsorption on the clay minerals and its lower diffusivity.

2.2 Lithium

Lithium has two stable isotopes with the following abundances (Rosman and Taylor 1998):

^{6}Li 7.59%
^{7}Li 92.41%

Lithium is one of the rare elements where the lighter isotope is less abundant than the heavier one. In order to be consistent with the other isotope systems lithium isotope ratios are reported as δ^{7}Li-values.

The large mass difference relative to the mass of the element between ^{6}Li and ^{7}Li of about 16% is a favorable condition for their fractionation in nature. Taylor and Urey (1938) found a change of 25% in the Li-isotope ratio when Li-solutions percolate through a zeolite column. Thus, fractionation of Li-isotopes might be expected in geochemical settings in which cation exchange processes are involved.

Early workers had to struggle with serious lithium fractionation effects during mass spectrometric analysis. Today most workers use the multicollector sector ICP-MS technique first described by Tomascak et al. (1999). Improvements of the analytical techniques in recent years have lead to an accuracy better than 0.3‰. Unfortunately, there are no internationally accepted Li isotope values for rocks or waters. James and Palmer (2000) have determined nine international rock standards ranging from basalt to shale relative to the so-called NIST L-SVEC standard.

i) Characteristic features of Li isotope geochemistry

Lithium isotope geochemistry is characterized by a difference close to 30‰ between ocean water ($\delta^{7}Li + 31‰$) and bulk silicate earth with a δ^{7} Li-value of 3.2‰ (Seitz et al. 2007). In this respect lithium isotope geochemistry is very similar to that of boron (see p. 45). The isotopic difference between the mantle and the ocean can be used as a powerful tracer to constrain water/ rock interactions (Tomaszak 2004). Figure 2.6 gives an overview of Li-isotope variations in major geological reservoirs.

During weathering ^{7}Li is preferentially mobilized, whereas ^{6}Li is enriched in the weathering residue. Rudnick et al. (2004) have demonstrated that Li isotope fractionation correlates directly with the degree of weathering and that very light $\delta^{7}Li$ of $-20‰$ can be produced in soils. Thus, very effective Li-isotope fractionation processes are operative in the sedimentary environment. By analyzing major rivers, Huh et al. (1998) observed a large variation in $\delta^{7}Li$ in river waters with the suspended load being systematically lighter than the dissolved load.

Mantle-derived basalts, on the other hand, have a relatively uniform composition with $\delta^{7}Li$ values of $4 \pm 2‰$ (Tomaszak 2004; Elliott et al. 2004). The continental crust generally has a lighter Li isotope composition than the upper mantle from which it was derived (Teng et al. 2004). Considering the small Li isotope fractionation at high temperature igneous differentiation processes (Tomaszak 2004), pristine

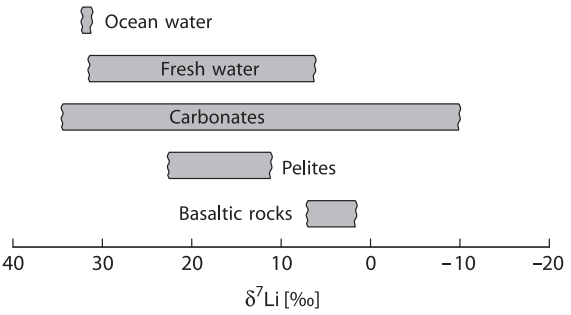

Fig. 2.6 Lithium isotope variations in major geological reservoirs

continental crust should not be too different in Li isotope composition from the mantle. Because this is not the case, the isotopically light crust must have been modified by secondary processes, such as weathering, hydrothermal alteration and prograde metamorphism (Teng et al. 2007).

Given the homogeneity of basaltic rocks, it is surprising that peridotites have a wide range in δ^7Li values from values as low as $-17‰$ (Nishio et al. 2004) to values as high as $+10‰$ (Brooker et al. 2004). This unexpected finding can be explained by diffusion processes that affect mantle minerals during melt migration (Parkinson et al. 2007). The latter authors have demonstrated that ^{6}Li diffuses 3% faster than ^{7}Li in silicate minerals consistent with diffusion experiments by Richter et al. (2003). Thus diffusion at magmatic temperatures is a very effective mechanism for generating large variations in ^{7}Li/^{6}Li ratios (Lundstrom et al. 2005; Teng et al. 2006; Rudnick and Ionov 2007). Although diffusion profiles will relax with time the existence of sharp δ^7 Li-profiles suggest diffusional Li isotope fractionation over short timescales (days to a few months) and therefore diffusion profiles in mantle minerals may be used as geospeedometers (Parkinson et al. 2007). At the same time diffusion may obliterate primary mantle signatures.

During fluid–rock interaction, Li as a fluid-mobile element will enrich in aqueous fluids. It might therefore be expected that δ^7Li enriched seawater incorporated into altered oceanic crust should be removed during subduction zone metamorphism. Continuous dehydration of pelagic sediments and altered oceanic crust results in ^{7}Li-depleted rocks and in ^{7}Li enriched fluids. A subducting slab therefore should introduce large amounts of ^{7}Li into the mantle wedge. To quantitatively understand this process Li isotope fractionation factors between minerals and coexisting fluids must be known. First attempts have been undertaken by Wunder et al. (2006, 2007) by determining experimentally the Li isotope fractionations between pyroxene, mica, staurolite and Cl^- and OH^- bearing fluids. These authors showed that ^{7}Li is preferentially partitioned into the fluid.

Because Li isotopes may be used as a tracer to identify the existence of recycled material in the mantle, systematic studies of arc lavas have been undertaken (Moriguti and Nakamura 1998; Tomascak et al. 2000; Leeman et al. 2004 and others). However, most arc lavas have δ^7Li values that are indistinguishable from those of MORB. Thus Li seems to be decoupled from other fluid mobile elements, because Li can partition into Mg-silicates (pyroxene, olivine) in the mantle (Tomascak et al. 2002).

Lithium is a conservative element in the ocean with a residence time of about one million year. Its isotope composition is maintained by inputs of dissolved Li from rivers (average $\delta^7\text{Li} + 23‰$, Huh et al. 1998) and high-temperature hydrothermal fluids at ocean ridges at one hand and low temperature removal of Li into oceanic basalts and marine sediments at the other. Any variance in these sources and sinks thus should cause secular variations in the isotope composition of oceanic Li. And indeed in a first attempt Hoefs and Sywall (1997) interpreted Li isotope variations in well preserved carbonate shells as indicating secular variations of the oceanic Li-cycle.

2.3 Boron

Boron has two stable isotopes with the following abundances (Rosman and Taylor 1998).

^{10}B 19.9%
^{11}B 80.1%

The large mass difference between ^{10}B and ^{11}B and large chemical isotope effects between different species (Bigeleisen 1965) make boron a very promising element to study for isotope variations. The utility of boron isotopes as a geochemical tracer stems from the high mobility of boron during high- and low-temperature fluid-related processes, showing a strong affinity for any vapor phases present.

The lowest observed δ^{11}B-values of around $-30‰$ are for certain tourmalines (Chaussidon and Albarede 1992) and some non-marine evaporite sequences (Swihart et al. 1986), whereas the most enriched ^{11}B-reservoir is given by brines from Australia and Israel (Dead Sea) which have δ^{11}B-values of up to 60‰ (Vengosh et al. 1991a, b). A very characteristic feature of boron geochemistry is the isotopic composition of ocean water with a constant δ^{11}B-value of 39.5‰ (Spivack and Edmond 1987), which is about 50‰ heavier than average continental crust value of $-10 \pm 2‰$ (Chaussidon and Albarede 1992). Isotope variations of boron in some geological reservoirs are shown in Fig. 2.7.

Methods
In recent years solid source mass-spectrometry has provided an effective means for B-isotope analysis. Two different methods have been developed, which have been summarized by Swihart (1996). The first was a positive thermal ionization technique using $Na_2BO_2^+$ ions initially developed by McMullen et al. (1961). Subsequently, Spivack and Edmond (1986) modified this technique by using $Cs_2BO_2^+$

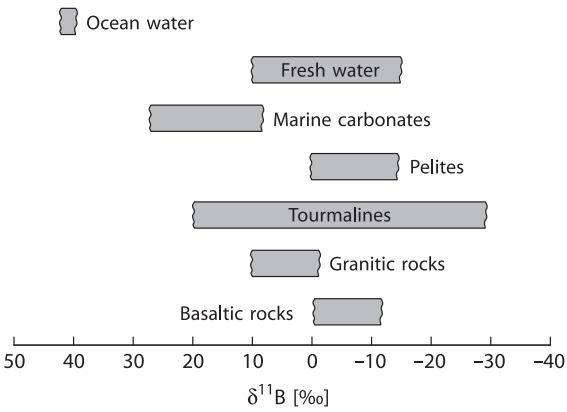

Fig. 2.7 Boron isotope variations in some geologically important reservoirs

ions (measurement of the masses 308 and 309). The substitution of ^{133}Cs for ^{23}Na increases the molecular mass and reduces the relative mass difference of its isotopic species, which limits the thermally induced mass dependent isotopic fractionation. This latter method has a precision of about ±0.25‰, which is better by a factor of 10 than the $Na_2BO_2^+$ method. Another method has been used by Chaussidon and Albarede (1992), who performed boron isotope determinations with an ion-microprobe having an analytical uncertainty of about ±2‰. Recently, Leceyer et al. (2002) described the use of MC–ICP–MS for B isotopic measurements of waters, carbonates, phosphates and silicates with an external reproducibilty of ±0.3‰.

As analytical techniques have been consistently improved in recent years, the number of boron isotope studies has increased rapidly. Reviews have been given by Barth (1993) and by Palmer and Swihart (1996). The total boron isotope variation documented to date is about 90‰. $\delta^{11}B$-values are generally given relative NBS boric acid SRM 951, which is prepared from a Searles Lake borax. This standard has a $^{11}B/^{10}B$ ratio of 4.04558 (Palmer and Slack 1989).

pH dependence of isotope fractionations

Boron is generally bound to oxygen or hydroxyl groups in either triangular (e.g., BO_3) or tetrahedral (e.g., $B(OH)_4^-$) coordination. The dominant isotope fractionation process occurs in aqueous systems via an equilibrium exchange process between boric acid ($B(OH)_3$) and coexisting borate anion ($B(OH)_4^-$). At low pH-values trigonal $B(OH)_3$ predominates, at high pH-values tetrahedral $B(OH)_4^-$ is the primary anion. The pH-dependence of the two boron species and their related isotope fractionation is shown in Fig. 2.8 (after Hemming and Hanson 1992). The pH dependence has been used reconstructing past ocean pH-values by measuring the boron isotope composition of carbonates e.g. foraminifera. This relies on the fact that mainly the charged species $B(OH)_4^-$ is incorporated into carbonate minerals with small to insignificant fractionations (Hemming and Hanson 1992; Sanyal et al. 2000).

Because of the inability to quantitatively separate the two species in solution, a theoretically calculated fractionation factor of about 1.0194 at 25°C has been widely used for p_H estimates (Kakihana et al. 1977). As recently shown by Zeebe (2005) and Klochko et al. (2006) the equilibrium fractionation factor appears to be significantly larger than the theoretical value of Kakihana et al. (1977) used in paleo-pH studies. Klochko et al. (2006), for instance, reported a fractionation factor of 1.0272.

This approach has been not only used to directly estimate the ocean pH from $\delta^{11}B$ of foraminifera but to estimate from the p_H the past atmospheric CO_2 concentrations (i.e. Pearson and Palmer 1999, 2000; Pagani et al. 2005). An increase in atmospheric CO_2 results in increased dissolved CO_2 in ocean water, which in turn causes a reduction in oceanic p_H. A note of caution was presented by Lemarchand et al. (2000) who suggested that boron isotope variations in foraminifera depend at least in part on variations in the supply of riverine boron to the ocean during the geologic past. And indeed the boron isotope composition of rivers can be extremely variable (Rose et al. 2000; Lemarchand et al. 2002). Joachimski et al. (2005) presented evidence

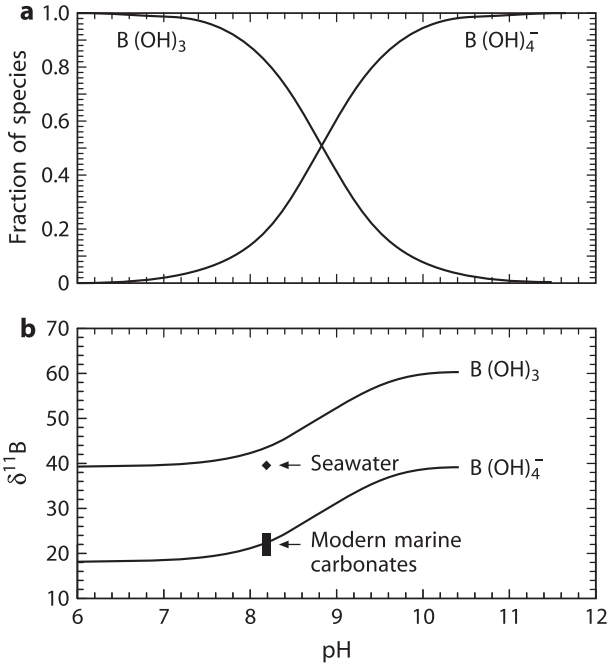

Fig. 2.8 (**a**) Distribution of aqueous boron species versus ph; (**b**) $\delta^{11}B$ of the two dominant species $B(OH)_3$ and $B(OH)_4^-$ versus ph (after Hemming and Hanson, 1992)

that Paleozoic oceans were lower in $\delta^{11}B$ by up to 10‰, which supports conclusions that boron isotope ratios cannot be used as a reliable paleo-pH indicator.

Fluid-rock interactions

Boron and – as already demonstrated – lithium are useful tracers for mass transfer estimates in subduction zones. Both elements are mobilized by fluids and melts and display considerable isotope fractionation during dehydration reactions. Concentrations of B and Li are low in mantle derived materials, whereas they are high in sediments, altered oceanic crust and continental crust. Any input of fluid and melt from the subducting slab into the overlying mantle has a strong impact on the isotope composition of the mantle wedge and on magmas generated there. Experimental studies of boron isotope fractionation between hydrous fluids, melts and minerals have shown that ^{11}B preferentially partitions into the fluid relative to minerals or melts (Palmer et al. 1987; Williams et al. 2001; Wunder et al. 2005; Liebscher et al. 2005), ranging from about 33‰ for fluid–clay (Palmer et al. 1987) to about 6‰ for fluid–muscovite at 700°C (Wunder et al. 2005) and to a few ‰ for fluid-melt above $1,000$°C (Hervig et al. 2002). The main fractionation effect seems to be due to the change from trigonal boron in neutral pH hydrous fluid to tetrahedrally coordinated boron in most rock forming minerals.

Tourmaline

Tourmaline is the most abundant reservoir of boron in metamorphic and magmatic rocks. It is stable over a very large p–T range. Since volume diffusion of B isotopes is insignificant in tourmalines (Nakano and Nakamura 2001), isotopic heterogeneities of zoned tourmalines should be preserved up to at least 600°C. Swihart and Moore (1989), Palmer and Slack (1989), Slack et al. (1993), Smith and Yardley (1996) and Jiang and Palmer (1998) analyzed tourmaline from various geological settings and observed a large range in δ^{11}B-values which reflects the different origins of boron and its high mobility during fluid related processes. By using the SIMS method, Marschall et al. (2008) demonstrated that boron isotopes in zoned tourmalines indeed may reflect different stages of tourmaline growth.

Because tourmaline is usually the only boron-bearing mineral of significance, recrystallization of tourmaline will not produce any change in its ^{11}B-content, unless boron is lost or gained by the system. If boron is lost from the rock, the δ^{11}B-value of the recrystallized tourmaline will be lower than the original value because ^{11}B is preferentially partitioned into the fluid phase. Meyer et al. (2008) experimentally determined the boron partitioning between tourmaline and fluid. In the temperature range from 400 to 700°C ^{11}B preferentially fractionates into the fluid, but to a smaller degree than determined by Palmer et al. (1992).

2.4 Carbon

Carbon occurs in a wide variety of compounds on Earth, from reduced organic compounds in the biosphere to oxidized inorganic compounds like CO_2 and carbonates. The broad spectrum of carbon-bearing compounds involved in low- and high-temperature geological settings can be assessed on the basis of carbon isotope fractionations.

Carbon has two stable isotopes (Rosman and Taylor 1998)

$^{12}\text{C} = 98.93\%$ (reference mass for atomic weight scale)
$^{13}\text{C} = 1.07\%$

The naturally occurring variations in carbon isotope composition are greater than 120‰, neglecting extraterrestrial materials. Heavy carbonates with δ^{13}C-values $> +20$‰ and light methane of < -100‰ have been reported in the literature.

2.4.1 Preparation Techniques

The gases used in $^{13}\text{C}/^{12}\text{C}$ measurements are CO_2 and recently CO during pyrolysis applications. For CO_2 the following preparation methods exist:

1. Carbonates are reacted with 100% phosphoric acid at temperatures between 20 and 90°C (depending on the type of carbonate) to liberate CO_2 (see also "oxygen").

2. Organic compounds are generally oxidized at high temperatures (850–1,000°C) in a stream of oxygen or by an oxidizing agent like CuO. In the last few years, a new methodology to measure ^{13}C-contents of individual compounds in complex organic mixtures has been developed. This so-called GC–C–MS technique employs a capillary column gas chromatograph, a combusion interface to produce CO_2 and a modified conventional gas mass–spectrometer and can measure individual carbon compounds in mixtures of sub-nanogram samples with a precision of better than $\pm 0.5‰$.

2.4.2 Standards

As the commonly used international reference standard PDB has been exhausted for several decades, there is a need for introducing new standards. Even though several different standards are in use today, the international standard the δ-values are referred to remains to be the PDB-standard (Table 2.2).

2.4.3 Fractionation Processes

The two main terrestrial carbon reservoirs, organic matter and sedimentary carbonates, have distinctly different isotopic characteristics because of the operation of two different reaction mechanisms:

1. Isotope equilibrium exchange reactions within the inorganic carbon system "atmospheric CO_2 – dissolved bicarbonate – solid carbonate" lead to an enrichment of 13C in carbonates.
2. Kinetic isotope effects during photosynthesis concentrate the light isotope 12C in the synthesized organic material.

1. The inorganic carbonate system is comprised of multiple chemical species linked by a series of equilibria:

$$CO_{2(aq)} + H_2O = H_2CO_3 \tag{2.2}$$

$$H_2CO_3 = H^+ + HCO_3^- \tag{2.3}$$

$$HCO_3^- = H^+ + CO_3^{2-} \tag{2.4}$$

Table 2.2 δ^{13}C-values of NBS-reference samples relative to PDB

NBS-18	Carbonatite	−5.00
NBS-19	Marble	+1.95
NBS-20	limestone	−1.06
NBS-21	Graphite	−28.10

The carbonate (CO_3^{2-}) ion can combine with divalent cations to form solid minerals, calcite and aragonite being the most common

$$Ca^{2+} + CO_3^{2-} = CaCO_3 \tag{2.5}$$

An isotope fractionation is associated with each of these equilibria, the ^{13}C-differences between the species depend only on temperature, although the relative abundances of the species are strongly dependent on pH. Several authors have reported isotope fractionation factors for the system dissolved inorganic carbon (DIC) – gaseous CO_2) (Vogel et al. 1970; Mook et al. 1974; Zhang et al. 1995). The major problem in the experimental determination of the fractionation factor is the separation of the dissolved carbon phases (CO_{2aq}, HCO^{3-}, CO^{3-}) because isotope equilibrium among these phases is reached within seconds. Figure 2.9 summarizes carbon isotope fractionations between various geologic materials and gaseous CO_2 (after Chacko et al. 2001).

The generally accepted carbon isotope equilibrium values between calcium carbonate and dissolved bicarbonate are derived from inorganic precipitate data of Rubinson and Clayton (1969), Emrich et al. (1970), and Turner (1982). What is often not adequately recognized is the fact that systematic C-isotope differences exist between calcite and aragonite. Rubinson and Clayton (1969) and Romanek et al. (1992) found calcite and aragonite to be 0.9 and 2.7‰ enriched in ^{13}C relative to bicarbonate at 25°C. Another complicating factor is that shell carbonate – precipitated by marine organisms – is frequently not in isotopic equilibrium with the ambient dissolved bicarbonate. Such so-called "vital" effects can be as large as a few permil (see discussion on p. 198).

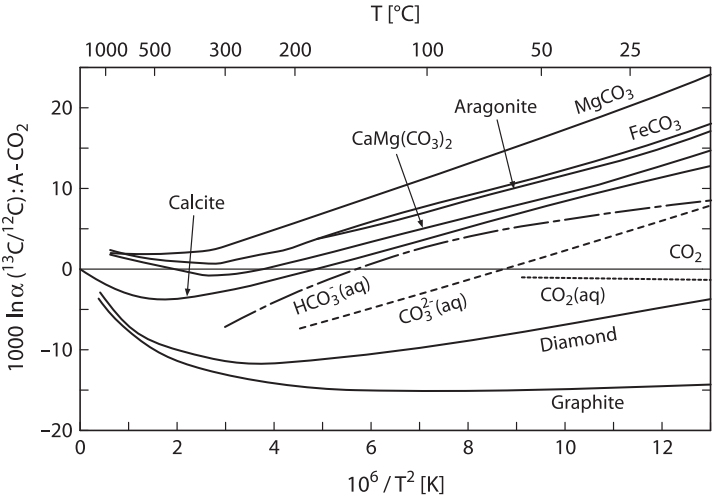

Fig. 2.9 Carbon isotope fractionations between various geologic materials and CO_2 (after Chacko et al. 2001)

Carbon isotope fractionations under equilibrium conditions are important not only at low-temperature, but also at high temperatures within the system carbonate, CO_2, graphite, and CH_4. Of these, the calcite–graphite fractionation has become a useful geothermometer (e.g., Valley and O'Neil 1981; Scheele and Hoefs 1992; Kitchen and Valley 1995) (see discussion on p. 227).

2. Early reviews by O'Leary (1981) and Farquhar et al. (1989) have provided the biochemical background of carbon isotope fractionations during photosynthesis, with more recent accounts by Hayes (2001) and Freeman (2001).

The main isotope-discriminating steps during biological carbon fixation are (1) the uptake and intracellular diffusion of CO_2 and (2) the biosynthesis of cellular components. Such a two-step model was first proposed by Park and Epstein (1960):

$$CO_{2(\text{external})} \leftrightarrow CO_{2(\text{internal})} \rightarrow \text{organic molecule}$$

From this simplified scheme, it follows that the diffusional process is reversible, whereas the enzymatic carbon fixation is irreversible. The two-step model of carbon fixation clearly suggests that isotope fractionation is dependent on the partial pressure of CO_2, i.e. pCO_2 of the system. With an unlimited amount of CO_2 available to a plant, the enzymatic fractionation will determine the isotopic difference between the inorganic carbon source and the final bioproduct. Under these conditions, ^{13}C fractionations may vary from -17 to $-40‰$ (O'Leary 1981). When the concentration of CO_2 is the limiting factor, the diffusion of CO_2 into the plant is the slow step in the reaction and carbon isotope fractionation of the plant decreases.

Atmospheric CO_2 first moves through the stomata, dissolves into leaf water and enters the outer layer of photosynthetic cells, the mesophyll cell. Mesophyll CO_2 is directly converted by the enzyme ribulose biphosphate carboxylase/oxygenase ("Rubisco") to a six carbon molecule that is then cleaved into two molecules of phosphoglycerate (PGA), each with three carbon atoms (plants using this photosynthetic pathway are therefore called C_3 plants). Most PGA is recycled to make ribulose biphosphate, but some is used to make carbohydrates. Free exchange between external and mesophyll CO_2 makes the carbon fixation process less efficient, which causes the observed large ^{13}C-depletions of C3 plants.

C4 plants incorporate CO_2 by the carboxylation of phosphoenolpyruvate (PEP) via the enzyme PEP carboxylase to make the molecule oxaloacetate which has 4 carbon atoms (hence C4). The carboxylation product is transported from the outer layer of mesophyll cells to the inner layer of bundle sheath cells, which are able to concentrate CO_2, so that most of the CO_2 is fixed with relatively little carbon fractionation.

In conclusion, the main controls on carbon fractionation in plants are the action of a particular enzyme and the "leakiness" of cells. Because mesophyll cells are permeable and bundle sheath cells are less permeable, C_3 vs C_4 plants have ^{13}C-depletions of $-18‰$ versus $-4‰$ relative to atmospheric CO_2 (see Fig. 2.10).

Work summarized by Hayes (1993) and Hayes (2001) has demonstrated that the final carbon isotope composition of naturally synthesized organic matter depends on a complex set of parameters. (1) the ^{13}C-content of the carbon source, (2) isotope

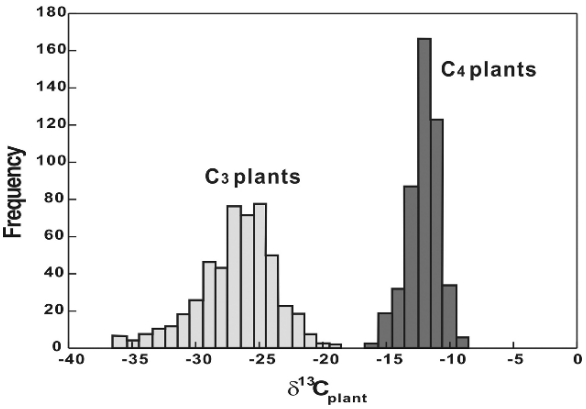

Fig. 2.10 Histogram of $\delta^{13}C$-values of C_3 and C_4 plants (after Cerling and Harris, 1999)

effects associated with the assimilation of carbon, (3) isotope effects associated with metabolism and biosynthesis and (4) cellular carbon budgets.

Even more complex is C-isotope fractionation in aquatic plants. Factors that control the $\delta^{13}C$ of phytoplankton include temperature, availability of $CO_2(aq)$, light intensity, nutrient availability, pH and physiological factors such as cell size and growth rate (Laws et al. 1995, 1997; Bidigare et al. 1997; Popp et al. 1998 and others). In particular the relationship between C-isotope composition of phytoplankton and concentration of oceanic dissolved CO_2 has been subject of considerable debate because of its potential as a palaeo-CO_2 barometer (see discussion).

Since the pioneering work of Park and Epstein (1960) and Abelson and Hoering (1961) it is well known that ^{13}C is not uniformly distributed among the total organic matter of plant material, but varies between carbohydrates, proteins and lipids. The latter class of compounds is considerably depleted in ^{13}C relative to the other products of biosynthesis. Although the causes of these ^{13}C-differences are not entirely clear, kinetic isotope effects seem to be more plausible (De Niro and Epstein 1977; Monson and Hayes 1982) than thermodynamic equilibrium effects (Galimov 1985a, 2006). The latter author argued that ^{13}C-concentrations at individual carbon positions within organic molecules are principally controlled by structural factors. Approximate calculations suggested that reduced C – H bonded positions are systematically depleted in ^{13}C, while oxidized C – O bonded positions are enriched in ^{13}C. Many of the observed relationships are qualitatively consistent with that concept. However, it is difficult to identify any general mechanism by which thermodynamic factors should be able to control chemical equilibrium within a complex organic structure. Experimental evidence presented by Monson and Hayes (1982) suggests that kinetic effects will be dominant in most biological systems.

2.4.4 Interactions between the Carbonate-Carbon Reservoir and Organic Carbon Reservoir

Variations in ^{13}C content of some important carbon compounds are schematically demonstrated in Fig. 2.11: The two most important carbon reservoirs on Earth, marine carbonates and the biogenic organic matter, are characterized by very different isotopic compositions: the carbonates being isotopically heavy with a mean $\delta^{13}C$-value around 0‰ and organic matter being isotopically light with a mean $\delta^{13}C$-value around −25‰. For these two sedimentary carbon reservoirs an isotope mass balance must exist such that:

$$\delta^{13}C_{input} = f_{org}\delta^{13}C_{org} + \left(1 - f_{org}\right)\delta^{13}C_{carb} \tag{2.6}$$

If δ input, δ_{org}, δ_{carb} can be determined for a specific geologic time, f_{org} can be calculated, where f_{org} is the fraction of organic carbon entering the sediments. It should be noted that f_{org} is defined in terms of the global mass balance and is independent of biological productivity referring to the burial rather than the synthesis of organic material. That means that large f_{org} values might be a result of high productivity and average levels of preservation of organic material or of low levels of productivity and high levels of preservation.

The $\delta^{13}C$-value for the input carbon cannot be measured precisely but can be estimated with a high degree of certainty. As will be shown later, mantle carbon has an isotopic composition around −5‰ and estimates of the global average isotope composition for crustal carbon also fall in that range. Assigning −5‰ to $\delta^{13}C$-input, a modern value for f_{org} is calculated as 0.2 or expressed as the ratio of $C_{org}/C_{carb} = 20/80$. As will be shown later (Chapter) f_{org} has obviously changed during specific periods of the Earth's history (e.g. Hayes et al. 1999). With each molecule of organic carbon being buried, a mole of oxygen is released to the atmo-

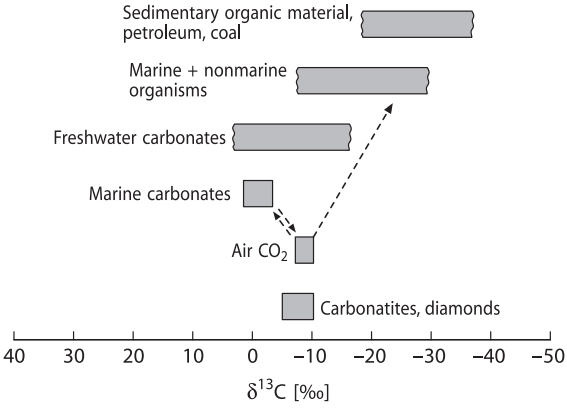

Fig. 2.11 $\delta^{13}C$-values of some important carbon reservoirs

sphere. Hence, knowledge of f_{org} is of great value in reconstructing the crustal redox budget.

2.5 Nitrogen

More than 99% of the known nitrogen on or near the Earth's surface is present as atmospheric N_2 or as dissolved N_2 in the ocean. Only a minor amount is combined with other elements, mainly C, O, and H. Nevertheless, this small part plays a decisive role in the biological realm. Since nitrogen occurs in various oxidation states and in gaseous, dissolved, and solid forms (N_2, NO_3^-, NO_2^-, NH_3, NH_4^+), it is a highly suitable element for the search of natural variations in its isotopic composition. Schoenheimer and Rittenberg (1939) were the first to report nitrogen isotopic variations in biological materials. Today, the range of reported $\delta^{15}N$-values covers 100‰, from about −50 to +50‰. However, most δ-values fall within the much narrower spread from −10 to +20‰, as described in more recent reviews of the exogenic nitrogen cycle by Heaton (1986), Owens (1987), Peterson and Fry (1987) and Kendall (1998).

Nitrogen consists of two stable isotopes, ^{14}N and ^{15}N. Atmospheric nitrogen, given by Rosman and Taylor (1998) has the following composition:

$^{14}N : 99.63\%$
$^{15}N : 0.37\%$.

N_2 is used for $^{15}N/^{14}N$ isotope ratio measurements, the standard is atmospheric N_2. Various preparation procedures have been described for the different nitrogen compounds (Bremner and Keeney 1966; Owens 1987; **? ?**; Kendall and Grim 1990; Scholten 1991 and others). In the early days of nitrogen isotope investigations the extraction and combustion techniques potentially involved chemical treatments that could have introduced isotopic fractionations. In recent years, simplified techniques for combustion have come into routine use, so that a precision of 0.1–0.2‰ for $\delta^{15}N$ determinations can be achieved. Organic nitrogen-compounds are combusted to CO_2, H_2O and N_2, the product gases are separated from each other cryogenically and the purified N_2 is trapped on molecular sieves for mass-spectrometric analysis.

To understand the processes leading to the nitrogen isotope distribution in the geological environment, a short discussion of the biological nitrogen cycle is required. Atmospheric nitrogen, the most abundant form of nitrogen, is the least reactive species of nitrogen. It can, however, be converted to "fixed" nitrogen by bacteria and algae, which, in turn, can be used by biota for degradation to simple nitrogen compounds such as ammonium and nitrate. Thus, microorganisms are responsible for all major conversions in the biological nitrogen cycle, which generally is divided into fixation, nitrification, and denitrification. Other bacteria return nitrogen to the atmosphere as N_2.

The term *fixation* is used for processes that convert unreactive atmospheric N_2 into reactive nitrogen such as ammonium, usually involving bacteria. Fixation commonly produces organic materials with δ^{15}N-values slightly less than 0‰ ranging from −3 to +1 (Fogel and Cifuentes 1993) and occurs in the roots of plants by many bacteria. The large amount of energy needed to break the molecular nitrogen bond makes nitrogen fixation a very inefficient process with little associated N-isotope fractionation.

Nitrification is a multi-step oxidation process mediated by several different autotrophic organisms. Nitrate is not the only product of nitrification, different reactions produce various nitrogen oxides as intermediate species. Nitrification can be described as two partial oxidation reactions, each of which proceeds separately.

Oxidation by Nitrosomas ($NH_4 \rightarrow NO_{2-}$) followed by oxidation by Nitrobacter (NO_2fiNO_3). Because the oxidation of nitrite to nitrate is generally rapid, most of the N-isotope fractionations is caused by the slow oxidation of ammonium by Nitrosomas. In N-limited systems fractionations are minimal.

Denitrification (reduction of more oxidized forms to more reduced forms of nitrogen) is a multi-step process with various nitrogen oxides as intermediate compounds resulting from biologically mediated reduction of nitrate. Denitrification takes place in poorly aerated soil and in stratified anaerobic water bodies. Denitrification supposedly balances the natural fixation of nitrogen, if it did not occur, then atmospheric nitrogen would be exhausted in less than 100 million years. Denitrification causes the δ^{15}N-values of the residual nitrate to increase exponentially as nitrate concentrations decrease. Experimental investigations have demonstrated that fractionation factors may change from 10 to 30‰, with the largest values obtained under lowest reduction rates. Generally, the same factors that influence isotope fractionation during bacterial sulfate reduction are also operative during bacterial denitrification. Table 2.3, which gives a summary of observed N-isotope fractionations, clearly indicates the dependence of fractionations on nitrogen concentrations and

Table 2.3 Naturally observed isotope fractionation for nitrogen assimilation (after Fogel and Cifuentes Fogel and Cifuentes 1993)

N_2 fixation	−3 to +1‰
NH_4^+ assimilation	
Cultures	
Millimolar concentrations	0 to −15‰
Micromolar concentrations	−3 to −27‰
Field observations	
Micromolar concentrations	−10‰
NO_3^- assimilation	
Cultures	
Millimolar concentrations	0 to −24‰
Micromolar concentrations	−10‰
Field observations	
Micromolar concentrations	−4 to −5‰

demonstrates, that at low nitrogen concentrations fractionations are nearly zero because virtually all the nitrogen is used.

So far, only kinetic isotope effects have been considered, but isotopic fractionations associated with equilibrium exchange reactions have been demonstrated for the common inorganic nitrogen compounds (Letolle 1980). Of special importance in this respect is the ammonia volatilization reaction:

$$NH_{3gas} \leftrightarrow NH^{+}_{4aq}$$

for which isotope fractionation factors of 1.025–1.035 have been determined (Kirshenbaum et al. 1947; Mariotti et al. 1981). Experimental data by Nitzsche and Stiehl (1984) indicate fractionation factors of 1.0143 at 250°C and of 1.0126 at 350°C very small ^{15}N-enrichment of about 0.1‰ occurs during the solution of atmospheric N_2 in ocean water (Benson and Parker 1961).

Nitrogen isotope studies are extremely important for evaluating the source and fate of nitrogen in the marine and terrestrial environment. $\delta^{15}N$-values measured in the water column of the ocean and in sediments depend on the many nitrogen isotope fractionation reactions in the biological cycle. Nitrogen isotopes have been used as a paleoceanographic proxy, because they record changes of nutrient dynamics and ventilation that affects denitrification in the water column (e.g. Farrell et al. 1995). This approach is based on the fact that particulate organic nitrogen depends on (1) the isotopic composition of dissolved nitrate, which in oxygenated waters has a $\delta^{15}N$-value of about -6‰ (in anoxic waters where denitrification occurs the $\delta^{15}N$-value is significantly higher, up to 18.8‰ in the tropical North Pacific; Cline and Kaplan 1975) and on (2) isotope fractionation that occurs during nitrogen uptake by phytoplankton. In the photic zone phytoplankton preferentially incorporates ^{14}N, which results in a corresponding ^{15}N-enrichment in the residual nitrate. The N-isotope composition of settling organic detritus thus varies depending on the extent of nitrogen utilization: low ^{15}N contents indicate low relative utilisation, high ^{15}N contents indicate a high utilization.

Much of the initial organic nitrogen reaching the sediment/water interface is lost during early diagenesis. Nevertheless the nitrogen isotope composition of sediments is primarely determined by the source organic matter. Source studies have been undertaken to trace the contribution of terrestrial organic matter to ocean water and to sediments (i.e. Sweeney et al. 1978; Sweeney and Kaplan 1980). Such studies are based, however, on the assumption that the ^{15}N content remains unchanged in the water column. Investigations by Cifuentes et al. (1989), Altabet et al. (1991), and Montoya et al. (1991) have demonstrated that there may be rapid temporal (even on a time scale of days) and spatial changes in the nitrogen isotope composition of the water column due to biogeochemical processes. This complicates a clear distinction between terrestrial and marine organic matter, although marine organic matter generally has a higher $^{15}N/^{14}N$ ratio than terrestrial organic matter.

The organic matter in sediments has a mean $\delta^{15}N$-value of around $+7$‰ (Sweeney et al. 1978). During diagenesis biological and thermal degradation of

the organic matter results in the formation of ammonium (NH_4) which can be incorporated for potassium in clay minerals. This nitrogen in the crystal lattice of clay minerals and micas is mainly derived from decomposing organic matter and thus has a very similar isotopic composition as the organic matter (Scholten 1991; Williams et al. 1995).

During metamorphism of sediments, there is a significant loss of ammonium during devolatilisation, which is associated with a nitrogen fractionation, leaving behind ^{15}N residues (Haendel et al. 1986; Bebout and Fogel 1992; Jia 2006). Thus high-grade metamorphic rocks and granites are relatively enriched in ^{15}N and typically have $\delta^{15}N$-values between 8 and 10‰. Sadofsky and Bebout (2000) have examined the nitrogen isotope fractionation among coexisting micas, but could not find any characteristic difference between biotite and white mica.

In summary, nitrogen in sediments and crustal rocks exhibits positive $\delta^{15}N$-values around 6‰. In contrast, mantle nitrogen extracted from MORB glasses (Marty and Humbert 1997; Marty and Zimmermann 1999) and from diamonds (Javoy et al. 1986; Cartigny et al. 1997) have average $\delta^{15}N$-values of around -5‰. These similar values for subcontinental and MORB mantle suggests a homogeneous distribution of nitrogen isotopes in the mantle. $\delta^{15}Nt$-values thus are an important tracer to distinguish mantle-derived from crustal derived nitrogen.

Many studies have shown that nitrogen isotopes can be used in environmental studies. Fertilizer, animal wastes or sewage are the main sources of nitrate pollution in the hydrosphere. Under favorable conditions, these N-bearing compounds can be isotopically distinguished from each other (Heaton 1986). Anthropogenic fertilizers have $\delta^{15}N$-values in the range -4 to $+4$‰ reflecting their atmospheric source, whereas animal waste typically has $\delta^{15}N$-values > 5‰. Soil-derived nitrate and fertilizer nitrate commonly have overlapping $\delta^{15}N$-values. $\delta^{15}N$ can potentially also be used as trophic level indicator.

Figure 2.12 gives an overview about the nitrogen isotope variations in some important reservoirs.

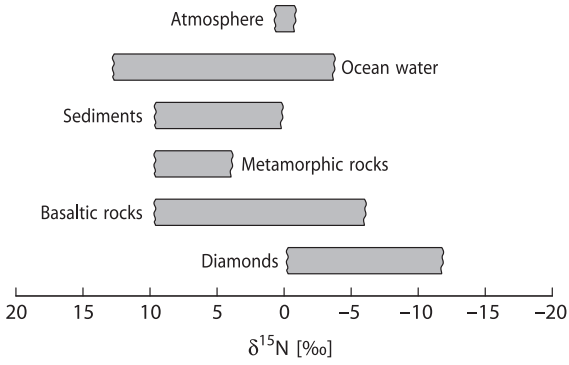

Fig. 2.12 $\delta^{15}N$-values of geologically important reservoirs

2.6 Oxygen

Oxygen is the most abundant element on Earth. It occurs in gaseous, liquid and solid compounds, most of which are thermally stable over large temperature ranges. These facts make oxygen one of the most interesting elements in isotope geochemistry.

Oxygen has three stable isotopes with the following abundances (Rosman and Taylor 1998)

$^{16}O : 99.757\%$
$^{17}O : 0.038\%$
$^{18}O : 0.205\%$

Because of the higher abundance and the greater mass difference, the $^{18}O/^{16}O$ ratio is normally determined, which may vary in natural samples by about 10% or in absolute numbers from about 1:475 to 1:525.

2.6.1 Preparation Techniques

CO_2 is the gas generally used for mass-spectrometric analysis. More recently CO and O_2 have also been used in high temperature conversion of organic material and in laser probe preparation techniques. A wide variety of methods have been described to liberate oxygen from the various oxygen-containing compounds.

Oxygen in silicates and oxides is usually liberated through fluorination with F_2, BrF_5 or ClF_3 in nickel-tubes at 500 to 650°C (Taylor and Epstein 1962; Clayton and Mayeda 1963; Borthwick and Harmon 1982) or by heating with a laser (Sharp 1990). Decomposition by carbon reduction at 1,000 to 2,000°C may be suitable for quartz and iron oxides but not for all silicates (Clayton and Epstein 1958). The oxygen is converted to CO_2 over heated graphite or diamond. Care must be taken to ensure quantitative oxygen yields, which can be a problem in the case of highly refractive minerals like olivine and garnet. Low yields may result in anomalous $^{18}O/^{16}O$ ratios, high yields are often due to excess moisture in the vacuum extraction line.

Conventional fluorination is usually done on 10–20 mg of whole-rock powder or minerals separated from much larger samples; the inability to analyze small quantities means that natural heterogeneity cannot be detected by such bulk techniques. Recent advances in the development of laser microprobes, first described by Sharp (1990), have revolutionized mineral analyses. Laser techniques have both the resolution and precision to investigate isotopic zoning within single mineral grains and mineral inter- and overgrowths.

The standard procedure for the isotope analysis of carbonates is the reaction with 100% phosphoric acid at 25°C first described by McCrea (1950). The following reaction equation:

$$MeCO_3 + H_3PO_4 \rightarrow MeHPO_4 + CO_2 + H_2O \qquad (2.7)$$

where Me is a divalent cation, shows that only two-thirds of the carbonate oxygen present in the product CO_2 is liberated, and thus a significant isotope effect is observed, which is on the order of 10‰, but varies up to a few ‰ depending on the cation, the reaction temperature and the preparation procedure. The so-called acid fractionation factor must be precisely known to obtain the oxygen isotope ratio of the carbonate. This can be done by measuring the $\delta^{18}O$-value of the carbonate by fluorination with BrF_5, first described by Sharma and Clayton (1965).

Experimental details of the phosphoric acid method vary significantly among different laboratories. The two most common varieties are the "sealed vessel" and the "acid bath" methods. In the latter method the CO_2 generated is continuously removed, while in the former it is not. Swart et al. (1991) demonstrated that the two methods exhibit a systematic ^{18}O difference between 0.2 and 0.4‰ over the temperature range 25 to 90°C. Of these the acid-bath method probably provides the more accurate results. A further modification of this technique is referred to as the "individual acid bath", in which contaminations from the acid delivery system are minimized. Wachter and Hayes (1985) demonstrated that careful attention must be given to the phosphoric acid. In their experiments best results were obtained by using a 105% phosphoric acid and a reaction temperature of 75°C. This high reaction temperature should not be used when attempting to discriminate between mineralogically distinct carbonates by means of differential carbonate reaction rates.

Because some carbonates like magnesite or siderite react very sluggishly at 25°C, higher reaction temperatures are necessary to extract CO_2 from these minerals. Reaction temperatures have varied up to 90 or even 150°C (Rosenbaum and Sheppard 1986; Böttcher 1996), but there still exist considerable differences in the fractionation factors determined by various workers. For example fractionations between aragonite and calcite remain controversial and different workers have reported fractionations from negative to positive. Nevertheless there seems to be a general agreement that the fractionation factor for aragonite is about 0.6‰ higher than for calcite (Tarutani et al. 1969; Kim and O'Neil 1997), although Grossman and Ku (1986) have reported a value of up to 1.2‰. The dolomite-calcite fractionation may vary depending on specific composition (Land 1980). Table 2.4 reports acid fractionation factors for various carbonates.

Phosphates are first dissolved, then precipitated as silver phosphate (Crowson et al. 1991). Ag_3PO_4 is preferred because it is non-hydroscopic and can be precipitated rapidly without numerous chemical purification steps (O'Neil et al. 1994). This Ag_3PO_4 is then fluorinated (Crowson et al. 1991), reduced with C either in a furnace (O'Neil et al. 1994) or with a laser (Wenzel et al. 2000) or pyrolyzed (Vennemann et al. 2002). Because PO_4 does not exchange oxygen with water at room temperature (Kolodny et al. 1983), the isotopic composition of the Ag_3PO_4 is that of the PO_4 component of the natural phosphate. As summarized by Vennemann et al. (2002) conventional fluorination remains the most precise and accurate analytical technique for Ag_3PO_4. Laser techniques on bulk materials have also been attempted (Cerling and Sharp 1996; Kohn et al. 1996; Wenzel et al. 2000), but because fossil phosphates invariably contain diagenetic contaminants, chemical processing and analysis of a specific component (CO_3 or PO_4) is ordinarily performed.

Table 2.4 Acid fractionation factors for various carbonates determined at 25°C (modified after Kim et al. 2007)

Mineral	α	Reference
Calcite	10.30	Kim et al. (2007)
Aragonite	10.63	Kim et al. (2007)
	11.14	Gilg (2007)
Dolomite	11.75	Rosenbaum and Sheppard (1986)
Magnesite	10.79 (50°C)	Das Sharma et al. (2002)
Siderite	11.63	Carothers et al. (1988)
Witherite	10.57	Kim and O·Neil (1997)

Sulfates are precipitated as $BaSO_4$, and then reduced with carbon at 1,000°C to produce CO_2 and CO. The CO is either measured directly or converted to CO_2 by electrical discharge between platinum electrodes (Longinelli and Craig 1967). Total pyrolysis by continuous flow methods has made the analysis of sulfate oxygen more precise and less time-consuming than the off-line methods. Bao and Thiemens (2000) have used a CO_2-laser fluorination system to liberate oxygen from barium sulfate.

The $^{18}O/^{16}O$ ratio of water is usually determined by equilibration of a small amount of CO_2 with a surplus of water at a constant temperature. For this technique the exact value of the fractionation for the CO_2/H_2O equilibrium at a given temperature is of crucial importance. A number of authors have experimentally determined this fractionation at 25°C with variable results. A value of 1.0412 was proposed at the 1985 IAEA Consultants Group Meeting to be the best estimate.

It is also possible to quantitatively convert all water oxygen directly to CO_2 by reaction with guanidine hydrochloride (Dugan et al. 1985) which has the advantage that it is not necessary to assume a value for the $H_2O - CO_2$ isotope fractionation in order to obtain the $^{18}O/^{16}O$ ratio. On-line pyrolysis using TC-EA systems represents another approach (de Groot 2004).

2.6.2 Standards

Two different δ–scales are in use: $\delta^{18}O(VSMOW)$ and $\delta^{18}O(VPDB)$, because of two different categories of users, who have traditionally been engaged in O-isotope studies. The VPDB scale is used in low-temperature studies of carbonate. PDB is a Cretaceous belemnite from the Pee Dee Formation and was the laboratory working standard used at the university of Chicago in the early 1950's when the paleotemperature scale was developed. The original supply of this standard has long been exhausted, therefore secondary standards have been introduced (see Table 2.5), whose isotopic compositions have been calibrated relative to PDB. All other oxygen isotope analyses (waters, silicates, phosphates, sulfates, high-temperature carbonates) are given relative to SMOW.

Table 2.5 δ^{18}O-values of commonly used O-isotope standards

Standard	Material	PDB scale	VSMOW scale
NBS-19	Marble	−2.20	(28.64)
NBS-20	Limestone	−4.14	(26.64)
NBS-18	Carbonatite	−23.00	(7.20)
NBS-28	Quartz	(−20.67)	9.60
NBS-30	Biotite	(−25.30)	5.10
GISP	Water	(−53.99)	−24.75
SLAP	Water	(−83.82)	−55.50

The conversion equations of δ^8O(PDB) versus δ^{18}O(VSMOW) and vice versa (Coplen et al. 1983) are:

$$\delta^{18}\mathrm{O}\,(\mathrm{VSMOW}) = 1.03091\delta^{18}\mathrm{O}\,(\mathrm{PDB}) + 30.91$$

and

$$\delta^{18}\mathrm{O}\,(\mathrm{PDB}) = 0.97002\delta^{18}\mathrm{O}\,(\mathrm{VSMOW}) - 29.98$$

Table 2.5 gives the δ^{18}O-values of commonly used oxygen isotope standards on both scales (parenthesis denote calculated values).

2.6.3 Fractionation Processes

Out of the numerous possibilities to fractionate oxygen isotopes in nature, the following are of special significance.

Knowledge of the oxygen isotope fractionation between liquid water and water vapor is essential for the interpretation of the isotope composition of different water types. Fractionation factors experimentally determined in the temperature range from 0 to 350°C have been summarized by Horita and Wesolowski (1994). This is shown in Fig. 2.13.

Addition of salts to water also affects isotope fractionations. The presence of ionic salts in solution changes the local structure of water around dissolved ions. Taube (1954) first demonstrated that the $^{18}O/^{16}O$ ratio of CO_2 equilibrated with pure H_2O decreased upon the addition of $MgCl_2$, $AlCl_3$ and HCl, remained more or less unchanged for NaCl, and increased upon the addition of $CaCl_2$. The changes vary roughly linearly with the molality of the solute (see Fig. 2.14).

To explain this different fractionation behavior, Taube (1954) postulated different isotope effects between the isotopic properties of water in the hydration sphere of the cation and the remaining bulk water. The hydration sphere is highly ordered, whereas the outer layer is poorly ordered. The relative sizes of the two layers are dependent upon the magnitude of the electric field around the dissolved ions. The strength of the interaction between the dissolved ion and water molecules is also dependent upon the atomic mass of the atom to which the ion is bonded.

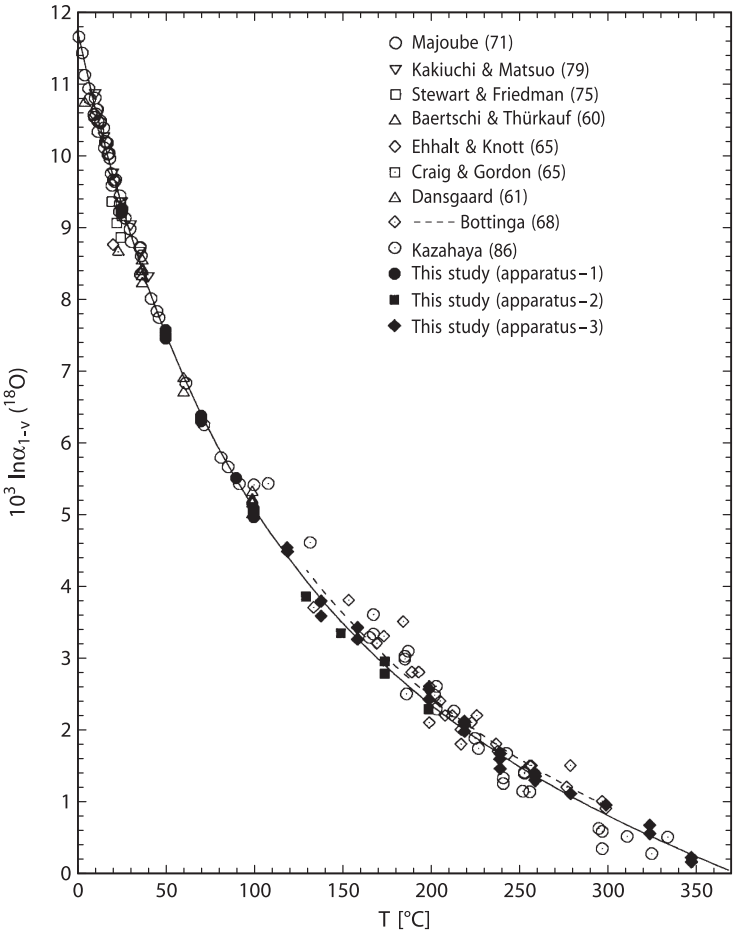

Fig. 2.13 Oxygen isotope fractionation factors between liquid water and water vapour in the temperature range 0 – 350°C (after Horita and Wesolowski 1994)

O'Neil and Truesdell (1991) have introduced the concept of "structure-making" and "structure-breaking" solutes: structure makers yield more positive isotope fractionations relative to pure water whereas structure breakers produce negative isotope fractionations. Any solute that results in a positive isotope fractionation is one that causes the solution to be more structured as is the case for ice structure, when compared to solutes that lead to less structured forms, in which cation – H_2O bonds are weaker than H_2O – H_2O bonds.

As already treated in the "hydrogen" section, isotope fractionations, the hydration of ions may play a significant role in hydrothermal solutions and volcanic vapors (Driesner and Seward 2000). Such isotope salt effects may change the oxygen isotope fractionation between water and other phases by several permil.

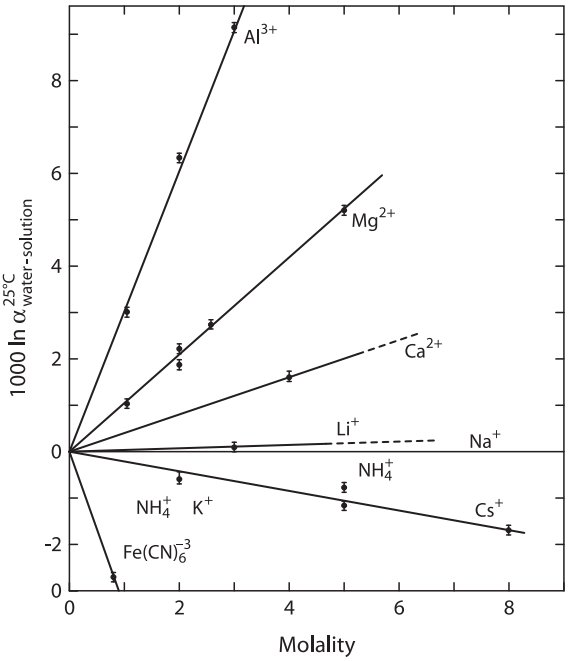

Fig. 2.14 Oxygen isotope fractionations between pure water and solutions of various ions (after O'Neil and Truesdell 1991)

Table 2.6 Experimentally determined oxygen isotope fractionation factors relative to water for the aqueous system $CO_2 - H_2O$ between 5 and 40°C according to $10^3\ \ln\alpha = A(10^6/T^{-2}) + B$ (Beck et al. 2005)

	A	B
HCO_3^-	2.59	1.89
CO_3^{2-}	2.39	−2.70
$CO_{2(aq)}$	2.52	12.12

Of equal importance is the oxygen isotope fractionation in the CO_2 – H_2O system. Early work concentrated on the oxygen isotope partitioning between gaseous CO_2 and water (Brennikmeijer et al. 1983). More recent work by Usdowski and Hoefs (1993), Beck et al. (2005) and Zeebe (2007) have determined the oxygen isotope composition of the individual carbonate species that are isotopically different at room temperature. Table 2.6 summarizes the equations for the temperature dependence between 5 and 40°C (Beck et al. 2005).

The fractionation (1,000 ln α) between dissolved CO_2 and water at 25°C is 41.6. dropping to 24.7 at high pH when CO_3^{2-} is the dominant species (see Fig. 2.15).

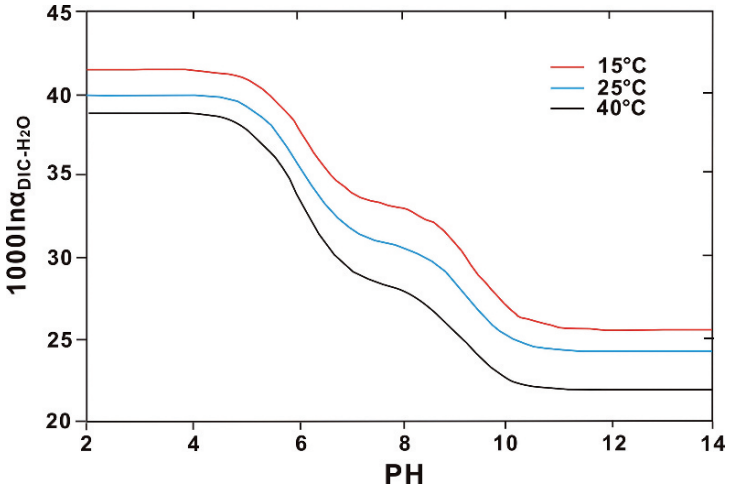

Fig. 2.15 Oxygen isotope fractionations between dissolved inorganic carbon (DIC) and water as a function of pH and temperatures (after Beck et al. 2005)

Table 2.7 Sequence of minerals in the order (bottom to top) of their increasing tendency to concentrate ^{18}O

Quartz
Dolomite
K-feldspar, albite
Calcite
Na-rich plagioclase
Ca-rich plagioclase
Muscovite, paragonite, kyanite, glaucophane
Orthopyroxene, biotite
Clinopyroxene, hornblende, garnet, zircon
Olivine
Ilmenite
Magnetite, hematite

The pH dependence of the oxygen isotope composition in the carbonate-water system has important implications in the derivation of oxygen isotope temperatures.

The oxygen isotope composition of a rock depends on the ^{18}O contents of the constituent minerals and the mineral proportions. Garlick (1966) and Taylor (1968) arranged coexisting minerals according to their relative tendencies to concentrate ^{18}O. The list given in Table 2.7 has been augmented by data from Kohn and Valley (1998a, b, c).

This order of decreasing ^{18}O-contents has been explained in terms of the bond-type and strength in the crystal structure. Semi-empirical bond-type calculations have been developed by Garlick (1966) and Savin and Lee (1988) by assuming that oxygen in a chemical bond has similar isotopic behavior regardless of the mineral in which the bond is located. This approach is useful for estimating fractionation

factors. The accuracy of this approach is limited due to the assumption that the isotope fractionation depends only upon the atoms to which oxygen is bonded and not upon the structure of the mineral, which is not strictly true. By using an electrostatic approximation to bond strength and taking into account cation mass Schütze (1980) developed an increment method for calculations of oxygen isotope fractionations in silicates, which has been modified and refined by Zheng (1991, 1993a, b). Kohn and Valley (1998a, b) determined empirically the effects of cation substitutions in complex minerals such as amphiboles and garnets spanning a large range in chemical compositions. Although isotope effects of cation exchange are generally less than 1‰ at $T > 500°C$, they increase considerably at lower temperatures. Thus use of amphiboles and garnets for thermometry requires exact knowledge of chemical compositions.

On the basis of these systematic tendencies of ^{18}O enrichment found in nature, significant temperature information can be obtained up to temperatures of 1,000°C, and even higher, if calibration curves can be worked out for the various mineral pairs. The published literature contains many calibrations of oxygen isotope geothermometers, most are determined by laboratory experiments, although some are based on theoretical calculations.

Although much effort has been directed toward the experimental determination of oxygen isotope fractionation factors in mineral- water systems, the use of water as an oxygen isotope exchange medium has several disadvantages. Some minerals become unstable in contact with water at elevated temperatures and pressures, leading to melting, breakdown and hydration reactions. Incongruent solubility and ill-defined quench products may introduce additional uncertainties. Most of the disadvantages of water can be circumvented by using calcite as an exchange medium (Clayton et al. 1989; Chiba et al. 1989). Mineral-mineral fractionations – determined by these authors (Table 2.8) – give internally consistent geothermometric information that generally is in accord with independent estimates, such as the theoretical calibrations of Kieffer (1982).

A more recent summary has been given by Chacko et al. (2001) (see Fig. 2.16).

Many isotopic fractionations between low-temperature minerals and water have been estimated by assuming that their temperature of formation and the isotopic composition of the water in which they formed (for example, ocean water) are well known. This is sometimes the only approach available in cases in which the rates of

Table 2.8 Coefficients A for silicate – pair fractionations ($1{,}000 \ln\alpha \, X - Y = A/T^2 \, 10^6$ (after Chiba et al. 1989)

	Cc	Ab	An	Di	Fo	Mt
Qtz	0.38	0.94	1.99	2.75	3.67	6.29
Cc		0.56	1.61	2.37	3.29	5.91
Ab			1.05	1.81	2.73	5.35
An				0.76	1.68	4.30
Di					0.92	3.54
Fo						2.62

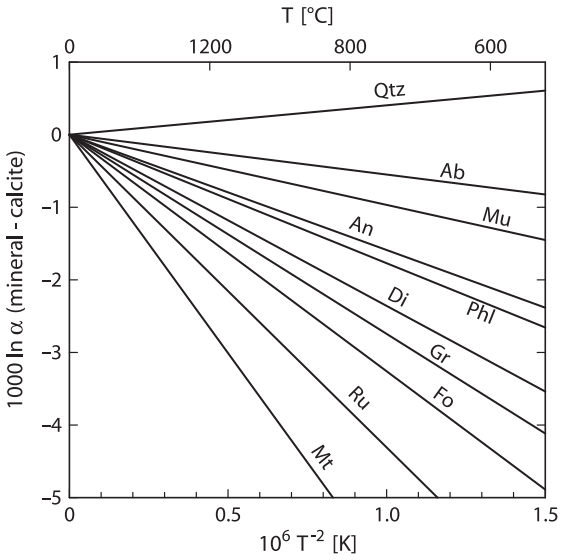

Fig. 2.16 Oxygen isotope fractionations between various minerals and calcite (after Chacko et al. 2001)

isotope exchange reactions are slow and in which minerals cannot be synthesized in the laboratory at appropriate temperatures.

2.6.4 Fluid-Rock Interactions

Oxygen isotope ratio analysis provides a powerful tool for the study of water/rock interaction. The geochemical effect of such an interaction between water and rock or mineral is a shift of the oxygen isotope ratios of the rock and/or the water away from their initial values, given that their compositions are not in equilibrium.

Detailed studies of the kinetics and mechanisms of oxygen isotope exchange between minerals and fluids show that there are three possible exchange mechanisms (Matthews et al. 1983b, c; Giletti 1985).

1. *Solution-precipitation*. During a solution-precipitation process, larger grains grow at the expense of smaller grains. Smaller grains dissolve and recrystallize on the surface of larger grains which decreases the overall surface area and lowers the total free energy of the system. Isotopic exchange with the fluid occurs while material is in solution.
2. *Chemical reaction*. The chemical activity of one component of both fluid and solid is so different in the two phases that a chemical reaction occurs. The breakdown of a finite portion of the original crystal and the formation of new crystals is implied. The new crystals would form at or near isotopic equilibrium with the fluid.

3. *Diffusion*. During a diffusion process isotopic exchange takes place at the interface between the crystal and the fluid with little or no change in morphology of the reactant grains. The driving force is the random thermal motion of the atoms within a concentration or activity gradient.

In the presence of a fluid phase, coupled dissolution – reprecipitation is known to be a much more effective process than diffusion. This has been first demonstrated experimentally by O'Neil and Taylor (1967) and later re-emphasized by Cole (2000) and Fiebig and Hoefs (2002).

The first attempts to quantify isotope exchange processes between water and rocks were made by Taylor (1974). By using a simple closed-system material balance equation these authors were able to calculate cumulative fluid/rock ratios.

$$W/R = \frac{\delta_{\mathrm{rock_f}} - \delta_{\mathrm{rock_i}}}{\delta_{\mathrm{H_2O}} - (\delta_{\mathrm{rock_f}} - \Delta)}, \tag{2.8}$$

where $\Delta = \delta_{\mathrm{rock}} f - \delta_{\mathrm{H_2O}} f$.

Their equation requires adequate knowledge of both the initial (i) and final (f) isotopic states of the system and describes the interaction of one finite volume of rock with a fluid. The utility of such "zero-dimensional" equations has been questioned by Baumgartner and Rumble (1988), Blattner and Lassey (1989), Nabelek (1991), Bowman et al. (1994) and others. Only under special conditions do one-box models yield information on the amount of fluid that actually flowed through the rocks. If the rock and the infiltrating fluid were not far out of isotopic equilibrium, then the calculated fluid/rock ratios rapidly approach infinity. Therefore, the equations are sensitive only to small fluid/rock ratios. Nevertheless, the equations can constrain fluid sources. More sophisticated one-dimensional models like the chromatographic or continuum mechanics models (i.e. Baumgartner and Rumble 1988) are physically more plausible and can describe how the isotopic composition of the rock and of the fluid change with time and space. The mathematical models are complex and are based on partial differential equations that must be solved numerically. Examples of fluid–rock interactions in contact metamorphic environments have been presented by Nabelek and Labotka 1993, Bowman et al. 1994 and application to contrasting lithologies by Bickle and Baker (1990) and Cartwright and Valley (1991).

Criss et al. (1987) and Gregory et al. (1989) developed a theoretical framework that describes the kinetics of oxygen isotope exchange between minerals and coexisting fluids. Figure 2.17 shows characteristic patterns in δ–δ plots for some hydrothermally altered granitic and gabbroic rocks. The $^{18}O/^{16}O$ arrays displayed on Fig. 2.17 cut across the 45° equilibrium lines at a steep angle as a result of the much faster oxygen isotope exchange of feldspar compared to that of quartz and pyroxene. If a low-^{18}O fluid such as meteoric or ocean water is involved in the exchange process, the slopes of the disequilibrium arrays can be regarded as "isochrons" where, with continued exchange through time the slopes become less steep and approach the 45° equilibrium line. These "times" represent the duration of a particular hydrothermal event.

Figure 2.18 summarizes the naturally observed oxygen isotope variations in important geological reservoirs.

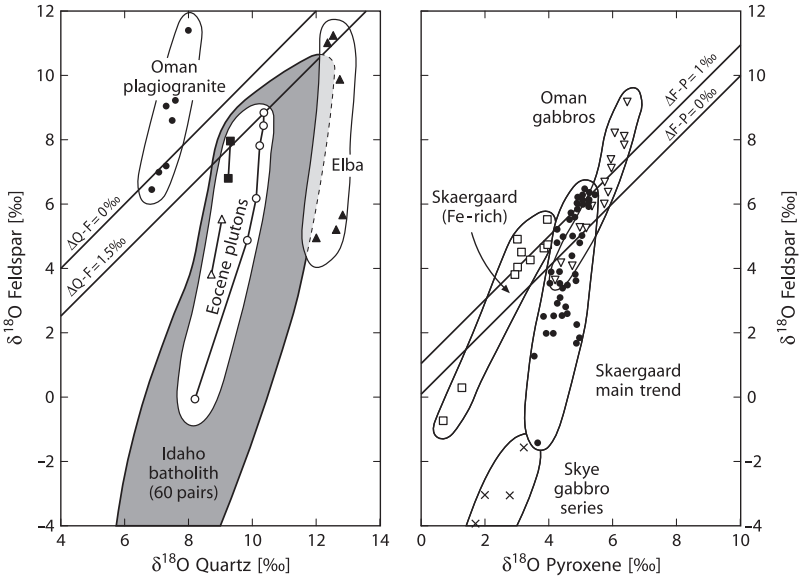

Fig. 2.17 $\delta^{18}O$ (feldspar) vs $\delta^{18}O$ (quartz) and vs $\delta^{18}O$ (pyroxene) plots of disequilibrium mineral pair arrays in granitic and gabbroic rocks. The arrays indicate open-system conditions from circulation of hydrothermal fluids (after Gregory et al. 1989)

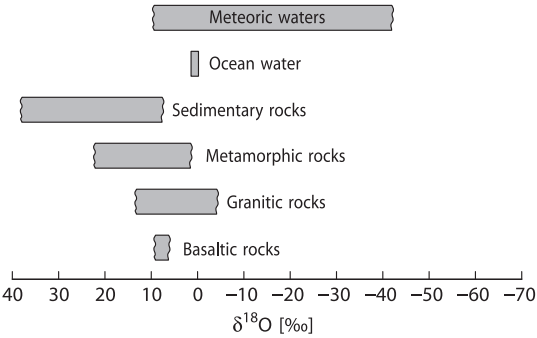

Fig. 2.18 $\delta^{18}O$ values of important geological reservoirs

2.7 Magnesium

Magnesium is composed of three isotopes (Rosman and Taylor 1998)

^{24}Mg 78.99%

^{25}Mg 10.00%

^{26}Mg 11.01%

Early investigations on Mg isotope variations have been limited by an uncertainty of 1 to 2‰. Catanzaro and Murphy (1966) for instance concluded that terrestrial Mg isotope variations are restricted to a few ‰. The introduction of multicollector-inductively coupled-plasma mass spectrometry (MC-ICP-MS) increased the precision by one order of magnitude and has initiated a new search of natural isotope variations (Galy et al. 2001, 2002). These authors obtained an overall 4‰ variation in δ^{26}Mg.

The oxidation state of magnesium always is two, thus it might be expected that the range in isotope composition is small. Mg is soluble and mobile during weathering, which, on the other hand, might initiate small fractionations during carbonate precipitation and clay formation. And indeed by investigating Mg isotope fractionation between speleothems and associated drip waters Galy et al. (2002) observed a characteristic difference in both phases, which might indicate equilibrium conditions. They further observed a 2–3‰ enrichment in dolomites relative to limestones, suggesting a mineralogical control on the isotope composition of carbonates.

Because of its relatively long mean residence time, ocean water has a constant isotope composition. Corals are about 1‰ and foraminifera are about 4.5‰ lighter than ocean water. Thus significant Mg isotope fractionations occur during biomineralization of carbonate secreting organisms which is larger than for Ca isotopes (see Section 2.11).

Tipper et al. (2006) have measured the Mg isotope composition of rivers. They observed a total variation in ^{26}Mg of 2.5‰. The lithology in the drainage area seems to be of limited significance, a major part of the variability has to be attributed to fractionations in the weathering environment.

One of the advantages of the MC-ICPMS technique compared to the SIMS technique is the ability to measure $^{25}Mg/^{24}Mg$ and $^{26}Mg/^{24}Mg$ ratios independently many times smaller than the magnitude of the natural variations. By doing this Young and Galy (2004) demonstrated that the relationship between $^{25}Mg/^{24}Mg$ and $^{26}Mg/^{24}Mg$ are diagnostic of kinetic vs equilibrium fractionations: for equilibrium processes the slope on a three-isotope diagram should be close to 0.521, for kinetic processes the slope should be 0.511. Evidence for equilibrium fractionation has been found for low-Mg calcite speleothems (Galy et al. 2002). Recently, however, Buhl et al. (2007) argued that a pure equilibrium mass fractionation cannot explain the Mg isotope data from speleothems. On the other hand biologically mediated precipitates such as foraminifera (Chang et al. 2004) and dolomites of bacterial origin (Carder et al. 2005) have a clear kinetic signature.

Galy et al. (2001) suggested that the mantle should have a homogeneous Mg isotope composition. Pearson et al. (2006), however, demonstrated that olivines from mantle xenoliths have a heterogeneous compositions with a δ^{26}Mg range of about 4‰. These authors suggested that the differences are due to diffusion-related metasomatic processes.

2.8 Silicon

Silicon has three stable isotopes with the following abundances (Rosman and Taylor 1998):

$$^{28}\text{Si } 92.23\%$$

$$^{29}\text{Si } 4.68\%$$

$$^{30}\text{Si } 3.09\%$$

Because of its high abundance on Earth, silicon is in principle a very interesting element to study for isotope variations. However, because there is no redox reaction for silicon (silicon is always bound to oxygen), only small isotope fractionations are to be expected in nature. Silicic acid, on the other hand, is an important nutrient in the ocean that is required for the growth of mainly diatoms and radiolaria. The silicon incorporation into siliceous organisms is associated with a Si isotope fractionation, because ^{28}Si is prefrentially removed as the organisms form biogenic silica. Early investigations by Douthitt (1982) and more recent ones by Ding et al. (1996) observed a total range of δ^{30}Si values in the order of 6‰. This range has extended to about 12‰ with the lowest δ^{30}Si value of -5.7‰ in siliceous cements (Basile-Doelsch et al. 2005) and the highest of $+6.1$‰ for rice grains (Ding et al. 2005).

Silicon isotope ratios have been generally measured by fluorination (Douthitt 1982; Ding et al. 1996). However, the method is time consuming and potentially hazardous, therefore, more recently MC-ICP-MS techniques have been introduced (Cardinal et al. 2003; Engstrom et al. 2006). Determinations with SIMS have been carried out by Robert and Chaussidon (2006). Very recently, Chmeleff et al. (2008) have shown that a UV-femtosecond laser ablation system coupled with MC-ICP-MS gives δ^{29}Si and δ^{30}Si-values with very high precision.

Igneous rocks have a rather uniform isotope composition with a rather constant δ^{30}Si-value of -0.3‰. In igneous rocks and minerals δ^{30}Si values exhibit small, but systematic variations with ^{30}Si enrichment increasing with the silicon contents of igneous rocks and minerals. The order of ^{30}Si enrichment is quartz, feldspar, muscovite and biotite, which is consistent with the order of ^{18}O enrichment. Thus felsic igneous rocks are slightly heavier than mafic igneous rocks.

Relative to igneous rocks rivers are isotopically enriched in ^{30}Si (De la Rocha et al. 2000a; Ding et al. 2004; Ziegler et al. 2005a, b; Basile-Doelsch et al. 2005; Reynolds et al. 2006; Georg et al. 2006). The enrichment in ^{30}Si is obviously produced during weathering which preferentially releases ^{28}Si into solution, followed by even stronger preferential incorporation of ^{28}Si during secondary mineral formation. Thus soil-clay mineral formation is responsible for high δ^{30}Si values of continental surface waters and ocean water. For the Yangtze river as an example, Ding et al. (2004) measured a δ^{30}Si range from 0.7 to 3.4‰, whereas the suspended matter has a more constant composition from 0 to -0.7‰.

In ocean water distinct ^{30}Si gradients with depth exist (Georg et al. 2006): surface waters are relatively rich in ^{30}Si whereas deep waters are more depleted in ^{30}Si, which is due to a silicon isotope fractionation during the uptake by organisms

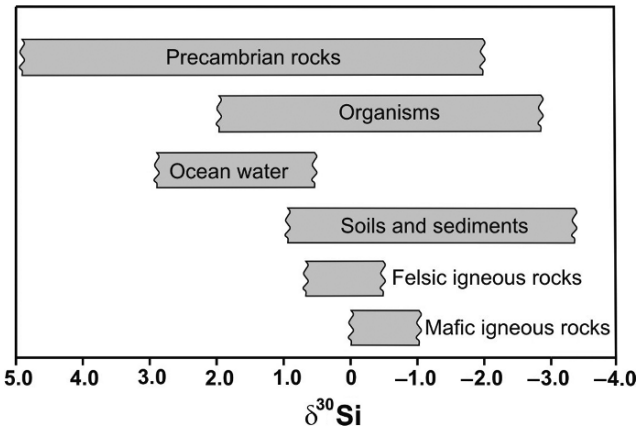

Fig. 2.19 δ^{30}Si ranges of various geologic reservoirs

in oceanic surface waters. De la Rocha et al. (1997, 1998) observed a 1‰ fractionation between dissolved and biogenic silica during opal formation by marine diatoms that does not vary with temperature nor among three species of diatoms. An increase in opal formation by diatoms results in more positive δ^{30}Si-values, whereas a decrease results in more negative δ-values. In this manner variations in ^{30}Si contents of diatoms may provide information on changes of oceanic silicon cycling (De la Rocha et al. 1998). Marine sponges fractionate silicon isotopes to a degree that is three times larger than observed by marine diatoms (De La Rocha 2003). Figure 2.19 summarizes natural silicon isotope variations.

A wide range of δ^{30}Si values from -0.8 to $+5.0$‰ have been reported for Precambrian cherts (Robert and Chaussidon 2006), much larger than for Phanerozoic cherts. These authors observed a positive correlation of δ^{18}O with δ^{30}Si values, which they interpreted as reflecting temperature changes in the ocean from about 70°C 3.5 Ga to about 20°C 0.8 Ga years ago.

2.9 Sulfur

Sulfur has four stable isotopes with the following abundances (Rosman and Taylor 1998)

^{32}S : 94.93%
^{33}S : 0.76%
^{34}S : 4.29%
^{36}S : 0.02%

Sulfur is present in nearly all natural environments. It may be a major component in ore deposits, where sulfur is the dominant nonmetal, and as sulfates in evaporites. It occurs as a minor component in igneous and metamorphic rocks, throughout

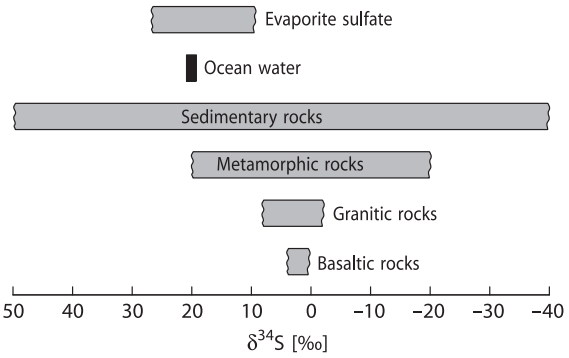

Fig. 2.20 δ^{34}S-values of some geologically important sulfur reservoirs

the biosphere in organic substances, in marine waters and sediments as both sulfide and sulfate. These occurrences cover the whole temperature range of geological interest. Thus, it is quite clear that sulfur is of special interest in stable isotope geochemistry.

Thode et al. (1949) and Trofimov (1949) were the first to observe wide variations in the abundances of sulfur isotopes. Variations on the order of 180‰ have been documented with the "heaviest" sulfates having δ^{34}S-values of greater than +120‰ (Hoefs, unpublished results), and the "lightest" sulfides having δ^{34}S-values of around −65‰. Some of the naturally occurring S-isotope variations are summarized in Fig. 2.20. Reviews of the isotope geochemistry of sulfur have been published by Nielsen (1979), Ohmoto and Rye (1979), Ohmoto (1986), Ohmoto and Goldhaber (1997), Seal et al. (2000), Canfield (2001a) and Seal (2006).

For many years the reference standard commonly referred to is sulfur from troilite of the Canyon Diablo iron meteorite (CDT). As Beaudoin et al. (1994) have pointed out, CDT is not homogeneous and may display variations in ^{34}S up to 0.4‰. Therefore a new reference scale, Vienna-CDT or V-CDT has been introduced by an advisory committee of IAEA in 1993, recommending an artificially prepared Ag_2S (IAEA-S-1) with a $\delta^{34}S_{VCDT}$ of −0.3‰ as the new international standard reference material.

2.9.1 Preparation Techniques

Chemical preparation of the various sulfur compounds for isotopic analysis have been discussed by Rafter (1957), Robinson and Kusakabe (1975) among others. The gas generally used for mass-spectrometric measurement is SO_2, although Puchelt et al. (1971) and Rees (1978) describe a method using SF_6 which has some distinct advantages: it has no mass spectrometer memory effect and because fluorine is monoisotopic, no corrections of the raw data of measured isotope ratios are necessary. Comparison of δ^{34}S-values obtained using the conventional SO_2 and the laser SF_6 technique has raised serious questions about the reliability of the SO_2

correction for oxygen isobaric interferences (Beaudoin and Taylor 1994). Therefore the SF_6 technique has been revitalized (Hu et al. 2003), demonstrating that SF_6 is an ideal gas for measuring $^{33}S/^{32}S$, $^{34}S/^{32}S$ and $^{36}S/^{32}S$ ratios.

For SO_2, pure sulfides have to be reacted with an oxidizing agent, like CuO, Cu_2O, V_2O_5 or O_2. It is important to minimize the production of sulfur trioxide since there is an isotope fractionation between SO_2 and SO_3. Special chemical treatment is necessary if pyrite is to be analyzed separately from other sulfides.

For the extraction of sulfates and total sulfur a suitable acid and reducing agent, such as tin(II)–phosphoric acid (the "Kiba" solution of Sasaki et al. 1979) is needed. The direct thermal reduction of sulfate to SO_2 has been described by Holt and Engelkemeier (1970) and Coleman and Moore (1978). Ueda and Sakai (1984) described a method in which sulfate and sulfide disseminated in rocks are converted to SO_2 and H_2S simultaneously, but analyzed separately. With the introduction of on-line combustion methods (Giesemann et al. 1994), multistep off-line preparations can be reduced to one single preparation step, namely the combustion in an elemental analyzer. Sample preparations have become less dependent on possibly fractionating wet-chemical extraction steps and less time-consuming.

Microanalytical techniques such as laser microprobe (Kelley and Fallick 1990; Crowe et al. 1990; Hu et al. 2003; Ono et al. 2006) and ion microprobe (Chaussidon et al. 1987, 1989; Eldridge et al. 1988, 1993) have become promising tools for determining sulfur isotope ratios. These techniques have several advantages over conventional techniques such as high spatial resolution and the capability for "in-situ" spot analysis. Sulfur isotopes are fractionated during ion or laser bombardment, but fractionation effects are mineral specific and reproducible.

2.9.2 Fractionation Mechanisms

Two types of fractionation mechanisms are responsible for the naturally occurring sulfur isotope variations:

1. Kinetic isotope effects during microbial processes. Micro-organisms have long been known to fractionate isotopes during their sulfur metabolism, particularly during dissimilatory sulfate reduction, which produces the largest fractionations in the sulfur cycle
2. Various chemical exchange reactions between both sulfate and sulfides and the different sulfides themselves

2.9.2.1 Dissimilatory Sulfate Reduction

Dissimilatory sulfate reduction is conducted by a large group of organisms (over 100 species are known so far, Canfield 2001a), that gain energy for their growth by reducing sulfate while oxidizing organic carbon (or H_2). Sulfate reducers are widely

distributed in anoxic environments. They can tolerate temperatures from −1.5 to over 100°C and salinities from fresh water to brines.

Since the early work with living cultures (Harrison and Thode 1957a, b; Kaplan and Rittenberg 1964) it is well known that sulfate reducing bacteria produce ^{32}S-depleted sulfide. Despite decades of intense research the factors that determine the magnitude of sulfur isotope fractionation during bacterial sulfate reduction are still under debate. The magnitude of isotope fractionation depends on the rate of sulfate reduction with the highest fractionation at low rates and the lowest fractionation at high rates. Kaplan and Rittenberg (1964) and Habicht and Canfield (1997) suggested that fractionations depend on the specific rate (cell^{-1} time^{-1}) and not so much on absolute rates (volume^{-1} time $^{-1}$). What is clear, however, is that the rates of sulfate reduction are controlled by the availabilty of dissolved organic compounds. One parameter which remains unclear is sulfate concentration. While for instance Boudreau and Westrich (1984) argued that the concentration of sulfate becomes important at rather low concentrations (less than 15% of the seawater value), Canfield (2001b) observed no influence of isotope fractionations on sulfate concentrations for natural populations. Another parameter, that has been thought to be important is temperature insofar as it regulates in natural populations the sulfate-reducing community (Brüchert et al. 2001). Furthermore differences in fractionation with temperature relate to differences in the specific temperature response to internal enzyme kinetics as well as cellular properties and corresponding exchange rates of sulfate in and out of the cell. Canfield et al. (2006) found in contrast to earlier belief high fractionations in the low and high temperature range and the lowest fractionations in the intermediate temperature range.

The reaction chain during anaerobic sulfate reduction has been described in detail by Goldhaber and Kaplan (1974). In general, the rate-limiting step is the breaking of the first S-O bond, namely the reduction of sulfate to sulfite. Pure cultures of sulfate reducing bacteria produce sulfide depleted in ^{34}S by 4–46‰ (Harrison and Thode 1957a, b; Kemp and Thode 1968; McCready et al. 1974; McCready 1975; Bolliger et al. 2001). More recently, sulfur isotope fractionations have been determined from natural populations covering a wide spectrum of environments (from rapidly metabolizing microbial mats to slowly metabolizing coastal sediments; Habicht and Canfield 1997, 2001; Canfield 2001a).

In marine coastal sediments typically 90% of the sulfide produced during sulfate reduction is reoxidized (Canfield and Teske 1996). The pathways of sulfide oxidation are poorly known but include oxidation to sulfate, elemental sulfur and other intermediate compounds. Systematic studies of sulfur isotope fractionations during sulfide oxidation are still needed, the few available data suggest that biologically mediated oxidation of sulfide to elemental sulfur and sulfate lead to only minimal isotope fractionation.

Naturally occurring sulfides in sediments and euxinic waters are commonly depleted in ^{34}S by up to 70‰ (Jørgensen et al. 2004), far beyond the apparent capabilities of sulfate reducing bacteria. As has been shown above, most of the sulfide produced by sulfate reduction in sediments is reoxidized, often via compounds in which sulfur has intermediate oxidation states that do not accumulate, but

are readily transformed and which can disproportionated by bactertia. Canfield and Thamdrup (1994) suggested that through a repeated cycle of sulfide oxidation to elemental sulfur and subsequent disproportionation, bacteria can generate the large ^{34}S depletion typical of many marine sulfides. Thus the oxidative part of the sulfur cycle may create circumstances by which sulfides become more depleted in ^{34}S than would be possible with sulfate reducing bacteria alone.

However, in contrast to microbiological experiments and near-surface studies, modelling of sulfate reduction in pore water profiles with in the ODP program has demonstrated that natural populations are able to fractionate S-isotopes by up to more than 70‰ (Wortmann et al. 2001; Rudnicki et al. 2001). Brunner et al. (2005) suggested that S isotope fractionations of around –70‰ might occur under hypersulfidic, substrate limited, but nonlimited supply of sulfate, conditions without the need of alternate pathways involving the oxidative sulfur cycle.

Another factor that is of great importance for the observed sulfur isotope variations of natural sulfides is whether sulfate reduction takes place in an open or closed system. An "open" system has an infinite reservoir of sulfate in which continuous removal from the source produces no detectable loss of material. Typical examples are the Black Sea and local oceanic deeps. In such cases, H_2S is extremely depleted in ^{34}S while consumption and change in ^{34}S remain negligible for the sulfate. In a "closed" system, the preferential loss of the lighter isotope from the reservoir has a feedback on the isotopic composition of the unreacted source material. The changes in the ^{34}S-content of residual sulfate and of the H_2S are modeled in Fig. 2.21, which shows that $\delta^{34}S$-values of the residual sulfate steadily increase with sulfate consumption (a linear relationship on the log-normal plot). The curve for the derivative H_2S is parallel to the sulfate curve at a distance which depends on the magnitude of

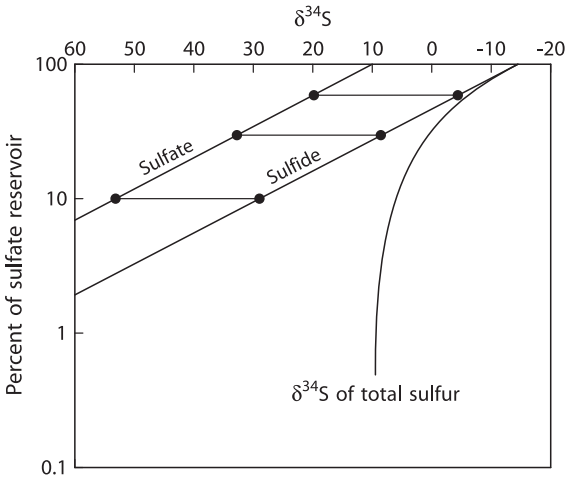

Fig. 2.21 Rayleigh plot for sulphur isotopic fractionations during the reduction of sulfate in a closed system. Assumed fractionation factor. 1.025, assumed starting composition of initial sulfate: +10‰

the fractionation factor. As shown in Fig. 2.21, H_2S may become isotopically heavier than the original sulfate when about 2/3 of the reservoir has been consumed. The $\delta^{34}S$-curve for "total" sulfide asymptotically approaches the initial value of the original sulfate. It should be noted, however, that apparent "closed-system" behavior of covarying sulfate and sulfide $\delta^{34}S$-values might be also explained by "open-system" differential diffusion of the different sulfur isotope species (Jørgensen et al. 2004).

In recent years additional informations on sulfur isotope fractionation mechanisms have been obtained from the analysis of the additional isotopes ^{33}S and ^{36}S (Farquhar et al. 2003; Johnston et al. 2005; Ono et al. 2006, 2007). For long it was thought $\delta^{33}S$ and $\delta^{36}S$ values carry no additional information, because sulfur isotope fractionations follow strictly mass-dependent fractionation laws. By studying all sulfur isotopes with very high precision these authors could demonstrate that bacterial sulfate reduction follows a mass-dependent relationship that is slightly different from that expected by equilibrium fractionations. On plots $\Delta^{33}S$ vs $\delta^{34}S$ mixing of two sulfur reservoirs is non-linear in these coordinates (Young et al. 2002). As a result samples with the same $\delta^{34}S$-value can have different $\Delta^{33}S$ and $\Delta^{36}S$ values. This opens the possibility to distinguish between different fractionation mechanisms and biosynthetic pathways (Ono et al. 2006, 2007). For instance, bacterial sulfate reduction shows slightly different fractionation relationships compared to sulfur disproportionation reactions (Johnston et al. 2005). Thus multiple sulfur isotope analyses might have great potential in identifying the presence or absence of specific metabolisms in modern environment or to have a fingerprint when a particular sulfur metabolism shows up in the geologic record.

Finally it should be mentioned that sulfate is labeled with two biogeochemical isotope systems, sulfur and oxygen. Coupled isotope fractionations of both sulfur and oxygen isotopes have been observed in experiments (Mizutani and Rafter 1973; Fritz et al. 1989; Böttcher et al. 2001) and in naturally occurring sediments (Ku et al. 1999; Aharon and Fu 2000; Wortmann et al. 2001). Brunner et al. (2005) argued that characteristic $\delta^{34}S$-$\delta^{18}O$ fractionation slopes do not exist, but depend on cell-specific reduction rates and oxygen isotope exchange rates. Despite the extremely slow oxygen isotope exchange of sulfate with ambient water, $\delta^{18}O$ in sulfate obviously depend on the $\delta^{18}O$ of water via an exchange of sulfite with water.

2.9.2.2 Thermochemical Reduction of Sulfate

In contrast to bacterial reduction thermochemical sulfate reduction is an abiotic process with sulfate being reduced to sulfide under the influence of heat rather than bacteria (Trudinger et al. 1985; Krouse et al. 1988). The crucial question, which has been the subject of a controversial debate, is whether thermochemical sulfate reduction can proceed at temperatures as low as about 100°C, just above the limit of microbiological reduction (Trudinger et al. 1985). There is increasing evidence from natural occurrences that the reduction of aqueous sulfates by organic compounds can occur at temperatures as low as 100°C, given enough time for the reduction to proceed (Krouse et al. 1988; Machel et al. 1995). S isotope fractionations during

thermochemical reduction generally should be smaller than during bacterial sulfate reduction. However, experiments by Kiyosu and Krouse (1990) have indicated S-isotope fractionations of 10 to 20‰ in the temperature range of 200 to 100°C.

To summarize, bacterial sulfate reduction is characterized by large and heterogeneous ^{34}S-depletions over very small spatial scales, whereas thermogenic sulfate reduction leads to smaller and "more homogeneous" ^{34}S-depletions.

2.9.2.3 Isotope Exchange Reactions

There have been a number of theoretical and experimental determinations of sulfur isotope fractionations between coexisting sulfide phases as a function of temperature. Theoretical studies of fractionations among sulfides have been undertaken by Sakai (1968) and Bachinski (1969), who reported the reduced partition function ratios and the bond strength of sulfide minerals and described the relationship of these parameters to isotope fractionation. In a manner similar to that for oxygen in silicates, there is a relative ordering of ^{34}S-enrichment among coexisting sulfide minerals (Table 2.9). Considering the three most common sulfides (pyrite, sphalerite and galena) under conditions of isotope equilibrium pyrite is always the most ^{34}S enriched mineral and galena the most ^{34}S depleted, sphalerite displays an intermediate enrichment in ^{34}S.

The experimental determinations of sulfur isotope fractionations between various sulfides do not exhibit good agreement. The most suitable mineral pair for temperature determination is the sphalerite–galena pair. Rye (1974) has argued that the Czamanske and Rye (1974) fractionation curve gives the best agreement with filling temperatures of fluid inclusions over the temperature range from 370 to 125°C. By contrast, pyrite – galena pairs do not appear to be suitable for a temperature determination, because pyrite tends to precipitate over larger intervals of ore deposition than galena, implying that these two minerals may frequently not be contemporaneous. The equilibrium isotope fractionations for other sulfide pairs are generally so small that they are not useful as geothermometers. Ohmoto and Rye (1979) critically examined the available experimental data and presented a

Table 2.9 Equilibrium isotope fractionation factors of sulfides with respect to H_2S. The temperature dependence is given by A/T^2 (after Ohmoto and Rye 1979)

Mineral	Chemical composition	A
Pyrite	FeS_2	0.40
Sphalerite	ZnS	0.10
Pyrrhotite	FeS	0.10
Chalcopyrite	$CuFeS_2$	−0.05
Covellite	CuS	−0.40
Galena	PbS	−0.63
Chalcosite	Cu_2S	−0.75
Argentite	Ag_2S	−0.80

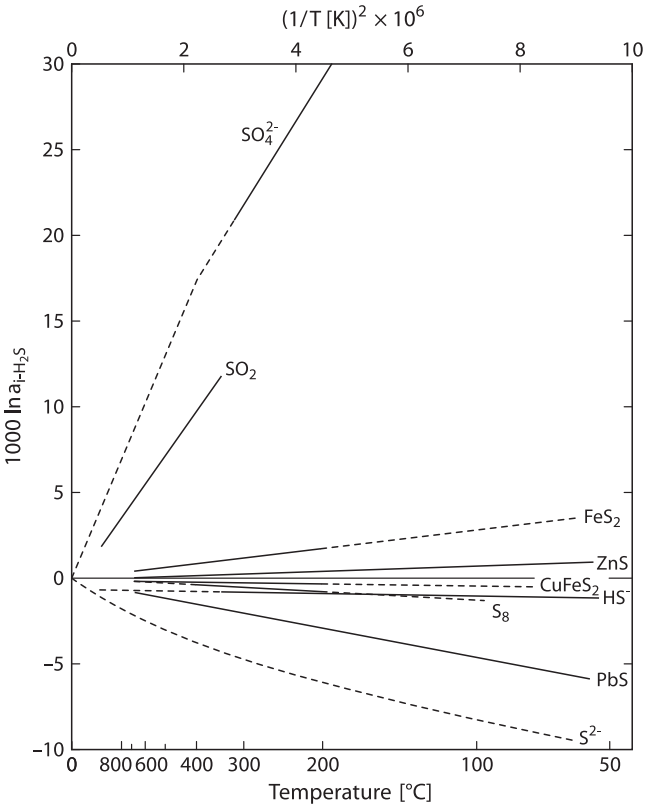

Fig. 2.22 Equilibrium fractionations among sulphur compounds relative to H_2S (*solid lines* experimentally determined, *dashed lines* extrapolated or theoretically calculated (after Ohmoto and Rye, 1979)

summary of what they believe to be the best S-isotope fractionation data. These S-isotope fractionations relative to H_2S are shown in Fig. 2.22.

Sulfur isotope temperatures from ore deposits often have been controversial; one of the reasons are strong ^{34}S zonations in sulfide minerals that have been observed by laser probe and ion probe measurements (McKibben and Riciputi 1998).

2.10 Chlorine

Chlorine has two stable isotopes with the following abundances (Coplen et al. 2002):

^{35}Cl 75.78%
^{37}Cl 24.22%

Natural isotope variations in chlorine isotope ratios might be expected due to both the mass difference between ^{35}Cl and ^{37}Cl as well as to variations in coordination of chlorine in the vapor, aqueous and solid phases. Schauble et al. (2003) calculated equilibrium fractionation factors for some geochemically important species. They showed that the magnitude of fractionations systematically varies with the oxidation state of Cl, but also depends on the oxidation state of elements to which Cl is bound with greater fractionations for 2+ cations than for 1+ cations. Silicates are predicted to be enriched compared to coexisting brines and organic molecules are enriched to dissolved Cl^-.

2.10.1 Methods

Measurements of Cl-isotope abundances have been made by different techniques. The first measurements by Hoering and Parker (1961) used gaseous chlorine in the form of HCl and the 81 samples measured exhibited no significant variations relative to the standard ocean chloride. In the early eighties a new technique has been developed by Kaufmann et al. (1984), that uses methylchloride (CH_3Cl). The chloride-containing sample is precipitated as AgCl, reacted with excess methyliodide, and separated by gas chromatography. The total analytical precision reported is near $\pm 0.1‰$ (Long et al. 1993; Eggenkamp 1994; Sharp et al. 2007). The technique requires relatively large quantities of chlorine (>1 mg), which precludes the analysis of materials with low chlorine concentrations or which are limited in supply. Magenheim et al. (1994) described a method involving the thermal ionization of Cs_2Cl^+, which, as argued by Sharp et al. (2007), is very sensitive to analytical artefacts and therefore might lead to erroneous results. δ-values are generally given relative to seawater chloride termed SMOC (Standard Mean Ocean Chloride).

2.10.2 Characteristic Features of Cl Isotope Geochemistry

Chlorine is the major anion in surface- and mantle-derived fluids. It is the most abundant anion in hydrothermal solutions and is the dominant metal complexing agent in ore forming environments (Banks et al. 2000). Despite its variable occurrence, chlorine isotope variations in natural waters commonly are small and close to the chlorine isotope composition of the ocean. This is also true for chlorine from fluid inclusions in hydrothermal minerals which indicate no significant differences between different types of ore deposits such as Mississippi-Valley and Porphyry Copper type deposits (Eastoe et al. 1989; Eastoe and Guilbert 1992).

Relatively large isotopic differences have been found in slow flowing groundwater, where Cl-isotope fractionation is attributed to a diffusion process (Kaufmann et al. 1984, 1986; Desaulniers et al. 1986). ^{37}Cl depletions detected in some pore waters have been attributed to processes such as ion filtration, alteration and dehydration

reactions and clay mineral formation (Long et al. 1993; Eggenkamp 1994; Eastoe et al. 2001; Hesse et al. 2006). A pronounced downward depletion of δ^{37}Cl-values to $-4‰$ has been reported by Hesse et al. (2006). Even lower δ^{37}Cl-values have been reported in pore waters from subduction-zone environments (Ransom et al. 1995; Spivack et al. 2002). The downward depletion trend might be explained by mixing of two fluids: shallow ocean water with a deep low ^{37}Cl fluid of unknown origin.

Controversial results have been reported for chlorine isotopes in mantle-derived rocks. According to Magenheim et al. (1995) δ^{37}Cl-values for MORB glasses show a surprisingly large range. As postulated by Magenheim et al. (1995), characteristic differences between mantle and crustal chlorine can be used as indicators of the source of volatiles in chlorine-rich mafic magmas, such as the Bushveld and Stillwater complexes (Boudreau et al. 1997; Willmore et al. 2002). For the Stillwater Complex chlorine isotopes are consistent with an influence of crustal derived fluid, whereas for the Bushveld Complex chlorine isotopes indicate a mantle-derived source. A similar approach has been taken by Markl et al. (1997) to trace the origin of chlorine in the lower crust. Since δ^{37}Cl values of granulite facies rocks cluster around ocean water composition, Markl et al. (1997) concluded that chlorine in the lower crust is derived from the upper crust and therefore does not reflect degassing of the mantle.

Recently Sharp et al. (2007) have questioned the findings of Magenheim et al. (1995). Sharp et al. (2007) found that the large differences between mantle and crustal material do not exist and that the mantle and the crust have very similar isotopic composition. A possible explanation for this apparent discrepancy might be related to analytical artifacts of the TIMS technique (Sharp et al. 2007). Bonifacie et al. (2008) also observed small Cl-isotope variations only in mantle derived rocks. They demonstrated that δ^{37}Cl values correlate with chlorine concentrations: Cl-poor basalts have low δ^{37}Cl values and represent the composition of uncontaminated mantle derived magmas, whereas Cl-rich basalts are enriched in ^{37}Cl and are contaminated by Cl-rich material such as ocean water.

Volcanic gases and associated hydrothermal waters have a large range in δ^{37}Cl-values from -2 to $+12‰$ (Barnes et al. 2006). To evaluate chlorine isotope fractionations in volcanic systems, HCl liquid-vapor experiments performed by Sharp (2006) yield large isotope fractionations of dilute HCl at 100°C. These results are in contrast to liquid–vapor experiments by Liebscher et al. (2006) observing very little fractionation at $400-450$°C. Clearly more data are needed to resolve these discrepancies.

2.10.3 Chlorine Isotopes in the Environment

Chlorine isotope studies have been applied to understand the environmental chemistry of anthropogenic organic compounds, such as chlorinated organic solvents or biphenyls. The primary goal of such studies is to identify and quantify sources and

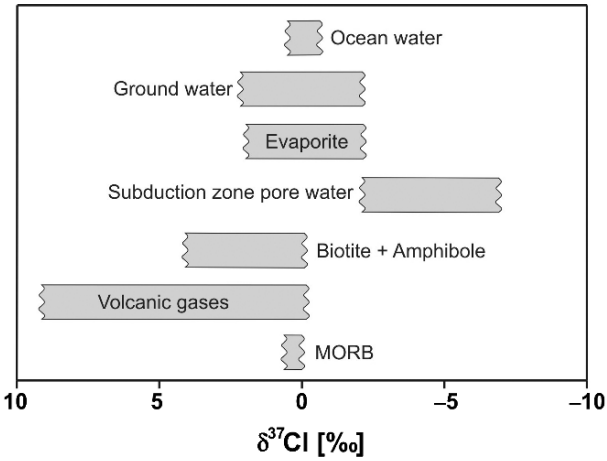

Fig. 2.23 δ^{37}Cl values in geologically important reservoirs

biodegration processes in the environment. To do this successfully chorine isotope values should differ among compounds and manufactorers. The range of reported δ^{37}Cl-values is from about -5 to $+6‰$ with distinct signatures from different suppliers (Van Warmerdam et al. 1995; Jendrzewski et al. 2001).

Perchlorate is another anthropogenic compound, which may contaminate surface and ground waters. The occurrence of natural perchlorate is limited to extremely dry environments, such as the Atacama desert. Large kinetic isotope effects during microbial reduction of perchlorate have been observed by Sturchio et al. (2003) and Ader et al. (2008), which may be used to document in-situ bioremediation.

A summary of the observed natural chlorine isotope variations is presented in Fig. 2.23. Ransom et al. (1995) gave a natural variation range in chlorine isotope composition of about 15‰ with subduction zone pore waters having δ^{37}Cl values as low as $-8‰$ whereas minerals in which Cl substitutes OH have δ^{37}Cl values as high as 7‰.

2.11 Calcium

Calcium plays an essential role in biological processes (calcification of organisms, formation of bones etc.). Calcium has six stable isotopes in the mass range of 40 to 48 with the following abundances (Rosman and Taylor 1998)

^{40}Ca : 96.94%
^{42}Ca : 0.647%
^{43}Ca : 0.135%
^{44}Ca : 2.08%
^{46}Ca : 0.004%
^{48}Ca : 0.187%

Its wide natural distribution and the large relative mass difference suggest a large isotope fractionation, which might be caused by mass-dependent fractionation processes and by radiogenic growth (radioactive decay of ^{40}K), the latter not being discussed here. Early studies on natural isotope variations found no differences or ambigous results. By using a double-spike technique and by using a mass-dependent law for correction of instrumental mass fractionation Russell et al. (1978) were the first to demonstrate that differences in the ^{44}Ca/^{40}Ca ratio are clearly resolvable to a level of 0.5‰. More recent investigations by Skulan et al. (1997) and by Zhu and MacDougall (1998) have improved the precision to about 0.1–0.15‰. These latter authors observed Ca-isotope variations – given as δ^{44}Ca-values – of about 5‰ (see also the review by DePaolo 2004). Comparing data from different laboratories, complications may arise from the use of different δ-definitions and from the use of different standards. By initiating a laboratory exchange of internal standards Eisenhauer et al. (2004) have suggested to use NIST SRM 915a as international standard.

New insights on biomineralization may be revealed by measuring Ca isotope variations in shell secreting organisms (e.g. Griffith et al. 2008). Two factors influence the Ca isotope composition of shells: (1) the chemistry of the solution, in which the organisms live and (2) the process by which Ca is precipitated.

The magnitude of Ca isotope fractionation during carbonate precipitation as well as the mechanism – either isotope equilibrium or kinetic effects – remain a matter of debate. Studies by Nägler et al. (2000), Gussone et al. (2005) and Hippler et al. (2006) reported temperature dependent Ca isotope fractionations precipitated in natural environments or under cultured laboratory conditions with a slope of about 0.02‰ per °C. The slope is identical for aragonite and calcite with an offset of about 0.6‰: aragonite being isotopically lighter (δ^{44}Ca ≈ 0.4‰) than calcite (δ^{44}Ca ≈ 1.0‰). An important question is whether the observed temperature-dependent fractionation results solely from temperature or whether it is influenced by temperature related changes in growth and calcification rates (Langer et al. 2007). And as pointed out by Gussone et al. (2006) similar temperature dependencies do not necessarily imply the same fractionation mechanism. Temperature dependent fractionations; however, have not been found in all shell secreting organisms (Lemarchand et al. 2004; Sime et al. 2005). Sime et al. (2005) analyzed 12 species of foraminifera and found negligible temperature dependence for all 12 species. Thus, no consensus on temperature controlled Ca isotope fractionations has been reached (Griffith et al. 2008).

Marine biogenic carbonates are isotopically depleted in ^{44}Ca relative to present-day seawater (Skulan et al. 1997; Zhu and MacDougall 1998). Zhu and MacDougall have made the first attempt to investigate the global Ca cycle. They found a homogeneous isotope composition of the ocean, but distinct isotope differences of the sources and sinks and suggested that the ocean is not in steady state. Since then several other studies have investigated secular changes in the Ca isotope composition of the ocean: De La Rocha and de Paolo (2000) and Fantle and de Paolo (2005) for the Neogene, Steuber and Buhl (2006) for the Cretaceous; Farkas et al. (2007). for the late Mesozoic; and Kasemann et al. (2005) for the Neoproterozoic. Model

simulations of the Ca cycle by Farkas et al. (2007) indicated that the observed Ca isotope variations can be produced by variable Ca input fluxes to the oceans. However, since the isotope effects that control the Ca isotope composition of marine carbonates are not well understood, any clear indication of secular changes in the Ca isotope composition of ocean waters must remain subject of further debate.

2.12 Chromium

Chromium has 4 stable isotopes with the following abundances (Rosman and Taylor 1998)

^{50}Cr 4.35%
^{52}Cr 83.79%
^{53}Cr 9.50%
^{54}Cr 2.36%

Chromium exists in two oxidation states, Cr(III), as a cation Cr^{3+} and Cr(VI), as an oxyanion (CrO_4^{2-} or $HCrO_4^-$) having different chemical behaviors: Cr^{3+} is the dominant form in most minerals and in water under reducing conditions, whereas Cr(VI) is stable under oxidizing conditions. These properties make Cr isotope investigations suitable to detect and quantify redox changes in different geochemical reservoirs.

Schoenberg et al. (2008) presented the first set of Cr isotope data for rocks and Cr(II) rich ores. Mantle derived rocks and chromite ores from layered intrusions have a uniform $^{53}Cr/^{52}Cr$ isotope ratio very close to the certified Cr standard NIST SRM 979. The Cr isotope composition of hydrothermal lead chromates is substantially heavier (δ^{53}Cr from 0.6 to 1.0‰) than the rocks from which the chromium was leached.

Chromium is a common anthropogenic contaminant in surface waters, therefore Cr isotope fractionations are of potential interest in tracking Cr^{6+} pollution in groundwaters. Ellis et al. (2002, 2004)) and Izbicki et al. (2008) analyzed groundwater samples from contaminated sites and observed an increase in $^{53}Cr/^{52}Cr$ ratios up to 6‰ during the reduction of chromate. Equilibrium fractionations between Cr(VI) and Cr (III) have been estimated by Schauble et al. (2002), who predicted Cr isotope fractionations >1‰ between Cr species with different oxidation states.

2.13 Iron

Iron has 4 stable isotopes with the following abundances (Beard and Johnson 1999)

^{54}Fe 5.84%
^{56}Fe 91.76%
^{57}Fe 2.12%
^{58}Fe 0.28%

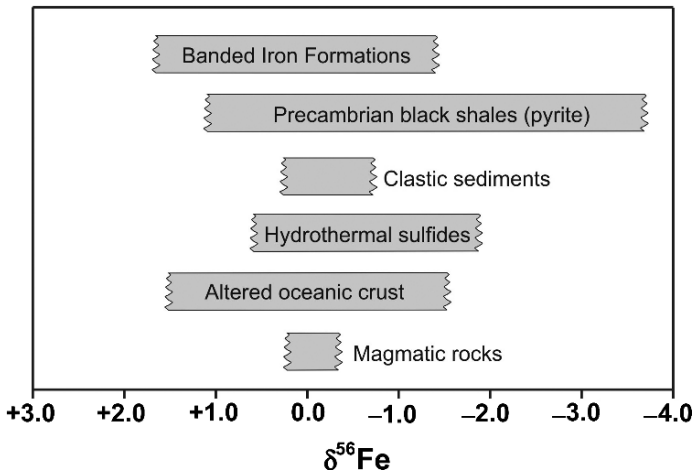

Fig. 2.24 δ^{56}Fe ranges in some important iron reservoirs

Iron is the third most abundant element that participates in a wide range of biotically and abiotically-controlled redox processes in different geochemical low- and high-temperature environments. Iron has a variety of important bonding partners and ligands, forming sulfide, oxide and silicate minerals as well as complexes with water. As is well known bacteria can use Fe during both dissimilatory and assimilatory redox processes. Because of its high abundance and its prominent role in high and low temperature processes, isotope studies of iron have received the most attention of the transition elements. Since the first investigations on Fe isotope variations by Beard and Johnson (1999), the number of studies on Fe isotope variations have increased exponentially. Recent reviews on Fe-isotope geochemistry have been given by Anbar (2004a), Beard and Johnson (2004), Johnson and Beard (2006), Dauphas and Rouxel (2006) and Anbar and Rouxel (2007). Figure 2.24 summarizes Fe-isotope variations in important geological reservoirs.

Literature data have been presented either in the form of $^{57}Fe/^{54}Fe$ or as $^{56}Fe/^{54}Fe$ ratios. In the following all data are given as $^{56}Fe/^{54}Fe$ ratios or as δ^{56}Fe values. δ^{57}Fe values would be 1.5 times greater than δ^{56}Fe values, because only mass-dependent fractionations are expected. Fe isotope aqnalysis is highly challenging because of interferences from $^{40}Ar^{14}N^+$, $^{40}Ar^{16}O^+$ and $^{40}Ar^{16}OH^+$ at masses 54, 56 and 57 respectively. Nevertheless δ-values can be measured routinely with a precision of $\pm 0.05‰$.

Theoretical studies by Polyakov (1997), Polyakov et al. (2007) and Schauble et al. (2001) predicted Fe isotope fractionations of several ‰ between various iron oxides, carbonates and sulfides from spectroscopic data, even at high temperatures. $^{56}Fe/^{54}Fe$ ratios will be usually higher in Fe^{3+} compounds than in Fe^{2+} bearing species. First experimental studies at magmatic temperatures were conducted by Schüßler et al. (2007) for equilibrium isotope fractionations between iron sulfide

(pyrrhotite) and silicate melt and by Shahar et al. (2008) for those between fayalite and magnetite, demonstrating that Fe isotope fractionations are relatively large at magmatic temperatures and can be used as a geothermometer. At low temperatures, Johnson et al. (2002) presented experimental evidence for equilibrium fractionations between Fe^{3+} and Fe^{2+} in aqueous solutions. They observed a 2.75‰ enrichment in Fe^{3+} relative to Fe^{2+} at 25°C which is about half of that predicted by Schauble et al. (2001). While it is conceivable that Fe isotope equilibrium can be reached at high temperatures, indications for equilibrium fractionations are less straightforward at much lower temperatures. Therefore kinetic fractionations might dominate Fe isotope fractionations at low temperatures.

Igneous rocks exhibit only small variations in Fe isotope compositions (Zhu et al. 2002; Beard and Johnson 2004; Poitrasson et al. 2004; Williams et al. 2005; Weyer et al. 2005). Weyer et al. (2005) found that the Fe isotope composition in mantle peridotites is slightly lower than in basalts. As suggested by Williams et al. (2005) the relative incompatibility of ferric iron during melting might incorporate heavy iron into the melt. During magmatic differentiation the Fe isotope composition remains more or less constant except in the very SiO_2-rich differentiates (Beard and Johnson 2004; Poitrasson and Freydier 2005). A possible mechanism is removal of isotopically ^{56}Fe depleted titanomagnetite (Schüßler et al. 2008).

Under low-temperature conditions the observed natural Fe isotope variations of around 4‰ have been attributed to a large number of processes, which can be divided into inorganic reactions and into processes initiated by micro-organisms. Up to 1‰ fractionation can result from precipitation of Fe-containing minerals (oxides, carbonates, sulfides) (Anbar and Rouxel 2007). Larger Fe isotope fractionations occur during biogeochemical redox processes, which include dissimilatory Fe(III) reduction (Beard et al. 1999; Icopini et al. 2004; Crosby et al. 2007), anaerobic photosynthetic Fe(II) oxidation (Croal et al. 2004), abiotic Fe (II) oxidation (Bullen et al 2001) and sorption of aqueous Fe(II) on Fe(III) hydoxides (Balci et al. 2006). Controversy still exists whether the iron isotope variations observed are controlled by kinetic/equilibrium factors or by abiological/microbiological fractionations. This complicates the ability to use iron isotopes to identify microbiological processing in the rock record (Balci et al. 2006). However, as demonstrated by Johnson et al. (2008) microbiological reduction of Fe^{3+} produces much larger quantities of iron with distinct $\delta^{56}Fe$ values than abiological processes.

The bulk continental crust has $\delta^{56}Fe$ values close to zero. Clastic sediments generally retain the zero ‰ value. Because of its very low concentration in the ocean, the Fe isotope composition of ocean water so far has not been determined, which complicates a quantification of the modern Fe isotope cycle. Hydrothermal fluids at mid-ocean ridges and river waters have $\delta^{56}Fe$ values between 0 and -1‰ (Fantle and dePaolo 2004; Bergquist and Boyle 2006; Severmann et al. 2004), whereas fluids in diagenetic systems show a significantly larger spread with a preferential depletion in ^{56}Fe (Severmann et al. 2006). Thus, most iron isotope variations are produced by diagenetic processes that reflect the interaction between Fe^{3+} and Fe^{2+} during bacterial iron and sulfate reduction. Processes dominated by sulfide formation during sulfate reduction produce high $\delta^{56}Fe$ values for porewaters, whereas the

opposite occurs when dissimilatory iron reduction is the major pathway (Severmann et al. 2006).

Especially large iron isotope fractionations have been found in Proterozoic and Archean sedimentary rocks with lithologies ranging from oxide to carbonate in banded iron formations (BIFs) and pyrite in shales (Rouxel et al. 2005; Yamaguchi et al. 2005). In particular BIFs have been investigated to reconstruct Fe cycling through Archean oceans and the rise of $O_{2(atm)}$ during the Proterozoic (see discussion under 3.8.4 and Fig. 3.28). The pattern shown in Fig. 3.28 distinguishes three stages of Fe isotope evolution, which might reflect redox changes in the Fe cycle (Rouxel et al. 2005). The oldest samples (stage 1) are characterized by depleted δ^{56}Fe values, whereas younger samples in stage 2 are characterized by enriched δ^{56}Fe values. Interplays of the Fe-cycle with the C- and S-record might reflect changing microbial metabolims during the Earth,s history (Johnson et al. 2008).

2.14 Copper

Copper has two stable isotopes

^{63}Cu 69.1%
^{65}Cu 30.9%.

Copper occurs in two oxidation states, Cu^{+} and Cu^{++} and rarely in the form of elemental copper. The major Cu-containing minerals are sulfides (chalcopyrite, bornite, chalcosite and others), and, under oxidizing conditions, secondary copper minerals in the form of oxides and carbonates. Copper is a nutrient element, although toxic for all aquatic photosynthetic microorganisms. Copper may form a great variety of complexes with very different coordinations such as square, trigonal and tetragonal complexes. These properties are ideal prerequisites for relatively large isotope fractionations.

Early work of Shields et al. (1965) has indicated a total variation of $\sim$12‰ with the largest variations in low temperature secondary minerals. Somewhat smaller differences, but still in the range of 7 to 9‰, have been observed by Maréchal et al. (1999), Maréchal and Albarede (2002), Zhu et al. (2002), Ruiz et al. (2002), which are larger than for Fe. Nevertheless most samples so far analyzed vary between δ^{65}Cu values from $+1$ to -1‰.

Experimental investigations have demonstrated that redox reactions between CuI and CuII species are the principal process that fractionates Cu isotopes in natural systems (Ehrlich et al. 2004; Zhu et al. 2002). Precipitated CuI species are 3 to 5‰ lighter than dissolved CuII species during CuII reduction. Pokrovsky et al. (2008) observed a change in sign of Cu isotope fractionations during adsorption experiments from aqueous solutions depending on the kind of surface, either organic or inorganic: on biological cell surfaces a depletion of ^{65}Cu, wheras an enrichment of ^{65}Cu on oxy(hydr)oxide surface is observed. Although little is known about the Cu isotope composition of ocean water, Zhu et al. (2002) suggested that Cu isotopes

may be a tracer of Cu biochemical cycling. The latter authors reported Cu isotope fractionations of 1.5‰ during biological uptake.

Recent studies of Cu isotope variations have concentrated on Cu isotope fractionations during ore formation (Larson et al. 2003; Rouxel et al. 2004; Mathur et al. 2005; Markl et al. 2006a). The magnitude of isotope fractionation in copper sulfides increases with secondary alteration and reworking processes. Investigations by Markl et al. (2006) on primary and secondary copper minerals from hydrothermal veins have confirmed this conclusion. They showed that hydrothermal processes do not lead to significant Cu isotope variations, but instead, low temperature redox processes are the main cause of isotope fractionations. Thus copper isotope ratios may be used to decipher details of natural redox processes, but cannot be used as reliable fingerprints for the source of copper – as suggested by Graham et al. (2004) – because the variation caused by redox processes within a single deposit is usually much larger than the inter-deposit variation.

2.15 Zinc

Zinc has 5 stable isotopes of mass 64, 66, 67, 68 and 70 with the following abundances:

^{64}Zn 48.63,
^{66}Zn 27.90,
^{67}Zn 4.10,
^{68}Zn 18.75,
^{70}Zn 0.62.

Zinc is an essential biological nutrient in the ocean where the concentration of Zn is controlled by phytoplankton uptake and remineralization. Zn is incorporated into carbonate shells and diatoms, therefore, Zn isotopes may have great potential for tracing nutrient cycling in seawater. John et al. (2007a) measured the isotope fractionation of Zn during uptake by diatoms and demonstrated that Zn isotope fractionations are related to the extent of biological Zn uptake. In a depth profile of the upper 400 m of Pacific seawater, Bermin et al. (2006) observed small isotope variations which they interpreted as being due to biological recycling. Surface waters have a lighter δ^{66}Zn signature than deeper waters suggesting that absorption of Zn on particle surfaces carries Zn out of surface waters (John et al. 2007a). Pichat et al. (2003) suggested that variations in Zn isotopes in marine carbonates over the last 175 kyr reflect changes in upwelling and nutrient availabilty. Although it has been assumed that there is negligible fractionation between Zn in seawater and precipitated minerals, biological usage and adsorption onto particles are likely to cause isotope fractionations (Gelabert et al. 2006).

Measurements of the ^{66}Zn/^{64}Zn ratio in ores, sediments and biological materials have so far yielded a small variation of about 1‰ (Maréchal et al. 1999, 2000; Maréchal and Albarede 2002 and others). One of the main reasons for this small

variability appears to be that Zn does not participate in any redox reaction, it always occurs in the divalent state. Recently Wilkinson et al. (2005) extended the range of Zn isotope variations to ~1.5‰ by analyzing sphalerites from one ore deposit. They interpreted the variations by postulating kinetic fractionations during rapid sphalerite precipitation. John et al. (2008) have found relatively large Zn isotope fractionation in hydrothermal fluids and suggested that Zn sulfide precipitation is an important factor in causing δ^{66}Zn variations. By analyzing common anthropogenic products in the environment, John et al. (2007b) showed that δ^{66}Zn values of industrial products are smaller than of Zn ores demonstrating Zn isotope homogenezation during processing and ore purification.

2.16 Germanium

Because of nearly identical ionic radii, Ge usually replaces Si in minerals, with average concentrations around 1 ppm in the earth,s crust. Thus Ge and Si have similar chemistries, which might indicate that both elements show similarities in their isotope fractionations.

Ge has five stable isotopes with the following abundances (Rosman and Taylor 1998):

^{70}Ge 20.84%
^{72}Ge 27.54%
^{73}Ge 7.73%
^{74}Ge 36.28%
^{76}Ge 7.61%

Early investigations using the TIMS method were limited to an uncertainty of several ‰. Over the past few years advances have been made with the MC-ICP-MS technique with a long term external reproducibility of 0.2–0.4‰ (Rouxel et al. 2006; Siebert et al. 2006a).

Based on a few measurements of basalts and granites Rouxel et al. (2006) concluded that the bulk silicate earth has a homogeneous isotope composition. However, chemical sediments like sponges and authigenic glauconites are enriched in δ^{74}Ge by about 2‰. This suggests that seawater – similar to silicon – is isotopically enriched in ^{74}Ge relative to the bulk earth. Ge isotopes might offer new insights into the biogeochemistry of the past and present ocean, but more data are needed.

2.17 Selenium

Because selenium to some extent is chemically similar to sulfur, one might expect to find some analogous fractionations of selenium isotopes in nature. Six stable selenium isotopes are known with the following abundances (Coplen et al. 2002)

^{74}Se 0.89%
^{76}Se 9.37%
^{77}Se 7.63%
^{78}Se 23.77%
^{80}Se 49.61%
^{82}Se 8.73%

Interest in selenium isotope studies has grown in recent years, since selenium is both a nutrient and a toxicant and may reach significant concentrations in soils and in watersheds. Starting with work by Krouse and Thode (1962) the SeF_6 gas technique used by the early workers required relatively large quantities of Se, limiting the applications of selenium isotopes. Johnson et al. (1999) developed a double-spike solid-source technique (spike ^{74}Se and ^{82}Se, measure $^{80}Se/^{76}Se$) that corrects for fractionations during sample preparation and mass spectrometry, yielding an overall reproducibility of $\pm 0.2‰$. This technique brings sample requirements down to submicrogram levels. Even lower Se amounts (10 ng) are required for measurements with the MC-ICP-MS technique (Rouxel et al. 2002).

Reduction of selenium oxyanions by bacteria is an important process in the geochemical cycle of selenium. Selenium reduction proceeds in three steps with Se(IV) and Se(0) species as stable intermediates (Johnson 2004). Se isotope fractionation experiments by Herbel et al. (2000) indicate about 5‰ fractionations ($^{80}Se/^{76}Se$) during selenate reduction to selenite and little or no fractionation for selenite sorption, oxidation of reduced Se in soils, or Se volatilization by algae. Johnson and Bullen (2003) investigated Se isotope fractionations induced by inorganic reduction of selenate by Fe(II)–Fe(III) hydroxide sulfate ("green rust"). The overall fractionation is 7.4‰, which is larger than during bacterial selenate reduction. This indicates that the magnitude of Se isotope fractionations depends on the specific reaction mechanism. More data are needed, but selenium isotopes should be useful tracers for selenate and selenite reduction processes as well as selenium sources.

2.18 Molybdenum

Mo consists of 7 stable isotopes that have the following abundances:

^{92}Mo 15.86%,
^{94}Mo 9.12%,
^{95}Mo 15.70%,
^{96}Mo 16.50%,
^{97}Mo 9.45%,
^{98}Mo 23.75%
^{100}Mo 9.62%.

Either $^{97}Mo/^{95}Mo$ or $^{98}Mo/^{95}Mo$ ratios have been reported in the literature. Therefore care has to be taken by comparing Mo isotope values. Mo isotope data are gen-

erally given relative to laboratory standards calibrated against ocean water (Barling et al. 2001; Siebert et al. 2003).

Because Mo is a redox sensitive element that becomes enriched in reducing, organic rich sediments, Mo-isotope fractionations during redox processes might be expected (Anbar 2004b; Anbar and Rouxel 2007). In oxygenated waters insoluble MoO_4^{2-} is the dominant Mo species, which is so unreactive that Mo is the most abundant transition metal in ocean water. Mo in ocean water should have a uniform isotope composition as is expected from its long residence time in the ocean. Oxic pelagic sediments and Fe-Mn crusts or nodules are depleted in ^{98}Mo by about 3‰ relative to sea water (Barling et al. 2001; Siebert et al. 2003). A comparable fractionation has been found in pore waters (McManus et al. 2002) and in an experimental study of Mo absorption on Mn oxides (Barling and Anbar 2004). The actual fractionation mechanism is unclear, but fractionations occur in solution, where Mo is in the hexavalent state. Therefore oxidizing conditions in the marine environment are a major requirement for Mo isotope fractionations (Siebert et al. 2005).

The largest isotope effect occurs during adsorption of dissolved Mo to Mn-oxide particles, so that dissolved Mo is heavier than particle bound Mo. First observed in oxic seawater and sediments by Barling et al. (2001), Barling and Anbar (2004) have verified the fractionation effect in the laboratory. Smaller isotope fractionations occur during the reduction of Mo in suboxic environments (McManus et al. 2002, 2006; Nägler et al. 2005; Poulson et al. 2006; Siebert et al. 2003, 2006b). Observed in different sedimentary settings these effects so far have not been verified in experimental studies.

Due to the preferential extraction of ^{95}Mo from ocean water, the ocean is the heaviest Mo reservoir of all sources analyzed so far Fig. 2.24, consequently the Mo isotope composition of the ocean is sensitive to redox changes and thus can be used as a paleo-redox proxy.

Black shales that are formed in an anoxic environment such as the Black Sea have a Mo isotope composition nearly identical to ocean water (Barling et al. 2001; Arnold et al. 2004; Nägler et al. 2005). Organic carbon rich sediments formed in suboxic environments have variable ^{98}Mo/^{95}Mo ratios intermediate between those of ocean water and oxic sediments (Siebert et al. 2003). Thus Mo isotope values in ancient black shales can be used as a paleo-oceanographic proxy of the oxidation state of the ocean, as for example has been discussed by Arnold et al. (2004) for the Proterozoic. Figure 2.25 summarizes natural Mo isotope variations.

2.19 Mercury

The heaviest elements with observed fractionations of about 3 to 4‰ are mercury and thallium. This is surprising because isotope variations due to mass-dependent fractionations should be much smaller. Schauble (2007) demonstrated that isotope variations for the heaviest elements are controlled by nuclear volume, a fractionation effect being negligible for the light elements. Nuclear volume fractionations may

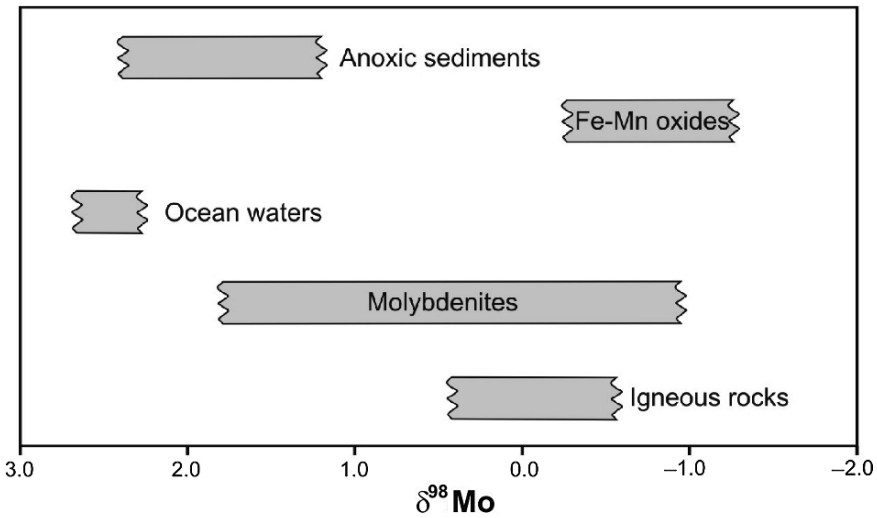

Fig. 2.25 δ^{97}Mo values in important geologic reservoirs

be about 1‰ per mass unit for Hg and Tl, declining to about 0.02‰ for sulfur. Nuclear volume fractionations also tend to enrich heavy isotopes in oxidized species (Schauble 2007).

Mercury has seven stable isotopes in the mass range from ^{196}Hg to ^{204}Hg with the following abundances (Rosman and Taylor 1998)

^{196}Hg 0.15
^{198}Hg 9.97
^{199}Hg 16.87
^{200}Hg 23.10
^{201}Hg 13.18
^{202}Hg 29.86
^{204}Hg 6.87

Due to the relative uniform isotope abundances in the mass range ^{198}Hg to ^{204}Hg, several possibilities exist for the measurement of isotope ratios, thus far δ-values are generally presented as ^{202}Hg/^{198}Hg ratios.

Mercury is very volatile and a highly toxic pollutant. Its mobility depends on its different redox states. Reduction of Hg species to Hg(0) vapor is the most important pathway for removal of Hg from aqueous systems to the atmosphere occurring by biotic and abiotic reactions. Data by Smith et al. (2005), Xie et al. (2005), Foucher and Hintelmann (2006) and Kritee et al. (2007), indicate that mercury isotopes are fractionated in hydrothermal cinnabar ores, sediments and environmental samples. The range in isotope composition (^{202}Hg/^{198}Hg) is likely to exceed 5‰, quite large considering the relatively small mass range of less than 4%. Smith et al. (2005, 2008) analyzed the Hg isotope composition of fossil hydrothermal systems and concluded that ore and spring deposits have a larger range in Hg isotope composition than

associated country rocks. They postulated that boiling of hydrothermal fluids and separation of a Hg-bearing vapor phase are the most important Hg fractionation processes.

Since Hg takes part in microbial processes, Hg fractionations should occur during methylation processes. Kritee et al. (2007) suggested that Hg isotopes might have the potential for distinguishing between different sources of mercury emissions based on the magnitude of isotope fractionations. Finally, it is important to note that abiological photochemical reduction of Hg^{2+} and CH_3Hg^+ by sunlight leads to a large mass-independent fractionation of ^{201}Hg and ^{199}Hg (Bergquist and Blum 2007).

2.20 Thallium

Thallium has two stable isotopes with masses 203 and 205.

^{204}Tl 29.54
^{205}Tl 70.48

Thallium is the heaviest element for which natural variations in isotope composition have been reported (Rehkämper and Halliday 1999). Tl exists in two valence states as Tl^+ and Tl^{3+} and forms in water a variety of complexes. Furthermore it is a highly volatile element which could induce kinetic fractionations during degassing processes. A systematic 2‰ difference between Fe–Mn crusts enriched in ^{205}Tl and seawater has been observed by Rehkämper et al. (2002), which was interpreted to be due to an fractionation effect during adsorption of Tl onto Fe–Mn particles. In a later study Rehkämper et al. (2004) found that growth layers of Fe–Mn crusts show a systematic change in Tl isotope composition with age, which they explained by time-dependent changes in Tl-isotope composition of seawater. No significant Tl isotope fractionations occur during weathering (Nielsen et al. 2005).

Tl isotope ratios might be also used as a tracer in mantle geochemistry (Nielsen et al. 2006; 2007). Since most geochemical reservoirs except Fe-Mn marine sediments and low temperature seawater altered basalts are more or less invariant in Tl isotope composition, admixing af small amounts of either of these two components into the mantle should induce small Tl isotope fractionations in mantle derived rocks. And indeed, evidence for the presence of Fe-Mn sediments in the mantle underneath Hawaii was presented by Nielsen et al. (2006).

Citation: Tiwari M, Singh AK, Sinha DK (2015) Stable isotopes: tools for understanding past climatic conditions and their applications in chemostratigraphy. In: Ramkumar Mu (ed) Chemostratigraphy: concepts, techniques and application. Elsevier, Amsterdam, pp 65–92

CHAPTER

3

STABLE ISOTOPES: TOOLS FOR UNDERSTANDING PAST CLIMATIC CONDITIONS AND THEIR APPLICATIONS IN CHEMOSTRATIGRAPHY

Manish Tiwari[1], Ashutosh K. Singh[2], Devesh K. Sinha[2]

[1]National Centre for Antarctic & Ocean Research, Vasco-da-Gama, Goa, India; [2]Department of Geology, Centre of Advanced Studies, University of Delhi, Delhi, India

3.1 INTRODUCTION

The climate of the earth can change drastically and has changed so in the past. This was first proposed by the European geologists in the late eighteenth and early nineteenth century including the Scottish geologist James Hutton who found the signature of glacial activity in presently unglaciated regions. The Swiss geologist Louis Agassiz and his colleagues proposed the theory of "Ice Age" in 1837 to explain the observations that hypothesized a succession of glaciation. Meanwhile, the French mathematician and physicist Joseph Fourier postulated in 1824 that the earth should have been much colder but for an insulating effect of its atmosphere (Fourier, 1824), which is widely regarded as the first reference toward the "greenhouse effect" of the atmosphere. The English physicist John Tyndall in mid-nineteenth century, intrigued by the Fourier's discovery and a need to explain the changing climate of the earth, found that water vapor, methane, and carbon dioxide strongly block infrared radiation and act as greenhouse gases (Tyndall, 1861). The celebrated Swedish scientist Svante August Arrhenius in 1896 quantified the effect of CO_2 increase on temperature rise and was first to predict that human produced CO_2 can cause warming (Arrhenius, 1896). Among these developments, the self educated Scottish scientist James Croll postulated in 1870s the link between the ice ages and the changes in earth's orbit. The Serbian climatologist, Milutin Milankovitch in 1920s, built upon the work of James Croll, and established that slight changes in earth's orbital parameters viz eccentricity, obliquity, and precession can cause the climate of the earth to change in a cyclic pattern (Milankovitch, 1930), which are known as Milankovitch Cycles. The theory, although mathematically elegant, was not accepted as it did not match with the timing of four ice ages (based on the records of glacial activities) widely recognized by geologists at that time. During that period, several theories including greenhouse effect, solar irradiance variability, orbital changes and so on were proposed but were not believed as they were not able to match the observations.

Chemostratigraphy. http://dx.doi.org/10.1016/B978-0-12-419968-2.00003-0

In such a puzzling scenario, chemostratigraphic techniques emerged in the forefront and helped to explain the past climatic changes. One of such advancements was the development of the "Radiocarbon Dating" method by Willard Libby in 1949 for which he was awarded the Nobel Prize in Chemistry. This revolutionary technique allowed the age determination of the organic matter till ~40,000 years using the radioactive isotope of carbon, which helped to precisely establish the chronology of the past climate change. But still, most of the records were land based and hence were disturbed due to erosion and other geological factors. In the year 1947, Harold Urey had found that the ratio of oxygen isotopes in carbonates depends on the ambient temperature using the newly developed technique of the isotope ratio mass spectrometry (Urey, 1947). This led the way for establishing the paleotemperature scale using marine carbonates (McCrea, 1950; Epstein et al., 1953) that avoided the limitations of the terrestrial records. Cesare Emiliani used oxygen isotope ratio of the calcium carbonate shells of microscopic organisms called foraminifera from deep-sea sediment cores to reconstruct the records of temperature changes for the past 300,000 years (Emiliani, 1955). These precisely dated, high-resolution records of the cold and warm periods stretching back continuously for thousands of years were instrumental in understanding the causes of climate change. Emiliani was able to correlate his record of climate change with the varying insolation according to Milankovitch's astronomical calculations for which he had to factor a lag of 5000 years considering the response time of the ice sheets. It was later proved that the oxygen isotopes of the foraminiferal shells not only reflected temperature but also the removal of large amounts of isotopically lighter water from the ocean and its storage over land during glacial periods—the so-called ice-volume effect (Shackleton, 1967). Still, the work of Emiliani and others provided a substantial credence to the orbital theory of climate change and to the fact that a little change in the forcing factors can have a major impact on the climate system of the earth (Broecker et al., 1968).

The next major step, when the chemostratigraphic techniques helped to decipher the climate change at much higher resolution than previously possible was the determination of isotopic ratios and trapped gases in the long ice cores obtained from Greenland and Antarctica. Willi Dansgaard and his team drilled several long cores in Greenland and measured oxygen isotope ratio that led to the discovery of the rapid climatic changes such as "Younger Dryas" when the earth cooled down abruptly within a few decades (Johnsen et al., 1992; Dansgaard et al., 1993; Alley, 2000). Such pattern of rapid climate change was also observed by Hans Oeschger in glacial-era lake deposits in Switzerland that came to be known as "Dansgaard-Oeschger events." Long ice cores from the Vostok Station from Antarctica revealed that the CO_2 also covaried with the temperature change implying a very strong link between them (Petit et al., 1999). Oceans are one of the largest reservoirs of the CO_2 that can exchange with the atmosphere on very short timescales. This led to the development of the hypothesis that reorganization of the thermohaline circulation can cause the abrupt climatic changes (e.g., Broecker and Denton, 1990). Although the magnitude of feedback from different components of the climate system was not clear, a consensus among the scientific community was established by 1980s that increasing anthropogenic CO_2 will result in adverse climatic change.

United Nations, in 1988, created an autonomous body—Intergovernmental Panel on Climate Change (IPCC)—that was entrusted with the task of producing reports that serve as the definitive word on the state of the climate change and its future impact. The first IPCC report was published in 1990 and since then it has produced periodic reports that serve a great purpose by putting before the general public the magnitude of anthropogenic climate change for which it was awarded the Nobel Peace Prize in 2007. The fifth and the most recent report of the IPCC shows that the earth's climate is warming

rapidly with an estimated 0.85 °C increase in globally averaged combined land and ocean surface temperatures from 1880 to 2012 of which the anthropogenic factors are the major causes. This warming of the climate system is beginning to show an adverse effect on the sea level, ocean acidification, ice melting, water cycle, and so on (IPCC, 2013).

This discussion leads us to the fact that the earth's climate change consists of a diversity of events that have occurred in its various spheres, i.e., atmosphere, ocean circulation change (hydrosphere), organic evolution (biosphere), ice-volume changes related to glacial and interglacial stages (cryosphere), large scale movements of the continents (asthenosphere and lithosphere), convection currents and volcanism (mesosphere), and paleomagnetic reversals (barysphere). A comprehensive understanding of the "Earth System Science" reveals that none of these spheres work in isolation; the changes in one sphere can cause perturbations in other spheres. The interplay among various spheres of the earth can be seen in operation in modern times and have been found to have occurred in geological past as well. In order to study the geological past, the geoscientists make use of what is known as "proxy." The past events are preserved in the geological material and the geologists use various kinds of proxies to infer the various parameters of the geological past. This constitutes the science of "paleoclimatology," which is defined as the study of past climate and its variation in space and time during the period before the instrumental documentation began. Stable isotopes are one of such powerful proxies that help us to infer the past geological events that have occurred in the various spheres of the earth. Like all other proxies, the application of stable isotopes also has some limitations. Nevertheless, they have been found to be of immense use for stratigraphic, paleoceanographic, and paleoclimatic studies. We present here the basics of the stable isotope methodology along with case studies of their application including high resolution paleoceanographic and paleoclimatic studies. The purpose is to make a new researcher acquainted with the potential of stable isotopes for application in paleoclimatological studies. The discussion is in no way an exhaustive summary of the available literature and only basic facts largely agreed upon, based on published work, have been highlighted.

3.2 STABLE ISOTOPE SYSTEMATICS

Atoms of an element having the same number of protons but different number of neutrons are called *isotopes*, i.e., they possess same atomic number but different mass number. The word "isotopes" in Greek means "equal places" indicating that they occupy the same position in the periodic table by virtue of their same atomic numbers. Isotopes, which spontaneously disintegrate with a measurable half-life, are called *radioactive* while those that do not disintegrate or have extremely long half-lives (comparable to the age of the earth) are considered *stable*. Such isotopes have existed in their current form before the formation of the Earth and therefore are also known as the "primordial isotopes." An isotope becomes unstable or radioactive when the electrostatic coulomb repulsion of the positively charged proton within the nucleus results in its spontaneous disintegration. To make an isotope stable, the repulsive force of the protons needs to be counterbalanced by neutrons. Till around mass number 40, same number of neutrons is sufficient to balance the repulsion generated by protons, i.e., neutron to proton ration (N/Z) is 1. This is known as the "Symmetry Rule." With increasing numbers of protons, the repulsion increases, thus requiring more neutrons than protons causing the N/Z ratio to exceed unity. The abundance of stable isotopes is explained by the "Oddo–Harkins Rule," which states that the cosmic abundance of elements with even number of protons is much more than the adjacent elements

with odd numbers of proton. It applies to the stability of isotopes as well. The elements with even number of protons and even number of neutrons have the maximum number of stable isotopes. Next in line are the elements with the combination of an even number of protons and odd number of neutrons followed by elements with odd number of protons and even number of neutrons. The elements with the least number of stable isotopes are those that possess an odd number of protons and odd number of neutrons (Hoefs, 2009). *Isotopologues* (shortened from "isotopic analogues") are molecules of the same compound that differ in isotopic composition and relative molecular mass, e.g., $H_2{}^{16}O$ and $H_2{}^{18}O$. Isotopomers (shortened from "isotopic isomers") differ only in the position of the isotopes and not in the composition, i.e., they possess same relative molecular mass, for e.g., $^{14}N^{15}N^{16}O$ and $^{15}N^{14}N^{16}O$.

The variations in the physical and chemical properties due to the presence of different isotopes (the so-called "Isotope Effect") arise due to very small, yet significant mass differences among them. For example, properties like density, melting point, boiling point, viscosity, etc., of the compounds with heavier isotopes are more than those composed of lighter isotopes. These differences are most significant for light elements (less than mass number 50) such as hydrogen, carbon, nitrogen, oxygen, etc., as the relative mass difference of their isotopes ($\Delta m/m$) is higher than heavier elements. In general, lighter isotopes are more mobile as the ratio of the velocity of the lighter molecule to that of the heavier molecule is inversely proportional to the square root of their masses. The mass of the constituent isotope also influences the vibrational motion of the molecule. The molecule with lighter isotope possesses a higher vibrational frequency, and hence higher vibrational energy than a molecule containing the heavier isotope. Therefore, lesser dissociation energy is required to break a bond formed by a lighter isotope than that formed by a heavier isotope. It implies that a molecule with lighter isotope will participate in a chemical process more readily than a molecule possessing heavier isotope. This leads to *isotopic fractionation*.

3.2.1 ISOTOPIC FRACTIONATION

Isotopic fractionation is defined as the relative partitioning of the heavier and lighter isotopes between two coexisting phases in a natural system. There are two types of isotopic fractionation processes, namely, "equilibrium" and "kinetic."

Equilibrium fractionation is a special case of chemical equilibrium reaction in which there is no net reaction but an exchange of isotopes takes place, which affects the equilibrium constant. In this case, isotopes can move to and fro and equilibrium is attained when the isotopic ratios do not change any more with time. For example, foraminifers (unicellular microorganism) secrete their calcitic shells in equilibrium with ambient seawater and the following isotopic exchange process takes place:

$$1/3CaC^{16}O_3 + H_2{}^{18}O \rightleftharpoons 1/3CaC^{18}O_3 + H_2{}^{16}O$$

The equilibrium constant "K" for this reaction can be written as:

$$K = \frac{\left[CaC^{18}O_3\right]^{1/3}\left[H_2{}^{16}O\right]}{\left[CaC^{16}O_3\right]^{1/3}\left[H_2{}^{18}O\right]}$$

$$\text{or, } K = \frac{\left(\left[CaC^{18}O_3\right] / \left[CaC^{16}O_3\right]\right)^{1/3}}{\left(\left[H_2{}^{18}O\right] / \left[H_2{}^{16}O\right]\right)}$$

Thus, equilibrium constant can be expressed as the ratio of $^{18}O/^{16}O$ in the carbonate phase to that in the water. This leads to the concept of *isotopic fractionation factor* "α" that represents the partitioning of isotopes between two phases. Fractionation factor is defined as the ratio of isotopes in one phase to the other coexisting phase. In the $CaCO_3$–H_2O system, the fractionation factor is defined as:

$$\alpha_{CaCO_3\text{-}H_2O} = \frac{\left(^{18}O/_{16}O\right)_{CaCO_3}}{\left(^{18}O/_{16}O\right)_{H_2O}}$$

The fractionation factor is related to the equilibrium constant by:

$$\alpha = K^{1/n}$$

where "n" is the number of atoms exchanged.

Kinetic fractionation is associated with incomplete and unidirectional processes and it affects the rate constant of the reaction. No isotopic equilibrium is attained in the case of kinetic fractionation. For example, in a reaction, where the k_L and k_H respectively depict different rate constants involving the lighter and the heavier isotopes. In such a case, the effect of isotopic substitution in the reactant can be expressed as the ratio of the rate constants, k_L/k_H. If this ratio is greater than 1, it means that the reactant with lighter isotope reacts more readily and is termed "normal." It is called "inverse" when the ratio is less than 1 signifying that the reactant with heavier isotope reacts more rapidly. Note that, if in an irreversible reaction, all the reactants are consumed to form a product, then no isotope effects and no fractionation will be observed in the final product.

The *isotopic fractionation*, ε, is defined as: $\varepsilon = \alpha - 1$. This is usually a small number, hence is multiplied by 10^3 and is then expressed in per mil (‰). The isotopic fractionation is temperature dependent (Urey, 1947). In this example, the $\alpha_{CaCO_3\text{–}H_2O}$ is 1.031 at 25 °C, i.e., the ε is $(1.031-1)10^3‰ = 31‰$. The $\alpha_{CaCO_3\,-\,H_2O}$ is 1.028 at 33.7 °C, i.e., the ε is 28‰. It indicates that the isotopic fractionation decreases with the increasing temperature. Theoretical studies demonstrate that α is inversely proportional to the square of the temperature (Hoefs, 2009).

Additionally, the nature of the chemical bonds also dictates the isotopic distribution. The bonds with higher ionic potential involving low atomic masses have higher vibrational frequencies and hence tend to accumulate heavier isotopes to reduce it. For example, the inorganically precipitated calcite is always enriched in the heavier isotope of the oxygen (^{18}O) as compared to the other minerals due to the presence of the small, highly charged C^{4+} ion to which the oxygen is bonded. Crystal structure also plays a role: the more orderly and closely packed structure tend to accumulate the heavier isotope. This effect is evident in the enrichment of ^{18}O in ice as compared to water (Beck and Münnich, 1988).

Rayleigh isotopic fractionation is an important type of fractional distillation or condensation under the *equilibrium* condition. It is used to calculate the changing isotopic ratios as the material is removed from one coexisting phase to the other during the evaporation–condensation processes. Considering an example of a cloud mass from which condensation (precipitation) is taking place the Rayleigh isotopic fractionation could be defined as: If, "R_o" is the original isotopic ratio of the vapor before the rain out, "R" is the new isotopic ratio of the remaining vapor, "α" is the vapor to liquid fractionation factor, and "f" is the fraction of the vapor remaining, i.e., ratio of the present amount to the initial total amount, then:

$$R = R_o(f)^{\alpha - 1}$$

In terms of δ-value (explained below):

$$\delta = \delta_o + \varepsilon \ln(f) \ \{\text{in } ‰\}$$

3.2.2 DELTA (δ) VALUE

It is very difficult to precisely measure the absolute abundance of isotopes owing to the very low abundance of heavier isotopes. Therefore, *isotope ratio* is determined, which is the ratio of the number of heavier isotopes to that of the lighter isotopes. The term "isotopic abundance" refers to the fraction or percentage of a particular isotope with respect to all other isotopes of that element in the same system (synonymous with the terms *isotope-amount fraction* or *atom fraction*). Isotope Ratio Mass Spectrometers (IRMS) are used for isotopic analysis, which are based on the principle of the separation of charged molecules and atoms under electromagnetic field according to their masses. The IRMS cannot measure the absolute isotopic ratio of a compound with sufficient precision. But it can measure the difference between the isotopic ratios of two compounds with very high precision and accuracy as both of them experience the same conditions during the analysis. Therefore, the isotopic abundances are reported in "δ" value, which is the relative difference of isotopic ratio of a sample from that of an international standard:

$$\delta_A = \left[\left(\frac{R_A}{R_{st}}\right) - 1\right]$$

where, R_A and R_{st} are the ratios of the abundance of the less abundant (heavier) to more abundant (lighter) isotope (e.g., $^{18}O/^{16}O$) in the sample and standard, respectively. δ-value is a dimensionless quantity as it is the ratio of the two quantities of the same kind. It is multiplied by extraneous numerical factors like 10^3 and expressed in "per mil" (‰) units for the sake of readability and ease of comprehension. When it is multiplied by 10^4, it shall be expressed in "pptt" (parts per ten thousand) and shall not be expressed as "ε" that has been erroneously reported so in several places in literature earlier (see Coplen, 2011 for detailed discussion). While expressing isotopic ratios, the heavier isotope is kept in numerator so that the δ-value is positive. A positive "δ" means that the sample comprises more number of heavier isotopes than the standard or, in other words, the atomic weight of the particular element is more in the sample than the standard.

3.2.3 ISOTOPIC STANDARDS

To be used as a standard or reference material for isotopic measurements, the substance should be sufficiently stable, homogeneous, widely available, and its isotope ratio shall be near the mean of the natural variation. Any such substance prepared in an individual laboratory is called as a "lab standard" or "working standard" but it needs to be calibrated with respect to an international standard so that the δ-values of the samples from all over the world are finally reported with respect to a common scale. The *primary reference materials* (international standards) for a few of the light elements are Vienna Standard Mean Ocean Water (VSMOW) for $\delta^{18}O$ and $\delta^{2}H$, Vienna Pee Dee Belemnite (VPDB) for $\delta^{18}O$ and $\delta^{13}C$, air-N_2 for $\delta^{15}N$, Vienna Canyon Diablo Troilite (an iron meteorite) for $\delta^{34}S$, SRM 951 (Boric Acid; formerly, NBS-951) for $\delta^{11}B$, and LSVEC (a lithium carbonate) for $\delta^{7}Li$ among others. Reputed institutions like International Atomic Energy Agency (IAEA, Vienna), National Institute of Standards and Technology (NIST, USA), and Institute for Reference Materials and Measurements (Belgium)

prepare and distribute such international standards and several other "certified isotopic reference materials" like VSMOW2, NBS-19, IAEA-N-1, etc., with an agreed upon δ-value, which are used to calibrate to the international standard's scale.

Two international standards viz PDB and SMOW are of historical importance in the development of the application of stable isotope techniques for climate related studies. For oxygen and hydrogen isotopic studies of water, the international standard SMOW holds special significance. SMOW is a hypothetical standard with $\delta^{18}O$ value close to the modern mean seawater value. The value of SMOW was defined by Craig (1961) with respect to an existing water standard NBS-1 (distilled Potomac River water) with $\delta^{18}O$ value of −7.94‰ versus SMOW. As SMOW does not actually exist as a real water sample so it cannot be used for calibrating laboratory measurements. Therefore a water sample with values identical to SMOW was distributed by IAEA that was called VSMOW where "V" stands for Vienna—the city where the IAEA is based. Prof. Harmon Craig of the University of California prepared it by mixing distilled ocean water (collected from the Pacific Ocean, 0° latitude 180° longitude, in July 1967) with small amounts of other waters to adjust the isotopic ratios to the required values (Gonfiantini, 1981). It has $\delta^{18}O$ and $\delta^{2}H$ value of 0‰ with respect to SMOW. This scale has been used for oxygen isotope analyses involving waters, silicates, phosphates, high temperature carbonates, etc. As VSMOW was getting exhausted, it was replaced by VSMOW2, which was prepared by the IAEA Isotope Hydrology Laboratory in 2006 with values similar to the original VSMOW. The other water standards currently in use are Standard Light Antarctic Precipitation 2 (SLAP2) and Greenland Ice Sheet Precipitation (GISP). The $\delta^{18}O$ and $\delta^{2}H$ value of SLAP2 are −55.50‰ and −427.5‰, respectively, with respect to VSMOW (Gröning, 2004). The $\delta^{18}O$ and $\delta^{2}H$ value of GISP are −24.76‰ and −189.5‰, respectively, with respect to VSMOW (Gröning, 2004). All the δ-values have to be reported on the VSMOW/SLAP scale, using VSMOW2 and SLAP2 as the calibration materials.

The PDB standard scale is used in the low temperature carbonate studies. The original PDB standard was a carbonate obtained from the fossilized rostrum (cigar shaped internal shell) of *Belemnitella americana*, a belemnite (an extinct cephalopod) from the Pee Dee Formation of the Cretaceous Period in South Carolina, USA. It was the laboratory working standard used by the Urey's group at the University of Chicago in the 1950s for developing the initial paleotemperature scale (McCrea, 1950). Over the decades, the original PDB standard has been exhausted and is no longer available. To overcome this problem, IAEA introduced a hypothetical standard VPDB with values nearly identical to PDB and is defined by its relationship to the carbonate reference material NBS-19 (NBS stands for the National Bureau of Standards—the earlier name of NIST). NBS-19 is calcium carbonate from a marble of geologically unidentified origin with $\delta^{18}O$ and $\delta^{13}C$ values of −2.20‰ and +1.95‰ respectively with respect to VPDB (Gröning, 2004).

3.2.4 A FEW IMPORTANT EQUATIONS USED IN STABLE ISOTOPE ANALYSIS

The conversion equations of $\delta^{18}O_{(VPDB)}$ to $\delta^{18}O_{(VSMOW)}$ and vice versa are (Coplen et al., 1983)

$$\delta^{18}O_{(VSMOW)} = 1.03091\delta^{18}O_{(VPDB)} + 30.91$$

$$\delta^{18}O_{(VPDB)} = 0.97002\delta^{18}O_{(VSMOW)} - 29.98$$

Usually in the mass spectrometry labs, a "Lab Standard" is used for measuring δ-values that need to be converted to the international standard scale. For example, δ-value of a sample "Smp" with respect to an international standard, say VPDB, can be determined if its value with respect to the lab standard, say "Lb," is measured and the δ-value of the lab standard with respect to the international standard is known after careful calibration. The conversion equation is

$$_{\text{VPDB}}\delta^{\text{Smp}} = {}_{\text{Lb}}\delta^{\text{Smp}} + {}_{\text{VPDB}}\delta^{\text{Lb}} + {}_{\text{Lb}}\delta^{\text{Smp}}\ {}_{\text{VPDB}}\delta^{\text{Lb}}\ 10^{-3}$$

The difference in the δ-values (*isotopic difference*, Δ) of the two coexisting phases, say $CaCO_3$ and H_2O, is approximately related to their fractionation factor (α) by the equation:

$$\delta_{CaCO_3} - \delta_{H_2O} = \Delta_{CaCO_3 - H_2O} \approx 10^3 \ln\alpha_{CaCO_3 - H_2O} \quad (\text{expressed in } ‰)$$

This approximation is especially good for δ-values where the difference ($\delta_A - \delta_B$) is less than 10.

Isotope ratio and δ-value of a mixture (say, M) is proportional to the mole fractions of its constituents (say, A and B):

$$R_M = X_A R_A + X_B R_B$$

$$\delta_M = X_A \delta_A + X_B \delta_B$$

where, R_M, R_A, R_B and δ_M, δ_A, R_B depict the *isotopic ratios* and the *δ-values* of the mixture, constituent A and constituent B, respectively; X_A, and X_B depict *mole fractions* of the constituent A and constituent B, respectively.

3.3 STABLES ISOTOPES OF A FEW ELEMENTS AND THEIR APPLICATIONS

Stable isotopes of several elements namely carbon and oxygen are used in paleoclimatic research. These are measured on the available geological archives such as foraminifera, speleothems, corals, and calcretes. In addition, carbon and nitrogen isotopes of organic matter preserved in sediments; oxygen and hydrogen isotopes of water including ice; carbon, hydrogen, nitrogen, and oxygen isotopes of greenhouse gases (CH_4, N_2O, CO_2) trapped in ice cores; oxygen and hydrogen isotopes of cellulose from trees; silicon and oxygen isotopes of silica from diatoms are also studied routinely. It is out of the scope of this paper to discuss the application of every isotope from different materials and environments. Therefore, as an example, we present a discussion on a few important isotopes from the marine realm used in paleoclimatological studies.

3.3.1 STABLE ISOTOPES OF OXYGEN AND CARBON IN CENOZOIC PALEOCEANOGRAPHY AND STRATIGRAPHY

The Cenozoic (past ~65 Ma) stable isotopic record of the oxygen and carbon has not only provided us the insight into global paleoceanographic signals but has been very useful for stratigraphic correlation of a large number of wells drilled for oil exploration. We shall first consider the basic premises of using oxygen and carbon isotopic record for long timescale, the major trends in the Cenozoic stable isotopic record, the limitations and lastly the future potential.

3.3.1.1 Oxygen Isotopes

Oxygen has three stable isotopes viz ^{16}O, ^{17}O, and ^{18}O with 99.763%, 0.0375%, and 0.1995% abundances, respectively. For paleoclimatological studies, the ratio $^{18}O/^{16}O$ is determined as ^{18}O has a higher abundance than ^{17}O and greater mass difference with ^{16}O. It was the Nobel laureate Harold Urey who in his classic paper published in the Journal of Chemical Society introduced the field of stable isotopic geochemistry (Urey, 1947). Urey was able to quantify the effect of temperature on oxygen isotope fractionation between calcium carbonate and water and came with the extraordinary idea that the isotopic composition of carbonate material could be used as a proxy for paleotemperature. Thereafter, McCrea (1950) studied the low temperature calcite–water oxygen isotopic fractionation and came out with the first empirical relationship between temperature and $\delta^{18}O$. However, these studies were based on inorganically precipitated calcites. Epstein et al. (1953) studied the biogenically precipitated calcite for establishing similar fractionation relationships. These workers gave an empirical relationship between the isotopic composition of water and temperature by growing mollusks in water at different temperatures. The oxygen isotope record of marine carbonates is a function of the isotopic composition of the ambient seawater besides temperature at which the calcification takes place. Emiliani (1955) used these studies to reconstruct the Pleistocene climatic cycles from the deep sea sediment cores. Another important study in this context was that of Craig (1965) who modified Epstein's equation and suggested corrections. Shackleton (1974) did an initial study of the T–$\delta^{18}O$ relationship in benthic foraminifera *Uvigerina*. Erez and Luz (1983) were among the first to derive temperature–$\delta^{18}O$ relationship in the tests of planktonic foraminifera *Globigerinoides sacculifer*. Bemis et al. (1998) did culture experiments on planktonic foraminiferal species *Orbulina universa* (with symbiotic algae) and *Globigerina bulloides* (without symbiotic algae) and gave revised paleotemperature equations. They demonstrated the influence over oxygen isotope of the *G. bulloides* by test size and offset in oxygen isotopic equilibration of *O. universa* introduced by the algal symbionts. Such studies have helped refine the paleoceanographic models based on isotopic analyses of the tests of various species. The researchers all over the world realized the importance of these empirical relationships as they provided a very powerful tool to infer the paleotemperature of the ambient water in which the ancient geological materials were formed. In most of the cases, the geological materials were the shells of macro- or microorganisms which were supposed to have grown in a medium whose paleotemperatures were to be estimated. The approximate temperature coefficient is –0.25‰ per °C, i.e., $\delta^{18}O$ of carbonate decreases by 0.25‰ for every 1 °C rise in temperature (Erez and Luz, 1983). These authors determined the following empirical temperature equation by comparing the isotopic composition of the planktonic foraminifera *G. sacculifer* with the actual growth temperature:

$$T\ ^{\circ}C = 17.0 - 4.52\ \left(\delta^{18}O_c - \delta^{18}O_w\right) + 0.03\ \left(\delta^{18}O_c + \delta^{18}O_w\right)^2$$

where T, $\delta^{18}O_c$, $\delta^{18}O_w$, are the estimated temperature (in °C), the isotopic composition of the shell carbonate, and the seawater, respectively. But there are few limitations that inhibit the widespread application of paleotemperature scale. To apply the paleotemperature equation, we must know the $\delta^{18}O$ value of the seawater with which a given specimen of $CaCO_3$ has equilibrated. This is not easy to establish with certainty; because, the isotopic composition of seawater as a whole depends on the amount of ice stored on the continents, which gives rise to the so-called "ice-volume effect." When water evaporates from the ocean surface, the water vapor gets enriched in the lighter isotopes, as vapor pressure of $H_2{}^{16}O$ is more than $H_2{}^{18}O$. For example, at 20 °C, the $\delta^{18}O$ value of the vapor is

lower by 10‰ than the liquid phase. Kinetic effects also take place that further deplete the vapor phase in the heavier isotope during molecular diffusion in the boundary layer at the water–air interface. This kinetic fractionation is directly proportional to the relative air humidity (Gonfiantini, 1986) and inversely proportional to the wind speed (Merlivat and Jouzel, 1979). With progressive evaporation, isotopically lighter water gets locked in the form of continental ice sheets, and the remaining ocean water gets increasingly enriched with the heavier isotope. It is believed that during the Last Glacial Maximum, the average seawater $\delta^{18}O$ was 1.3‰ more than the present (Labeyrie et al., 1987; Fairbanks, 1989). Simultaneously, the sea level also fell by 120 m that resulted in a scale of 0.011‰ increase in $\delta^{18}O$ of marine carbonate for every meter fall in sea level, which can be used to reconstruct the sea level curve (Fairbanks and Matthews, 1978; Fairbanks, 1989). Presently, the temperature of sea water is independently determined using techniques like trace element ratio (Mg/Ca, Sr/Ca) of carbonates, alkenone unsaturation index, Tex_{86} (membrane lipid composition of single celled microorganisms), clumped isotope method, etc., which is then used to calculate the $\delta^{18}O$ of seawater using the paleotemperature equations. The $\delta^{18}O$ of seawater thus obtained is used to calculate the past salinity values using the $\delta^{18}O$–salinity relationships for specific oceanic regions (Tiwari et al., 2013 and references cited therein).

3.3.1.2 Carbon Isotopes

Carbon has two stable isotopes, namely, ^{12}C and ^{13}C with an abundance of 98.89% and 1.11%, respectively (Craig, 1953). Photosynthesis causes preferential uptake of ^{12}C due to the kinetic fractionation in the organic matter. Within the inorganic carbon system, "atmospheric CO_2—dissolved bicarbonate—solid carbonate," equilibrium fractionation causes enrichment in the heavier isotope in the carbonates. The carbonate equilibria in the marine system can be represented by the following equations (Faure, 1986):

$$CO_2\ (g) \leftrightarrow CO_2\ (aq.)$$

$$CO_2\ (aq.) + H_2O \leftrightarrow H^+ + HCO_3^-\ (aq.)$$

$$CaCO_3\ (s) + H^+ \leftrightarrow Ca^{2+}\ (aq.) + HCO_3^-\ (aq.)$$

Total dissolved inorganic carbon (DIC) comprises HCO_3^- (aq.), CO_3^{2-} and CO_2 (aq.). The equilibrium fractionation factors for carbon isotope in this system at 20 °C are (Emrich et al., 1970)

$$\alpha_{CaCO_3(s)-HCO_3^-\ (aq.)} = 1.00185$$

$$\alpha_{HCO_3^-\ (aq.)-CO_2\ (g)} = 1.00838$$

$$\alpha_{CaCO_3(s)-CO_2\ (aq.)} = 1.01017$$

At low temperatures, the largest fractionation occurs between the dissolved CO_2 and the bicarbonate ion. The bicarbonate ion is the dominant species at the prevailing pH of seawater and DIC can be conveniently approximated by HCO_3^- (aq.). The temperature coefficient shows 0.035‰ increase of $\delta^{13}C$ per degree Celsius increase in temperature (Grossman, 1984; Emrich et al., 1970). Thus temperature has a negligible effect on $\delta^{13}C$ of calcite.

The $\delta^{13}C$ of the planktonic foraminiferal tests are also very valuable in ranking them according to the depth. This is possible because of the presence of a vertical gradient in the total dissolved CO_2 of the oceans (Kroopnick, 1985; Berger and Vincent, 1986). This gradient is a function of the biological activity and productivity at various depths in the water column. In the photic zone, the organic productivity is very high due to the phytoplanktons and thus the isotope of carbon used in this process is mostly the lighter isotope ^{12}C. Thus, the surface waters become enriched in ^{13}C and accordingly the planktonic foraminifera calcifying their test in isotopic equilibrium with sea water has higher $\delta^{13}C$. As one goes into the thermocline and deeper ocean, the biological productivity decreases and ^{12}C is released due to the decay of the organic matter and respiration thereby depleting the waters with ^{13}C. Thus the planktonic foraminifera living in the mixed layer, thermocline and below thermocline have progressively lower values of $\delta^{13}C$ in a region with well stratified water column and thus isotopic depth ranking can be made with the help of carbon isotope also. In summary, the planktonic foraminiferal oxygen and carbon isotope values are functions of their depth habitat and thus can be used as proxies for their isotopic depth ranking (Gasperi and Kennett, 1992). Such studies have been used to provide an isotopic depth ranking of a number of extinct foraminifera. There are many publications that successfully utilized this trait to infer the depth, thickness of the thermocline, and mixed layer during the Cenozoic. For example, Srinivasan and Sinha (1998, 2000), based on the Neogene planktonic foraminiferal biostratigraphy and isotopic depth ranking of planktonic foraminiferal species *Pulleniatina spectabilis*, an extinct species, inferred the closing of Indonesian seaway to thermocline water during the early Pliocene.

3.3.1.3 Oxygen Isotope Stratigraphy

The advent of the Deep Sea Drilling Project (DSDP) in 1968 was a major step in the development of Cenozoic stable isotope record and later resulted into a robust chemostratigraphic application on marine strata for worldwide correlation. An important aspect of the Cenozoic oxygen isotope record is its dependence on the global ice volume, which is termed "ice-volume effect" as explained in preceding sections. During glacial intervals, when the global ice volume increases, a large portion of the ocean water is locked in the form of polar ice sheets which are depleted in the heavier isotope of oxygen (^{18}O). Thus, the resultant effect during glacial interval is enriched ocean waters and depleted glacial ice with respect to the heavier isotope ^{18}O. The foraminifera calcifying their test in isotopic equilibrium with sea water during glacial times are thus enriched in ^{18}O as compared to those calcifying during interglacial intervals. Usually, benthic foraminifera are used as they, unlike planktonic, are not affected by short term temperature and salinity fluctuations (Shackleton and Opdyke, 1973). This leads to an oxygen isotope curve whose trends parallel the glacial–interglacial fluctuation, i.e., the changing global ice volumes. This phenomenon has resulted in the establishment of the marine oxygen isotope stages (MIS) for the later part of the Cenozoic while efforts are being made to extend the record back in time with more and more advancements of techniques. Several workers have stacked together $\delta^{18}O$ values of foraminifera from several well dated deep sea records using the orbitally forced ice-volume tuning to obtain global, high-resolution isotope chronostratigraphic curves (Imbrie et al., 1984; Pisias et al., 1984; Prell et al., 1986; Martinson et al., 1987; Imbrie et al., 1992; Lisiecki and Raymo, 2005). Such curves are not only used for global correlation but also as a relative dating method. The latest stack LR04 based on 57 deep sea records of $\delta^{18}O$ of benthic foraminifera is by Lisiecki and Raymo (2005) that spans for the past 5.3 Ma (Fig. 1).

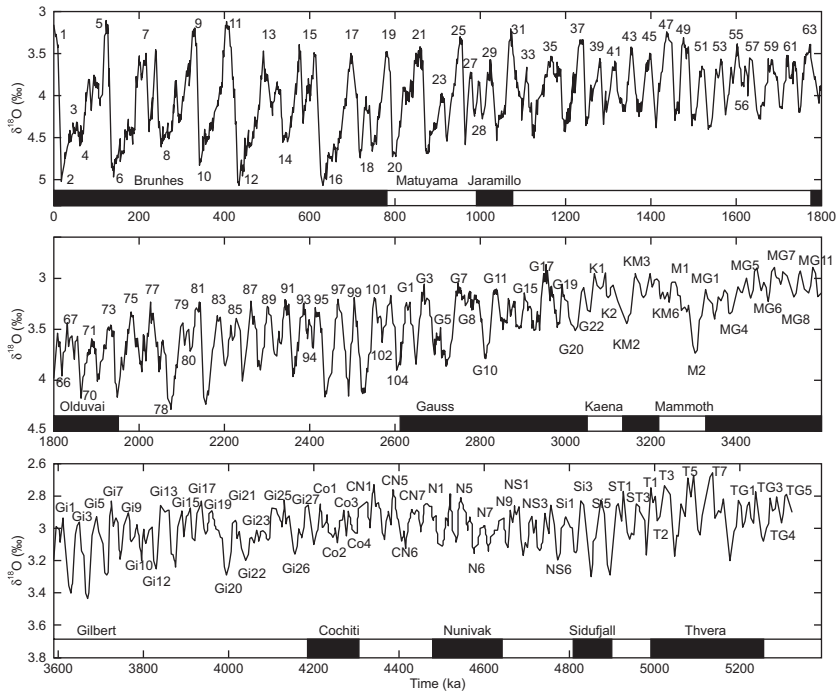

FIGURE 1

The oxygen isotope stratigraphy curve (LR04 stack) based on 57 stacked records of $\delta^{18}O$ values of benthic foraminifera spanning the past ~5.3 Ma.

Reprinted Lisiecki and Raymo (2005); Copyright 2005, with permission from John Wiley and Sons.

MIS 1 represents the Holocene and higher numbers indicate successively older periods with odd numbers depicting warmer stages and even numbers depicting colder stages. In addition, the later interglacial stages have been subdivided into separate warmer and colder episodes. For example, the MIS 5 is subdivided into five substages with 5a, 5c, and 5e as warmer conditions while 5b and 5d are colder intervals. Recently, decimal notation has been introduced to denote the isotopic substages so that the warmer episodes have odd numbers while the colder one possess even numbers. So, the MIS 5a, 5c, and 5e becomes 5.1, 5.3, and 5.5 respectively while the MIS 5b and 5d become 5.2 and 5.4 respectively. This scheme is followed till MIS 104 (~2.6 Ma). Thereafter, the isotopic stages are identified using the magnetic subchrons in which they appear. For example, the MIS G1 refers to the first warm episode in the Gauss subchron while the MIS G2 denotes the next colder episode; odd and even numbers again referring to the warmer and colder periods respectively. A distinctive feature of the oxygen isotope curve is the presence of the sawtooth pattern with the most rapid changes occurring at the termination of the glacial stages. These rapid changes from glacial to interglacial periods are called as "Terminations" and constitute major "events" in the oxygen isotope stratigraphy. For example, Termination 1 at ~14,000 years ago (Lisiecki and Raymo, 2005) is the rapid decline in $\delta^{18}O$ values at the end of the last glacial period, i.e., MIS 2.

3.3.1.4 Oxygen Isotopic Variation of Planktonic Foraminifera in Ocean Water Column

Though there is no strict rule to demonstrate the variation of $\delta^{18}O$ and $\delta^{13}C$ in the tests of planktonic foraminifera in the upper ocean water columns in the world's oceans, there is some agreement about the pattern of stable isotope composition if the water column is well stratified. The upper layer of the oceans receives kinetic energy from winds and heat energy from the sun. Due to this, the upper layer is well mixed and attains a uniform temperature. In the low latitudes this temperature is higher due to high amount of radiation received. This "mixed layer" can range in thickness from a few meters to few tens of meters and is characterized by a uniform temperature, i.e., the temperature does not decrease with depth within this layer. Below this mixed layer is the thermocline, a zone where the temperature declines sharply and reaches low values. Below the thermocline, the temperature declines very slowly till the bottom of the ocean is reached. This temperature distribution has implications on the oxygen isotopic composition of planktonic foraminifera. It is now well established that planktonic foraminifera are depth stratified in the upper ocean water columns. Several attempts were made to understand the distribution pattern with the help of plankton tows (Berger, 1969; Bé et al., 1973), sediment trap (Kahn and Williams, 1981; Fairbanks et al., 1982; Curry et al., 1983; Sautter and Thunell, 1991), and core top (Hemleben et al., 1989; Bijma et al., 1990). As described in the previous section, the oxygen isotope fractionation between sea water and calcium carbonate of the foraminifera is dependent on the ambient temperature in a way that lower the temperature of ambient water, more enrichment of the heavier isotope (^{18}O) takes place, i.e., $\delta^{18}O$ will be higher in $CaCO_3$. In a nutshell, the $\delta^{18}O$ of the planktonic foraminiferal test calcified in isotopic equilibrium indicates the temperature and isotopic composition of the sea water in which it lived (Gasperi and Kennett, 1992). Due to this relationship, the planktonic foraminifera residing at various depths in the ocean water column have different $\delta^{18}O$ values. Those residing in the warm mixed layer have lower values of $\delta^{18}O$ than those living in or below the thermocline. This property of depth (temperature) relationship with $\delta^{18}O$ values has been used to rank the extinct species also according to the depth habitat (Gasperi and Kennett, 1992; Douglas and Savin, 1978; Keller, 1985; Savin et al., 1985; Barrera et al., 1985).

3.3.1.5 Use of Oxygen and Carbon Isotopes in Upwelling Systems

The isotopic depth ranking as described in the preceding section can be used to detect the upwelling intervals in regions affected by seasonal upwelling. The planktonic foraminifera are depth stratified and their isotopic composition can be used to rank them according to depth. In the case of upwelling, the stratification of the water column is disturbed and surface waters are invaded by the cold, nutrient-rich waters. The invasion introduces two events, namely, the temperature gradient is reduced to minimum and the isotopic composition of the thermocline becomes uniform. Under such conditions, the foraminifera calcifying their tests in isotopic equilibrium with ambient water will have similar values of $\delta^{18}O$ and $\delta^{13}C$. Thus, if a time series data are obtained for the oxygen and carbon isotopic composition of shallow (mixed layer) and deep dwelling (thermocline and below) planktonic foraminifera, then the maximum divergence in the isotopic values indicate well-stratified water column while the minimum divergence or convergence indicate the upwelling conditions. Steens et al. (1992) studied the $\delta^{18}O$ and $\delta^{13}C$ of planktonic foraminiferal species including surface dwelling *G. bulloides* and the thermocline dwelling *Neogloboquadrina dutertrei* from the Hole 728A (ODP 117) located at a typical seasonal upwelling region of the Arabian Sea close to the Oman margin. These authors

interpreted the mixing of the water column during upwelling situations when the isotopic values of the two species converge or have minimum difference and diverge during well-stratified conditions. The difference in $\delta^{13}C$ isotope distribution between the two species was found to be smallest within the upwelling areas (Steens et al., 1992). These authors also showed that from isotopic stage 2 till stage 11, the upwelling was stronger during interglacial periods, and that upwelling intensified downcore for the same period. In older sediments (stages 12 and 13), the signal from the upwelling indicators were found to be reversed, showing stronger upwelling during glacial (Steens et al., 1992) periods.

3.3.1.6 Major Trends in Cenozoic Oxygen Stable Isotopic Record

Perhaps one of the best curves to show the overall major trends in the Cenozoic oxygen isotopic record is by Miller et al. (1987) as shown in Fig. 2. It shows the composite $\delta^{18}O$ record of the last 70 Ma. As discussed previously, the curve shows the pattern of global ice volume and deep-sea temperature variations (benthic $\delta^{18}O$ value) since the beginning of the Cenozoic.

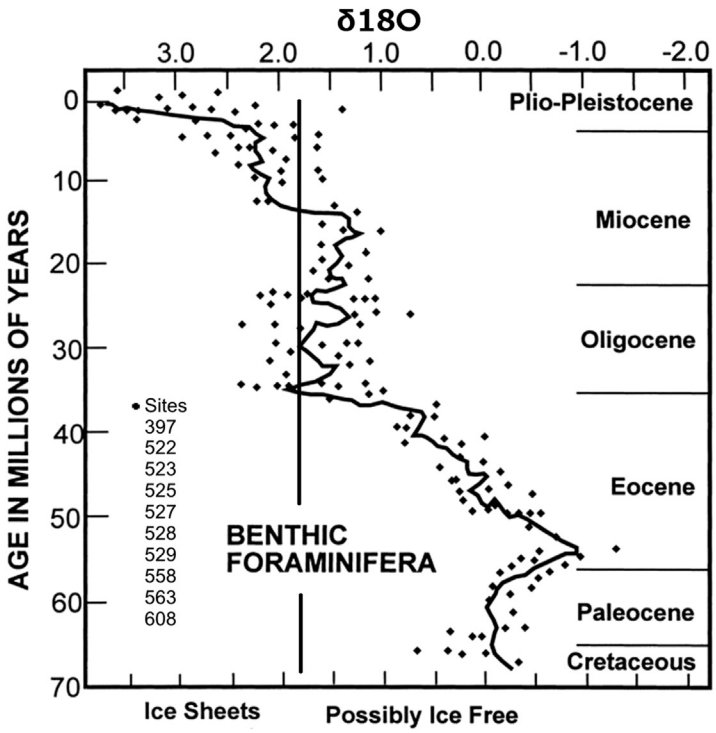

FIGURE 2

Cenozoic $\delta^{18}O$ record from the Atlantic Deep Sea Drilling Project sites. The vertical line is at 1.8‰ indicating the periods when the earth was either ice free or had major ice sheets.

Reprinted from Miller et al. (1987); Copyright 1987, with permission from John Wiley and Sons.

The minimum $\delta^{18}O$ value is observed at around ~55 Ma (million years ago)—a period known as the Paleocene-Eocene Thermal Maxima. Then onward, a long-term cooling trend is indicated by a steady increase in $\delta^{18}O$ values interrupted by times of relatively rapid change. This trend continues till the base of the Oligocene; after which, the cooling trend is not enhanced but remains steady till the Middle Miocene. After the Middle Miocene, the cooling trend is more significant and reaches the maximum values in the late Miocene. From the late Miocene to early Pliocene, again the steady state is maintained followed by a sharp increase in cooling trend during late Pliocene and Pleistocene. The steep increase in the isotopic values of the early Eocene–Oligocene boundary probably reflect the major ice cap expansion (Antarctic glaciation) event in the Cenozoic (Miller et al., 1987; Barrett et al., 1987). Later increases in the Middle Miocene and Late Pliocene indicate the subsequent growth of the ice volume with Arctic ice sheet coming into existence during the late Pliocene (Haug and Tiedemann, 1998). The high-resolution data superimposed over the long-term trends indicate Milankovitch forcing on the ice volume and all the three cycles of eccentricity, obliquity, and precession have been detected on a large number of deep sea cores.

3.3.1.7 Cenozoic Carbon Isotopic Record

Compared to the Cenozoic oxygen isotopic record, the interpretation of the carbon isotopic record has not been simple owing to its intrinsic interaction with the biological activity. The early work of Shackleton and Kennett (1975) provided an overview of the Cenozoic carbon isotopic record generated from planktonic and benthic foraminifera from DSDP sites 277, 279, and 281 from the southwest Pacific Ocean. While there is a general positive $\delta^{18}O$ shift from Paleocene to Pleistocene, no long term trend exists in the $\delta^{13}C$ record (Williams et al., 1988). While the oxygen isotope trend in the Neogene has been explained as the result of changing ice volume, initiation of major glaciations, waxing and waning of ice sheets, etc., the exact reasons for the shift in the carbon isotope record are not explained (Williams et al., 1988).

Kennett (1986) interpreted the Neogene $\delta^{13}C$ changes to have been caused by average oceanic compositional changes resulting from fractionation between continental and oceanic organic carbon reservoirs. Loutit et al. (1983) and Woodruff and Savin (1985) showed the existence of correlation between changes in Neogene carbon isotopic values and sea level as inferred from the onlap-offlap curve of Vail and Hardenbol (1979). During large-scale marine transgression corresponding to eustatic sea level rise during interglacials, the exposed land areas are reduced world over and continental shelves increase in size, which supports a diversity of organisms. Such organisms, their shell growth, and subsequent changes in food chain result in the removal of organic carbon from the ocean waters, which gets accumulated on the continental shelves and ocean waters became more enriched in ^{13}C. On the other hand, during a eustatic fall of sea level leading to large scale marine regression during glacial periods, large areas of the continental shelves are exposed and subjected to erosion. This results in the supply of organic carbon to the ocean basins and as a result, the oceans became more depleted in ^{13}C. Here, the scale of transgression and regression is of prime importance and should be large enough to cause the changes in organic carbon exchange at global level. Small rise and fall of sea level is reflected in the oxygen isotope values due to ice-volume effect but the same is not paralleled by the carbon isotopic fluctuation. The magnitude of the $\delta^{13}C$ change depends upon the areas of shallow shelves covered or exposed by a given change in sea level. This in turn, is directly related to the hypsometry (elevation relative to the sea level) of the continental margins and the magnitude of the sea-level change (Kennett, 1986).

3.3.1.7.1 Late Early to Early Middle Miocene Positive $\delta^{13}C$ Shift

In the early part of the Neogene, a positive shift in the $\delta^{13}C$ of 1‰ was demonstrated by Vincent and Berger (1985), which they termed as the "Monterey Carbon Isotope Excursion." Kennett (1986) explained this and agreed with several other workers regarding the explanation for this positive shift due to a global marine transgression (Loutit et al., 1983; Woodruff and Savin, 1985). Vincent and Berger (1985) stated that during this interval, large-scale transgression occurred throughout the circum-Pacific region, and, as explained above, huge amount of organic carbon was extracted from the oceans. This had resulted in the deposition of organic and phosphate-rich sediments within the Monterey Formation of California (John et al., 2002) throughout the Pacific margin. Vail and Hardenbol (1979) documented a period of coastal onlap that began at about 19 Ma (million years ago) and terminated about 14 Ma, and was contemporaneous with the interval containing the especially positive $\delta^{13}C$ values (Kennett, 1986). This positive carbon shift also corresponds to Early Neogene climatic optimum or warmth as reflected from the negative oxygen isotope excursion of benthic and planktonic foraminifera. Due to this climatic optimum, large amount of organic biomass in the form of forests could have grown on the continents and have contributed to the positive $\delta^{13}C$ values during this interval (Kennett, 1986). This climatic optimum was followed by middle Miocene global cooling as explained in the previous section corresponding with a negative carbon isotope excursion.

3.3.1.7.2 Late Miocene Negative Carbon Isotope Shift

The latest Miocene at 6.2 Ma is marked by a distinct, rapid shift of $\delta^{13}C$ up to–0.75‰ in all of the southwest Pacific sites, both in the benthic and planktonic records (Kennett, 1986). This depletion in $\delta^{13}C$ was followed markedly by low values during much of the remainder of the late Neogene, which led to the suggestion that it was "permanent" (Kennett, 1986; Keigwin, 1979). This well-known late Miocene carbon isotope shift is recorded throughout the Indo-Pacific and South Atlantic (Kennett, 1986; Keigwin, 1979; Bender and Keigwin, 1979; Loutit and Kennett, 1979; Keigwin and Shackleton, 1980; Vincent et al., 1980; Haq et al., 1980; Hodell and Kennett, 1984). This shift was of a very short duration and was assigned an age of ~6 Ma by Haq et al. (1980) and of 6.2 Ma by Loutit and Kennett (1979). Loutit and Keigwin (1982) summarized a number of global events associated with this negative carbon shift which included a global lowering of the sea level.

3.3.1.7.3 Messinian Salinity Crisis and Negative Carbon Shift

The world wide lowering of the global sea levels causing the negative carbon isotopic shift was also associated with isolation of the Mediterranean due to the closure of the Gibraltar Strait and resulted into the "Messinian Salinity Crisis" (Cita, 1982). The expansion of the ice sheets resulted in intensive circulation of bottom water and ocean ventilation (Kennett, 1986). Estimates of the magnitude of the marine regression are similar, ranging from 40 to 80 m (Loutit and Kennett, 1979; Berggren and Haq, 1976; Cita and Ryan, 1979).

3.3.1.8 Limitations

3.3.1.8.1 Vital Effects

The biological activities of foraminifera give rise to several effects due to which its calcite is not precipitated in isotopic equilibrium with the ambient water. The consequent offsets of isotopic values of the tests are collectively referred to as the "*Vital Effects*," which can be either metabolic or kinetic (McConnaughey, 1989a,b). Metabolic effects are due to the inclusion of ambient dissolved carbon

and oxygen, which are produced during the respiration or photosynthesis into the calcite shell. Preferential uptake of lighter isotopes during the hydration and hydroxylation of CO_2 that are generally associated with rapid calcification constitute the kinetic effects. Vital effects, thus, are a result of the processes like respiration, ontogeny, and secretion of gametogenic calcite, etc. Lower $\delta^{18}O$ values result when respiration products depleted in the heavier isotopes (Lane and Doyle, 1956) are utilized for shell formation. This is the reason for the progressive $\delta^{18}O$ enrichment from juvenile to mature chambers as higher metabolic rates in the juvenile specimen as compared to an adult would cause the stronger depletions (Wefer and Berger, 1991). Planktonic foraminifera inhabit different depths at various stages of their ontogeny. Foraminifera secrete shells at deeper and cooler waters toward the end of their life cycles resulting in higher $\delta^{18}O$ values (Bouvier-Soumagnac and Duplessy, 1985). Toward the end of their life cycle, foraminifera also secrete gametogenic calcite. Foraminifera move to deeper, cooler waters before gamete release and secrete a layer of calcite over its shell. This calcite layer with higher $\delta^{18}O$ values can comprise 18–28% of the shell mass of foraminifera (Bé, 1980). Furthermore, the $\delta^{18}O$ decreases with increasing irradiance, which causes enhanced photosynthesis that leads to a higher rate of shell formation and hence stronger kinetic fractionation (Spero and Lea, 1993; Wefer and Berger, 1991). The $\delta^{18}O$ in foraminiferal carbonate decreases with increasing carbonate ion concentration that was also ascribed to biological, kinetic fractionation effect (Spero et al., 1997) as this effect was also observed in rapidly precipitating inorganic $CaCO_3$ (McCrea, 1950). The disequilibria due to the vital effects can be avoided by choosing those species, which are known to precipitate their shells in equilibrium with seawater and by picking mature shells from a particular size range.

3.3.1.8.2 Effect of Diagenesis

This section addresses the studies involving long term stable isotope record of benthic and planktonic foraminifera from stratigraphic columns where foraminiferal carbonate is supposed to have undergone diagenesis. Our entire premise of using stable isotopes of foraminifera for paleoceanographic interpretation is based on the belief that the long term burial and diagenesis will not affect the primary isotopic values. Although the oxygen isotopic values may be affected by diagenesis involving recrystallization and significant dissolution (Baker et al., 1982; Elderfield and Gieskes, 1982; Killingley, 1983), it has been observed that diagenesis is usually absent or negligible in sediments of Pleistocene–Pliocene age (Williams et al., 1988). Anderson and Arthur (1983) stated that the $\delta^{13}C$ values of marine carbonates are thought to be less affected by diagenesis than the oxygen isotope values because of the differences in respective reservoirs for potential isotopic changes. The controlling factor for the diagenetic effect on isotopic composition is the $\delta^{18}O$ of the pore water. Williams et al. (1988) found that unless the diagenesis is severe, the $\delta^{18}O$ pattern or signal is not obliterated in many sections. Presence of significant amounts of organic matter can affect the $\delta^{13}C$ values of marine carbonates.

In general, the $\delta^{13}C$ values of the marine carbonates can be affected only when the recrystallization occurs in the presence of pore water bicarbonate in which $\delta^{13}C$ has been considerably altered due to the addition of ^{12}C from organic matter oxidation and microbial activity. Recently, Edgar et al. (2013) concluded that even extensive recrystallization of benthic foraminiferal calcite results in minimal shifts from primary $\delta^{18}O$ and $\delta^{13}C$ values.

Thus, the Cenozoic oxygen and carbon isotopic records of foraminifera have a tremendous scope of paleoceanographic and stratigraphic studies and also in the hydrocarbon exploration where at times biostratigraphic datum do not serve the purpose or have limitations.

3.3.2 NITROGEN ISOTOPES OF SEDIMENTARY ORGANIC MATTER AS DENITRIFICATION INDICATOR

Nitrogen has two isotopes viz ^{14}N and ^{15}N with abundances of 99.64% and 0.36%, respectively. Nitrogen gets into the biological systems via "Nitrogen Fixation," which involves the reduction of N_2 to ammonia (NH_3), NH_4^+, or any other nitrogen compound by the microorganisms (e.g., *Rhizobium*) under anaerobic conditions. Nitrogen fixing bacteria are called as diazotrophs. "Nitrification" is the conversion of the NH_3, NH_4^+ to nitrate (NO_3^-) or nitrite (NO_2^-) by the bacteria of *Nitrosamonas* and *Nitrobacter*. If ammonia is directly assimilated, then it is called as "ammonia assimilation" but free ammonium ions cannot exist for long in the aerobic soils as they are oxidized to nitrate or nitrite and hence nitrification is the dominant step. Dentrification is the process by which nitrate is reduced to any gaseous nitrogen species, generally N_2 or nitrous oxide (N_2O) under the anaerobic conditions (Deuser et al., 1978; Naqvi, 1987).

In the world's oceans, there are three regions that support perennial anaerobic conditions in the water depths of ~250–1250 m, also called as oxygen minima zone (OMZ) where oxygen concentration fall below 0.05 ml/l (Wyrtki, 1971; Deuser et al., 1978; Naqvi, 1987). This is due to the occurrence of high overhead productivity that consumes the available oxygen during their descent/degradation. These regions are the eastern tropical North Pacific, eastern tropical South Pacific, and the Arabian Sea (Christensen et al., 1987; Naqvi, 1987, 1994). Due to the lack of oxygen in the OMZ, the NO_3^- acts as an electron acceptor and is reduced by the anaerobic bacteria for the decomposition of organic matter. During this process, they preferentially consume NO_3^- with lighter isotope (^{14}N), thus enriching the residual nitrate in the heavier isotope, which gets upwelled to the sea surface and is taken by the organisms as a nutrient. The $\delta^{15}N$ of the organic matter is governed by the isotopic composition of the source NO_3^- that is upwelled from below and fractionation experienced by NO_3^- during its uptake by the phytoplanktons (Altabet and Francois, 1994). In the oxic waters of the euphotic zone, the $\delta^{15}N$ of the nitrate is 5–6‰ (Liu and Kaplan, 1989) whereas, in the regions receiving waters upwelled from the OMZ the $\delta^{15}N$ is in the excess of 18‰ (Cline and Kaplan, 1975) that explains the highly enriched $\delta^{15}N$ values observed in the particulate organic matter. This enriched $\delta^{15}N$ signature is preserved even when the organic matter settles down and gets preserved in sea sediments (Saino and Hattori, 1987). Thus, a high $\delta^{15}N$ can be related to increased dentrification, which in turn is controlled by the climate induced productivity increase (Ganeshram et al., 1995).

In the Arabian Sea, the OMZ is due to the high oxygen consumption below the thermocline for the oxidation of organic matter supplied by the high overhead surface productivity. The sluggish flow of the oxygen-poor intermediate water (Olson et al., 1993; You and Tomczak, 1993) along with a strong tropical thermocline (due to relatively high sea surface temperature that prevents mixing of the oxygen rich surface waters with the deeper waters) maintains the OMZ (Qasim, 1982). As an example, a dentrification record from the western Arabian Sea that reflects overhead surface productivity related to the intensity of the Southwest (SW) Monsoon winds is presented herein. The surface circulation of the western Arabian Sea is controlled by the seasonal reversal of monsoon winds. During the boreal summer, the summer or the SW Monsoon winds blowing along the Somali and Omani coast induce intense upwelling with upwelling velocities close to 3×10^{-3} cm/s and an upwelling transport of 1.5–2 Sv in the upper 50 m (Smith and Bottero, 1977; Shi et al., 2000). The reasons attributed for such intense coastal upwelling is the Ekman divergence due to the flow of strong winds parallel to the coast. As the surface water moves away from the coast, water from below upwells to occupy its place. The offshore upwelling takes place due to the strong positive wind stress curl to the NW of the axis of the Somali jet, which

is a low level cross-equatorial jet (Smith and Bottero, 1977). The upwelling injects nutrients into the euphotic zone leading to the increase in the productivity. The typical productivity values for the western Arabian Sea are 2.0 gC/m^2/day (gram carbon per meter square per day) during the SW monsoon period and 0.5 gC/m^2/day during the intermonsoon period (Codispoti, 1991; Barber et al., 2001). The Fig. 3 shows the $\delta^{15}N$ variations for the past 20,000 years from the western Arabian Sea (Altabet et al., 2002; Tiwari et al., 2010).

Altabet et al. (2002) analyzed the nitrogen isotope ratio ($\delta^{15}N$), nitrogen content, and chlorin (a pigment found in algae and plants, e.g., chlorophyll is a magnesium containing chlorin) abundance of sediment cores from Oman continental margin at millennial scale. Nitrogen and chlorin abundances are manifestations of the overhead surface productivity, which is controlled by the SW monsoon wind intensity. Altabet et al. (2002) found that all the three proxies varied in unison leading them to propose that $\delta^{15}N$ is a productivity indicator at least on century to millennial timescales. Their record also found a close correlation with the Greenland Ice Sheet Project 2 (GISP2) temperature record (Grootes and Stuiver, 1997) signifying strong teleconnection between the SW monsoon intensity and high latitude climate change. As evident from Fig. 3, during the Holocene (past 11,700 years), the $\delta^{15}N$ values show a maximum at around 10,000 years after which they decline slightly and then increase uniformly since 9000 years till the core top. It implies that an episode of monsoon intensification took place during early Holocene coinciding with the maximum summer insolation. Thereafter, the SW monsoon intensity did not decrease during the rest of Holocene unlike insolation that declined monotonically. Tiwari et al. (2010) also determined $\delta^{15}N$ values from a nearby sediment core (Fig. 3). The trend exhibited by the

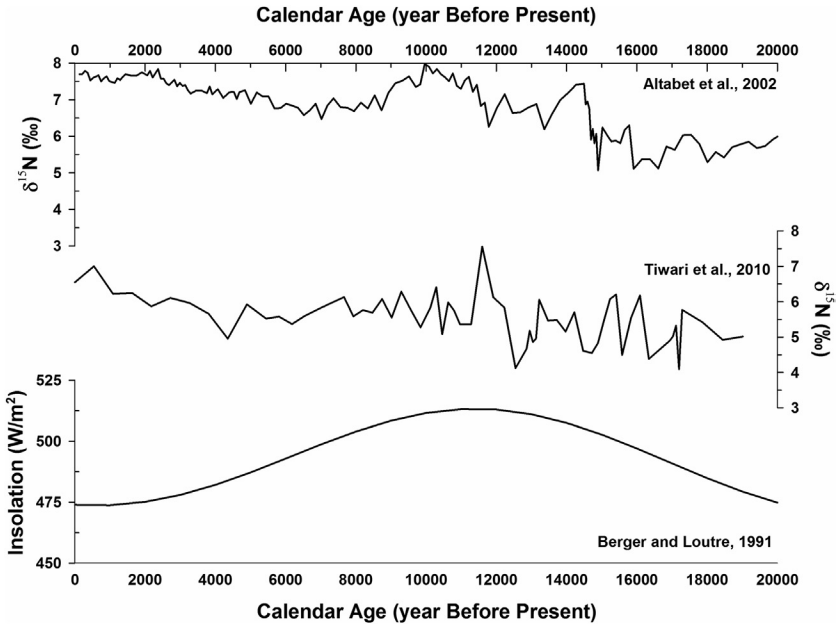

FIGURE 3

Denitrification records from the western Arabian Sea for the past 20,000 years.

Data taken from Berger and Loutre (1991), Berger (1992), Altabet et al. (2002), and Tiwari et al. (2010).

$\delta^{15}N$ values of the Tiwari et al. (2010) matches with that exhibited by Altabet et al. (2002) corroborating the fact that the SW monsoon did not decline during the Holocene. Thus, during the Holocene, SW monsoon did not follow insolation, signifying the importance of understanding internal feedbacks on nitrogen budgets.

3.3.3 CARBON ISOTOPES OF SEDIMENTARY ORGANIC MATTER AS PROVENANCE INDICATOR

The concentration of the organic carbon is a widely used proxy in the field of paleoclimatology to reconstruct the past productivity variability that can be related to various climatic factors. But this organic matter can be from marine as well as terrestrial sources. Therefore, it is important to ascertain the source of the organic matter for precise interpretation. Currently, the $\delta^{13}C$ value of the atmospheric CO_2 is around −8‰ (Hoefs, 2009). Plants preferentially incorporate ^{12}C due to the kinetic isotope effect during the photosynthesis. A two step model is proposed to explain the kinetic fractionation of carbon isotopes during photosynthesis that involves (1) fractionation during the uptake of gaseous CO_2 by the leaves through stomata and (2) then the fractionation during the carbon fixation using a suitable enzyme (Farquhar et al., 1989). In different categories of plants, the carbon fixation reaction involves different enzymes following diverse pathways. The first category comprising 90% of present day plants is of "C3 plants" that use an enzyme called as "ribulose bisphosphate carboxylase oxygenase (RuBisCO)." Such plants use what is known as Calvin Cycle wherein three molecules of CO_2 finally produce one molecule of a carbohydrate which is a three-carbon sugar phosphate molecule. The $\delta^{13}C$ values of C3 plants range from −20‰ to −36‰ with a mean value of −27‰ (Farquhar et al., 1989). The other important pathway is the Hatch–Slack Cycle which occurs in plants called as the C4 plants. The first stable compound of this pathway is a four-carbon compound namely oxaloacetic acid, hence such plants are called as C4 plants. This pathway utilizes water much more efficiently. Hence the C4 plants readily colonize the arid environments. The main enzyme used in this cycle is the PEP carboxylase that fractionates carbon isotopes much less than the RuBisCO leading to much higher $\delta^{13}C$ values than the C3 plants. The $\delta^{13}C$ values of the C4 plants range from −9‰ to −17‰ with a mean value of −13‰ (Farquhar et al., 1989). The marine organic matter plants/phytoplanktons are enriched in the heavier isotope (higher $\delta^{13}C$ values) as compared to the C3 plants as equilibrium fractionation leads to the enrichment of ^{13}C in the dissolved bicarbonate ion (HCO_3^-) as compared to the gaseous CO_2 ($\alpha_{HCO_3^-\ (aq.)-CO_2\ (g)} = 1.00838$); at 20 °C; (Faure, 1986). This enriched HCO_3^- is used by phytoplanktons for photosynthesis due to its higher concentration than the dissolved CO_2 at the prevailing pH of the ocean leading to the higher $\delta^{13}C$ values of the marine organic matter. The $\delta^{13}C$ value of marine organic matter ranges from −11 to −39‰ and the mean value is −21‰ (Farquhar et al., 1989).

It is clear from this discussion that the $\delta^{13}C$ value of the organic materials from different sources overlap. Therefore, it is advisable to use $\delta^{13}C$ in combination with C/N ratio, which is the carbon to nitrogen ratio by weight of the organic matter. The elemental composition of phytoplanktons and zooplanktons were given by Redfield (1934, 1958) and are called as "Redfield ratios." The Redfield ratios for marine organic matter are carbon:nitrogen:phosphorus = 106:16:1 that yields a C/N value of 6.6. This estimate was revised by Takahasi et al. (1985) who gave the ratio as C:N:P = 122 (±18):16:1 that provide a range of 6.5–8.7 as the C/N ratio. The C/N ratio of recent sediments comprising marine

organic matter has a value of 8–10 whereas the ancient sediments have a value of 12–15 (Müller, 1977). In contrast, terrestrial sources exclusively possess some compounds such as cellulose, lignin, etc., that are rich in carbon and poor in nitrogen (protein) as compared to aquatic algae resulting in much higher C/N ratios. Organic matter derived from land plants has C/N values between 20 and 100 (Premuzic et al., 1982; Meyers, 1994). Diageneis of organic matter tends to lower the C/N ratio as nitrogenous compounds break down to produce ammonia, which is retained by clay minerals (Müller, 1977) whereas carbon in the form of CO_2 diffuses out.

As an example, new data from a sediment core—SK 274/4G—from the eastern Arabian Sea is presented here. The core—SK 274/4G—has a total length of 359 cm and was collected off Goa (13°59′45″ N; 72°0′24″ E) from a water depth of 1290 m. For the present study, the samples have been selected at every 5 cm. The Fig. 4 shows the $\delta^{13}C$ values of the sedimentary organic matter versus its C/N ratio that would help to identify the origin of the organic matter in the core.

Eastern Arabian Sea receives abundant surface runoff from the adjacent Western Ghats (*Sahyadri* Hills) that results in intense orographic precipitation during the SW monsoon. The monsoon winds also induce moderate upwelling in the coastal regions of the eastern Arabian Sea. The transfer of nutrients via upwelling and the surface runoff lead to the enhanced marine productivity. For the eastern Arabian Sea, the typical productivity values are 0.6 and 0.2 gC/m^2/day during the SW monsoon and the inter-monsoon periods, respectively (Bhattathiri et al., 1996). However, there is a possibility of considerable contribution of the terrestrial organic matter as well through the surface runoff.

The $\delta^{13}C$ values in this core vary from −19‰ to −21‰ indicative of predominantly marine phytoplankton and some contribution from the terrestrial organic matter. The C/N ratio of the present study varies from 8 to 32, which is indicative of the presence of both terrestrial as well as the marine organic matter due to its coastal location. This example also stresses the fact that instead of relying solely on $\delta^{13}C$ values or C/N ratios to determine the provenance of organic matter, it is helpful to use them in conjunction.

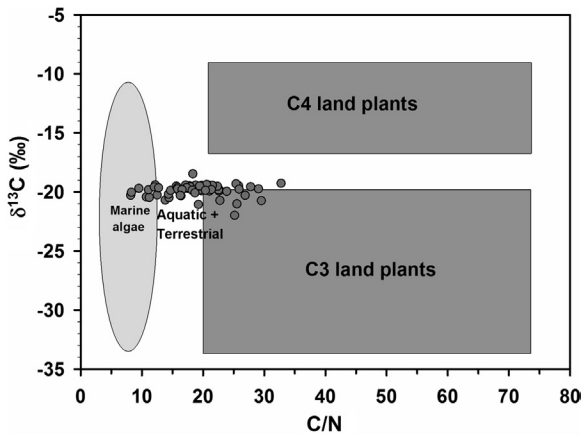

FIGURE 4

$\delta^{13}C$ values versus C/N ratios as indicator of the provenance of the organic matter; shaded areas approximately show the range of the $\delta^{13}C$ values for that particular group.

3.4 CONCLUSION

The stable isotopes of oxygen, carbon, and nitrogen are useful to reconstruct the past climatic and oceanographic changes. Besides, the oxygen isotopic stratigraphy of marine sediments provides a robust time frame work to correlate widely separated marine sections and also to correlate the paleoceanographic and paleoclimatic events. This helps us to interpret the cause and effect relationship among various events recorded in diversely located stratigraphic columns. The stable isotopic studies have become thus one of the most important tools in paleoceanographic and paleoclimatic studies. The aim of the paleoclimatology is far beyond the plain documentation of past climate changes. It will improve our understanding of the *mechanism* of climate variability including abrupt climate changes, especially under the greenhouse gases forcing expected toward the end of the century. It is necessary to determine the natural component to delineate the anthropogenic forcing to create viable models of future climate scenarios. Additionally, the trends/periodicities exhibited by the climatic phenomenon may indicate their future course. It would aid in gauging the severity, likely long-term effects, and possible consequences of changes.

ACKNOWLEDGMENT

MT is grateful to the Secretary, Ministry of Earth Sciences and Director NCAOR for their constant encouragement and support under the project Past Climate and Oceanic Variability (NCAOR Contribution no. 43/2014). DKS and MT thank ISRO-GBP Project for the financial support. AKS acknowledges DST Fast Track Project (SR/FTP/ES-85/2009) for the financial assistance. DKS and AKS thank Department of Geology, CAS in Geology, Delhi University for necessary facilities.

REFERENCES

Alley, R.B., 2000. The Younger Dryas cold interval as viewed from central Greenland. Quaternary Science Reviews 19, 213–226.

Altabet, M.A., Francois, R., 1994. Sedimentary nitrogen isotopic ratios as a recorder for surface ocean nitrate utilization. Global Biogeochemical Cycles 8, 103–116.

Altabet, M.A., Higginson, M.J., Murray, D.W., 2002. The effect of millennial-scale changes in Arabian Sea denitrification on atmospheric CO_2. Nature 415, 159–162.

Anderson, T.F., Arthur, M.A., 1983. Stable isotopes of oxygen and carbon and their application to sedimentologic and paleoenvironmental problems. In: Stable Isotopes in Sedimentary Geology M.A.

Arrhenius, S., 1896. On the influence of carbonic acid in the air upon the temperature of the ground. Philosophical Magazine 41, 237–276.

Baker, P.A., Gieskes, J.M., Elderfield, H., 1982. Diagenesis of carbonates in deep-sea sediments: evidence from Sr/Ca ratios and interstitial dissolved Sr^{2+} data. Journal of Sedimentary Petrology 52, 71–82.

Barber, R.T., Marra, J., Bidigare, R.C., Codispoti, L.A., Halpern, D., Johnson, Z., Latara, M., Goericke, R., Smith, S.L., 2001. Primary productivity and its regulation in the Arabian Sea during 1995. Deep-Sea Research Part II: Topical Studies in Oceanography 48, 1127–1172.

Barrera, E., Keller, G., Savin, S.M., 1985. Evolution of the Miocene ocean in the eastern North pacific as inferred from oxygen and carbon isotopic ratios of foraminifera. Geological Society of America, Memoir 163, 83–102.

Barrett, P.J., Elston, D.P., Harwood, D.M., McKelvey, B.C., Webb, P.N., 1987. Mid Cenozoic record of glaciation and sea level change on the margin of the Victorian land basin, Antarctica. Geology 15, 634–637.

Bé, A.W.H., 1980. Gametogenic calcification in a spinose planktonic foraminifer, *Globigerinoides sacculifer* (Brady). Marine Micropaleontology 5, 283–310.

Bé, A.W.H., Harrison, S.M., Lott, L., 1973. *Orbulina universa* in the Indian Ocean. Micropaleontology 19, 150–192.

Beck, N., Münnich, K.O., 1988. Freezing of water: isotopic fractionation. Chemical Geology 70, 168.

Bemis, B.E., Howard, J.S., Jelle, B., David, W.L., 1998. Reevaluation of the oxygen isotopic composition of planktonic foraminifera: experimental results and revised paleotemperature equations. Paleoceanography 13, 150–160.

Bender, M.L., Keigwin, L.D., 1979. Speculations about the Upper Miocene change in abyssal Pacific dissolved bicarbonate $\delta^{13}C$. Earth and Planetary Science Letters 45, 383–393.

Berger, A., 1992. Orbital Variations and Insolation Database. IGBP PAGES/World Data Center for Paleoclimatology Data Contribution Series # 92-007. NOAA/NGDC Paleoclimatology Program, Boulder CO.

Berger, A., Loutre, M.F., 1991. Insolation values for the climate of the last 10 million years. Quaternary Science Reviews 10, 297–317.

Berger, W.H., 1969. Ecological patterns of living foraminifera. Deep-Sea Research 16, 1–24.

Berger, W.H., Vincent, E., 1986. Deep-sea carbonates: reading the carbon isotope signal. Geologische Rundschau 75, 249–269.

Berggren, W.A., Haq, B.U., 1976. The Andalusian Stage (late Miocene): biostratigraphy, biochronology, and paleoecology. Palaeogeography, Palaeoclimatology, Palaeoecology 20, 67–129.

Bhattathiri, P.M.A., Pant, A., Sawant, S., Gauns, M., Matondakar, S.G.P., Mohanraju, R., 1996. Phytoplankton production and chlorophyll distribution in the eastern and central Arabian Sea in 1994–1995. Current Science 71, 857–862.

Bijma, J., Faber Jr., W.W., Hembleben, C., 1990. Temperature and salinity limits for the growth and survival of some planktonic foraminifera in laboratory cultures. Journal of Foraminiferal Research 20 (2), 95–116.

Bouvier-Soumagnac, Y., Duplessy, J.C., 1985. Carbon and isotopic composition of planktonic foraminifera from the laboratory culture, plankton tows and recent sediment: implications for the reconstruction of paleoclimatic conditions and of the global carbon cycle. Journal of Foraminiferal Research 15, 302–320.

Broecker, W.S., Thurber, D.L., Goddard, J., Ku, T.-L., Matthews, R.K., Mesolella, K.J., 1968. Milankovitch hypothesis supported by precise dating of coral reef and deep-sea sediments. Science 159, 297–300.

Broecker, W.S., Denton, G.H., 1990. The role of ocean-atmosphere reorganizations in glacial cycles. Quaternary Science Reviews 9, 305–341.

Cita, M.B., 1982. The Messinian salinity crisis in the mediterranean: a review. Alpine mediterranean Geodynamics series, vol. 7, American Geophysical Union, Washington. pp. 113–140.

Cita, M.B., Ryan, W.B.R., 1979. Late Neogene environmental evolution. In: von Rad, U., Ryan, W.B.R., et al. (Eds.), Init. Repts. DSDP, vol. 47 (Pt.1). U.S. Government Printing Office, Washington, pp. 447–459.

Christensen, J.P., Murray, J.W., Devol, A.H., Codispoti, L.A., 1987. Denitrification in continental shelf sediments has major impact on the oceanic nitrogen budget. Global Biogeochemical Cycles 1, 97–116.

Cline, J.D., Kaplan, I.R., 1975. Isotopic fractionation of dissolved nitrate during denitrification in the eastern tropical North Pacific Ocean. Marine Chemistry 3, 271–299.

Codispoti, L.A., 1991. Primary productivity and carbon and nitrogen cycling in the Arabian Sea. In: Smith, S.L., Banse, K., Cochran, J.K., Codispoti, L.A., Ducklow, H.W. (Eds.), Arabian Sea Process Study (M. E).

Coplen, T.B., 2011. Guidelines and recommended terms for expression of stable isotope-ratio and gas-ratio measurement results. Rapid Communications in Mass Spectrometry 25, 2538–2560.

Coplen, T.B., Kendall, C., Hopple, J., 1983. Comparison of stable isotope reference samples. Nature 302, 236–238.

Craig, H., 1953. The geochemistry of the stable carbon isotopes. Geochimica et Cosmochimica Acta 3, 53–92.

Craig, H., 1961. Standard for reporting concentrations of deuterium and oxygen-18 in natural waters. Science 133, 1833–1834.

Craig, H., 1965. Measurement of oxygen isotope paleotemperatures. In: Tongiorgi, E. (Ed.), Stable Isotopes in Oceanographic Studies and Paleotemperatures. Consiglio Nazionale delle Ricerche, Spoleto, Italy, pp. 161–182.

Curry, W.B., Thunnel, R.C., Honjo, S., 1983. Seasonal changes in the isotopic composition of planktonic foraminifera collected in Panama basin sediment traps. Earth and Planetary Science Letters 64, 33–43.

Dansgaard, W., Johnsen, S.J., Clausen, H.B., Dahl-Jensen, D., Gundestrup, N.S., Hammer, C.U., Hvidberg, C.S., Steffensen, J.P., Sveinbjörnsdottir, A.E., Jouzel, J., Bond, G., 1993. Evidence for general instability of past climate from a 250-kyr ice-core record. Nature 364, 218–220.

Deuser, W.G., Ross, E.H., Mlodzinska, Z.J., 1978. Evidence for and the rate of denitrification in the Arabian Sea. Deep-Sea Research 25, 431–445.

Douglas, R.G., Savin, S.M., 1978. Oxygen isotopic evidence for the depth stratification of Tertiary and Cretaceous planktonic foraminifera. Marine Micropaleontology 3, 175–196.

Edgar, K.M., Pälike, H., Wilson, P.A., 2013. Testing the impact of diagenesis on the $\delta^{18}O$ and $\delta^{13}C$ of benthic foraminiferal calcite from a sediment burial depth transect in the equatorial Pacific. Paleoceanography 28, 468–480.

Elderfield, H., Gieskes, J.M., 1982. Sr isotopes in interstitial waters of marine sediments from Deep Sea Drilling Project cores. Nature 300, 493–497.

Emiliani, C., 1955. Pleistocene temperatures. Journal of Geology 63, 538–578.

Emrich, K., Ehhalt, D.H., Vogel, J.C., 1970. Carbon isotope fractionation during the precipitation of calcium carbonate. Earth and Planetary Science Letters 8, 363–371.

Epstein, S., Buchsbaum, R., Lowenstam, H., Urey, H., 1953. Revised carbonate-water isotopic temperature scale. Geological Society of America Bulletin 64, 1315–1326.

Erez, J., Luz, B., 1983. Experimental paleotemperature equation for planktonic foraminifera. Geochimica et Cosmochimica Acta 47, 1025–1031.

Fairbanks, R.G., 1989. A 17,000-year glacio-eustatic sea level record: influence of glacial melting rates on the Younger Dryas event and deep ocean circulation. Nature 342, 637–642.

Fairbanks, R.G., Matthews, R.K., 1978. The marine oxygen isotope record in Pleistocene coral, Barbados, West Indies. Quaternary Research 10, 181–196.

Fairbanks, R.G., Sverdlove, M.S., Free, R., Wiebe, P.H., Bé, A.W.H., 1982. Vertical distribution and isotopic fractionation of living planktonic foraminifera from the Panama Basin. Nature 298, 841–844.

Farquhar, G.D., Ehleringer, J.R., Hubick, K.T., 1989. Carbon isotope discrimination and photosynthesis. Annual Review of Plant Physiology and Plant Molecular Biology 40, 503–537.

Faure, G., 1986. Principles of Isotope Geology, second ed. John Wiley and Sons. p. 589.

Fourier, J., 1824. Remarques générales sur les températures du globe terrestre et des espaces planétaires. Annales de chimie et de physique 27, 136–167.

Ganeshram, R.S., Pederson, T.F., Calvert, S.E., Murray, J.W., 1995. Large changes in oceanic inventories from glacial to interglacial periods. Nature 376, 755–758.

Gasperi, J.T., Kennett, J.P., 1992. Isotopic evidence for depth stratification and paleoecology of Miocene planktonic foraminifera: western equatorial Pacific DSDP site 289. In: Tsuchi, R., Ingle Jr., J. (Eds.), Pacific Neogene Events. University of Tokyo, press, pp. 117–147.

Gonfiantini, R., 1981. The δ-notation and the mass spectrometric measurement techniques. Technical Reports Series no. 210. In: Gat, J.R., Gonfiantini, R. (Eds.), Stable Isotope Hydrology: Deuterium and Oxygen-18 in the Water Cycle. IAEA, Vienna, pp. 35–84.

Gonfiantini, R., 1986. Environmental isotopes in lake studies. In: Fritz, P., Fontes, J.C. (Eds.), Handbook of Environmental Isotope Geochemistry, vol. 2. Elsevier, pp. 113–168.

Gröning, M., 2004. International stable isotope reference materials. In: first ed. In: de Groot, P.A. (Ed.), Handbook of Stable Isotope Analytical Techniques, vol. 1. Elsevier, pp. 874–906.

Grootes, P.M., Stuiver, M., 1997. Oxygen 18/16 variability in Greenland snow and ice with 103 to 105 year time resolution. Journal of Geophysical Research 102, 26455–26470.

Grossman, E.L., 1984. Carbon isotopic fractionation in live benthic foraminifera: comparison with inorganic precipitate studies. Geochimica et Cosmochimica Acta 48, 1505–1512.

Haq, B.U., Worsley, T.R., Burckle, L.H., Douglas, R.G., Keigwin Jr., L.D., Opdyke, N.D., Savin, S.M., Sommer II, M.A., Vincent, E., Woodruff, R., 1980. Late Miocene marine carbon isotopic shift and synchroneity of some phytoplanktonic biostratigraphic events. Geology 8, 427–431.

Haug, G.H., Tiedemann, R., 1998. Effect of the formation of the Isthmus of Panama on Atlantic Ocean thermohaline circulation. Nature 393, 673–676.

Hemleben, C., Spindler, M., Anderson, O.R., 1989. Modern Planktonic Foraminifera. Springer. p. 363.

Hodell, D., Kennett, J.P., 1984. Late Miocene carbon shift in DSDP Site 516A, western south Atlantic. Geological Society of America 16, 540.

Hoefs, J., 2009. Stable Isotope Geochemistry, sixth ed. Springer-Verlag. p. 285.

Imbrie, J., Boyle, E.A., Clemens, S.C., Duffy, A., Howard, W.R., Kukla, G., Kutzbach, J., Martinson, D.G., McIntyre, A., Mix, A.C., Molfino, B., Morley, J.J., Peterson, L.C., Pisias, N.G., Prell, W.L., Raymo, M.E., Shackleton, N.J., Toggweiler, J.R., 1992. On the structure and origin of major glaciation cycles. 1. Linear responses to Milankovitch forcing. Paleoceanography 7, 701–738.

Imbrie, J., Shackleton, N.J., Pisias, N.G., Morley, J.J., Prell, W.L., Martinson, D.G., Hays, J.D., McIntyre, A., Mix, A.C., 1984. The orbital theory of Pleistocene climate: support from a revised chronology of the marine $\delta^{18}O$ record. In: Berger, A., Imbrie, J., Hays, J., Kukla, G., Saltzman, B. (Eds.), Milankovitch and Climate: Understanding the Response to Astronomical Forcing. D. Reidel, Hingham, Massachusetts, USA, pp. 269–305.

IPCC, 2013. Summary for Policymakers. In: Stocker, T.F., Qin, D., Plattner, G.-K., Tignor, M., Allen, S.K., Boschung, J., Nauels, A., Xia, Y., Bex, V., Midgley, P.M. (Eds.), Climate Change 2013: The Physical Science Basis. Contribution of Working Group I to the Fifth Assessment Report of the Intergovernmental Panel on Climate Change. Cambridge University Press, Cambridge, UK and New York, NY, USA, pp. 3–29.

John, C.M., Follmi, K.B., Kaenel, E.D., Adatte, T., Steinman, P., Badertscher, C., 2002. Carbonaceous and phosphate rich sediments of the Miocene Monterey Formation at El Captain State Beach California, USA. Journal of Sedimentary Research 72, 252–267.

Johnsen, S.J., Clausen, H.B., Dansgaard, W., Fuhrer, K., Gundestrup, N., Hammer, C.U., Iversen, P., Jouzel, J., Stauffer, B., Steffensen, J.P., 1992. Irregular glacial interstadials recorded in a new Greenland ice core. Nature 359, 311–313.

Kahn, M.I., Williams, D.F., 1981. Oxygen and carbon isotopic composition of living planktonic foraminifera from the northeast Pacific Ocean. Palaeogeography, Palaeoclimatology, Palaeoecology 33, 47–69.

Keigwin Jr., L.D., 1979. Late Cenozoic stable isotope stratigraphy and paleoceanography of DSDP sites from the east equatorial and central North Pacific Ocean. Earth and Planetary Science Letters 45, 361–382.

Keigwin Jr., L.D., Shackleton, N.J., 1980. Uppermost Miocene carbon isotope stratigraphy of a piston core in the equatorial Pacific. Nature 284, 613–614.

Keller, G., 1985. Depth stratification of planktonic foraminifera in the Miocene ocean. Geological Society of America, Memoir 163, 177–195.

Kennett, J.P., 1986. Miocene to early Pliocene oxygen and carbon isotope stratigraphy in the Southwest Pacific. Initial reports. Deep Sea Drilling Project, vol. 90, pp. 1383–1412.

Killingley, J.S., 1983. Effect of diagenetic recrystallization on the $^{18}O/^{16}O$ values of the deep sea sediments. Nature 301, 594–597.

Kroopnick, P.M., 1985. The distribution of $\delta^{13}C$ of CO_2 in the world oceans. Deep-Sea Research 32, 57–84.

Labeyrie, L.D., Duplessy, J.C., Blanc, P.L., 1987. Deep water formation and temperature variations over the last 125,000 years. Nature 327, 477–482.

Lane, G.A., Doyle, M., 1956. Fractionation of oxygen isotopes during respiration. Science 123, 574–576.

Lisiecki, L.E., Raymo, M.E., 2005. A Pliocene-Pleistocene stack of 57 globally distributed benthic $\delta^{18}O$ records. Paleoceanography 20, PA1003.

Liu, K., Kaplan, I.R., 1989. The eastern tropical Pacific as a source of 15N-enriched nitrate in seawater off southern California. Limnology and Oceanography 34, 820–830.

Loutit, T.S., Keigwin Jr, L.D., 1982. Stable isotopic evidence for latest Miocene sea-level fall in the Mediterranean region. Nature 300 (5888), 163–166.
Loutit, T.S., Kennett, J.P., 1979. Application of carbon isotope stratigraphy to late Miocene shallow marine sediments. Science 204, 1196–1199.
Loutit, T.S., Kennett, J.P., Savin, S.M., 1983. Miocene equatorial and southwest Pacific paleoceanography from stable isotope evidence. Marine Micropaleontology 8, 215–233.
Martinson, D.G., Pisias, N.G., Hayes, J.D., Imbrie, J., Moore, T.C., Shackleton, N.J., 1987. Age dating and the orbital theory of the ice-ages: development of a high-resolution 0 to 300,000 year chronostratigraphy. Quaternary Research 27, 1–29.
McConnaughey, T., 1989a. ^{13}C and ^{18}O disequilibrium in biological carbonates.1. Patterns. Geochimica et Cosmochimica Acta 53, 151–162.
McConnaughey, T., 1989b. ^{13}C and ^{18}O disequilibrium in biological carbonates. 2. In vitro simulation of kinetic isotope effects. Geochimica et Cosmochimica Acta 53, 163–171.
McCrea, J.M., 1950. The isotopic chemistry of carbonates and a paleotemperature scale. Journal of Chemical Physics 18, 849–857.
Merlivat, L., Jouzel, J., 1979. Global climatic interpretation of the deuterium-oxygen 18 relationship for precipitation. Journal of Geophysical Research 84, 5029–5033.
Meyers, P.A., 1994. Preservation of elemental and isotopic source identification of sedimentary organic matter. Chemical Geology 114, 289–302.
Miller, K.G., Fairbanks, R.G., Mountain, G.S., 1987. Tertiary oxygen isotope synthesis, sea level history and continental margin erosion. Paleoceanography 2, 1–19.
Milankovitch, M., 1930. Mathematische Klimalehre und Astronomische Theorie der Kilimaschwankungen. In: Köppen, W., Geiger, R. (Eds.), Handbuch der Klimatologie, vol. 1 (Pt. A). Borntraeger, Berlin, pp. 1–176.
Müller, P.J., 1977. CN ratios in Pacific deep-sea sediments: effect of inorganic ammonium and organic nitrogen compounds sorbed by clays. Geochimica et Cosmochimica Acta 41, 765–776.
Naqvi, S.W.A., 1987. Some aspects of the oxygen deficient conditions and denitrification in the Arabian Sea. Journal of Marine Research 29, 459–469.
Naqvi, S.W.A., 1994. Denitrification process in the Arabian Sea. Proceedings of the Indian Academy of Sciences 103, 181–202.
Olson, D.B., Hitchcock, G.L., Fine, R.A., Warren, B.A., 1993. Maintenance of the low oxygen layer in the central Arabian Sea. Deep-Sea Research Part II: Topical Studies in Oceanography 40, 673–685.
Petit, et al., 1999. Climate and atmospheric history of the past 420,000 years from the Vostok ice core, Antarctica. Nature 399, 429–436.
Pisias, N.G., Martinson, D.G., Moore, T.C., Shackleton, N.J., Prell, W., Hays, J.D., Boden, G., 1984. High resolution stratigraphic correlation of benthic oxygen isotope records spanning the last 300,000 years. Marine Geology 56, 119–136.
Prell, W.L., Imbrie, J., Martinson, D.G., Morley, J.J., Pisias, N.G., Shackleton, N.J., Streeter, H.F., 1986. Graphic correlation of oxygen isotope stratigraphy application to the late Quaternary. Paleoceanography 1, 137–162.
Premuzic, E.T., Benkovitz, C.M., Gaffney, J.S., Walsh, J.J., 1982. The nature and distribution of organic matter in the surface sediments of the world oceans and seas. Organic Geochemistry 4, 63–77.
Qasim, S.Z., 1982. Oceanography of the northern Arabian Sea. Deep-Sea Research 29, 1041–1068.
Redfield, A.C., 1934. On the proportion of organic derivatives in seawater and their relation to the composition of plankton. In: James Johnstone Memorial Volume. Liverpool University Press, pp. 177–192.
Redfield, A.C., 1958. The biological controls of chemical factors in the environment. American Journal of Science 46, 205–221.
Saino, T., Hattori, A., 1987. Geographical variation of the water column distribution of suspended particulate organic nitrogen and its 15N natural abundance in the Pacific and its marginal seas. Deep-Sea Research 34, 807–827.

Savin, S.M., Abel, L., Barrera, E., Hodell, D., Keller, G., Kennett, J.P., Killingley, J., Murphy, M., Vincent, E., 1985. The evolution of Miocene surface and near surface marine temperatures: oxygen isotopic evidence. Geological Society of America, Memoir 163, 40–82.

Shackleton, N.J., 1967. Oxygen isotope analyses and Pleistocene temperatures re-assessed. Nature 215, 15–17.

Shackleton, N.J., 1974. Attainment of isotopic equilibrium between ocean water and benthonic foraminifera genus Uvigerina. Isotopic changes in the ocean during the last glacial. CNRS, Colloques Internationals 219, 203–209.

Shackleton, N.J., Kennett, J.P., 1975. Paleotemperature history of the Cenozoic and the initiation of the Antarctic glaciation:Oxygen and carbon isotope analyses in DSDP sites 277,279 and 281. Initial Reports. Deep Sea Drilling Project, vol. 29, pp. 743–756.

Shackleton, N.J., Opdyke, N.D., 1973. Oxygen isotope and paleomagnetic stratigraphy of equatorial Pacific core V28-238: oxygen isotope temperatures and ice volumes on a 105 and 106 year scale. Quaternary Research 3, 39–55.

Shi, W., Morrison, J.M., Bohm, E., Manghnani, V., 2000. The Oman upwelling zone during 1993, 1994 and 1995. Deep-Sea Research Part II: Topical Studies in Oceanography 47, 1227–1247.

Smith, R.L., Bottero, J.S., 1977. On upwelling in the Arabian Sea. In: Angel, M. (Ed.), A Voyage of Discovery. Pergamon Press, pp. 291–304.

Spero, H.J., Bijma, J., Lea, D.W., Bemis, B.E., 1997. Effect of seawater carbonate concentration on foraminiferal carbon and oxygen isotopes. Nature 390, 497–500.

Spero, H.J., Lea, D.W., 1993. Intraspecific stable isotope variability in the planktic foraminifera Globigerinoides sacculifer: results from laboratory experiments. Marine Micropaleontology 22, 221–234.

Srinivasan, M.S., Sinha, D.K., 1998. Early Pliocene closing of the Indonesian Seaway: evidence from northeast Indian Ocean and southwest Pacific deep sea cores. Journal of Southeast Asian Earth Sciences 16, 29–44.

Srinivasan, M.S., Sinha, D.K., 2000. Ocean circulation changes in the Indo-Pacific during 5.6 to 4.2 Ma: planktic foraminiferal and isotopic evidences. Proceedings of the Indian Academy of Sciences 109, 315–328.

Sautter, L., Thunell, R., 1991. Seasonal variability in the $\delta^{18}O$ and $\delta^{13}C$ of planktonic foraminifera from an upwelling environment: sediment trap results from the San Pedro Basin, Southern California Bight. Paleoceanography 6, 307–334.

Steens, T.N.F., Ganssen, G., Kroon, D., 1992. Oxygen and carbon isotope in planktonic foraminifera as indicators of upwelling intensity and upwelling induced high productivity in sediments from the northwestern Arabian Sea. In: Summerhayes, C.P., Prell, W.L., Emeis, K.C. (Eds.), Upwelling Systems Evolution since the early Miocene.Special Publication, vol. 64. Geological Society, London, pp. 107–120.

Takahasi, T., Broecker, W.S., Langer, S., 1985. Redfield ratio based on chemical data from isopycnal surfaces. Journal of Geophysical Research 90, 6907–6924.

Tiwari, M., Nagoji, S.S., Kartik, T., Drishya, G., Parvathy, R.K., Rajan, S., 2013. Oxygen isotope-salinity relationships of discrete oceanic regions from India to Antarctica vis-à-vis surface hydrological processes. Journal of Marine Systems 113–114, 88–93.

Tiwari, M., Ramesh, R., Sheshshayee, M., Bhushan, R., Somayajulu, B.L.K., Jull, A.J.T., Burr, G.S., 2010. Did the Indo-Asian summer monsoon decrease during the Holocene following insolation? Journal of Quaternary Science 25, 1179–1188.

Tyndall, J., 1861. On the absorption and radiation of heat by gases and vapours, and on the physical connection of radiation, absorption, and conduction. Philosophical Magazine Series 4, 22 (169–194), 273–285.

Urey, H., 1947. The thermodynamic properties of isotopic substances. Journal of Chemical Society 562–581.

Vail, P.R., Hardenbol, J., 1979. Sea-level changes during the Tertiary. Oceanus 22, 71–79.

Vincent, E., Berger, W.H., 1985. Carbon dioxide and polar cooling in the Miocene: the Monterey hypothesis. In: Sundquist, E.T., Broecker, W.S. (Eds.), The Carbon Cycle and Atmospheric CO_2: Natural Variations Archean to Present. American Geophysical Union, vol. 32, pp. 455–468.

Vincent, E., Killingley, J.S., Berger, W.H., 1980. The magnetic Epoch-6 carbon shift: a change in the ocean's 13C/12C ratio 6.2 million years ago. Marine Micropaleontology 5, 185–203.

Wefer, G., Berger, W.H., 1991. Isotope paleontology: growth and composition of extant calcareous species. Marine Geology 100, 207–248.

Williams, D., Lerche, I., Full, W.E., 1988. Isotope Chronostratigraphy, Theory and Methods. Academia Press Inc. p. 345.

Woodruff, F., Savin, S.M., 1985. $\delta^{13}C$ values of Miocene Pacific benthic foraminifera: correlations with sea level and biological productivity. Geology 13, 119–122.

Wyrtki, K., 1971. Oceanographic Atlas of the International Indian Ocean Expedition. National Science Foundation Publications, OCE/NSF 86-00-001, Washington, DC. p. 531.

You, Y., Tomczak, M., 1993. Thermocline circulation and ventilation in the Indian Ocean derived from water mass analysis. Deep-Sea Research 40, 13–56.

Chapter 7

Teleconnections between the Indian summer monsoon and climate variability: a proxy perspective

S. Chakraborty[a], Aasif M. Lone[b], Anant Parekh[a], P.M. Mohan[c]
[a]*Indian Institute of Tropical Meteorology, Ministry of Earth Sciences, Pune, Maharashtra, India,* [b]*Indian Institute of Science Education and Research, Bhopal, India,* [c]*Pondicherry University, Port Blair, India*

7.1 Introduction

7.1.1 Monsoon variability

Monsoon is a natural process composed of multiple complex interactions among atmosphere, land, ocean, vegetation, ice sheet, etc., over a broad spectrum of temporal and spatial scales (e.g., Gadgil 2003). Its variability is influenced by several global-scale events, such as the El Niño-Southern Oscillation (ENSO) (Tudhope et al., 2001; Moy et al., 2002;), Indian Ocean Dipole (IOD) (Ashok et al., 2001; DiNezio et al., 2020), Pacific Decadal Oscillation (PDO) (Newman et al., 2016; Zhang and Delworth, 2016), Atlantic Multi Decadal Oscillation (AMO) (Knudsen et al., 2011) shifts in the moisture source (Polanski et al., 2014; Jasechko, 2015) volcanic forcing (Singh et al., 2020) and changes in earth's orbital configurations (Jalihal et al., 2020).

One of the reliable means of studying the interactions among atmosphere, land, ocean, vegetation, and ice over a long period is proxy-based paleoclimatic investigations. The palaeoclimate reconstruction methods are widely used to study past monsoon variability and their causative mechanism(s) (Bolton et al., 2013; Dahl and Oppo, 2006; Tiwari et al., 2015). The use of paleoclimate reconstruction methods has significantly advanced in the past few decades involving changes in the chemical, physical, and biological processes of the Earth system in coherence with temperature and rainfall variations (Mann et al., 2008; PAGES2k Consortium, 2013). Among these methods, one of the means is to study the geophysical, geochemical, and biological characteristics of natural archives known to preserve records of these interaction processes reliably. The physical processes that govern these interactions and, in turn, determine the

Indian Summer Monsoon Variability: El Niño-teleconnections and beyond.
DOI: https://doi.org/10.1016/B978-0-12-822402-1.00070-3

climatic phenomena are evaporation, precipitation, atmospheric and oceanic circulation, transfer of heat energy, etc. (Doose-Rolinski et al., 2001).

In recent times, several studies have been compiled to draw inferences on Indian summer monsoon variability using single-multi-archived proxy records (Banerji et al., 2020 and reference therein). These climate archives include cave deposits, i.e., speleothems, ocean and lake sediments, tree rings, corals, etc. They are known to respond to changes in the atmospheric conditions associated with the monsoon through physical, chemical, or biological processes. Hence, variability in the Indian summer monsoon over decadal, centennial, and millennial timescales is apparent in these climate archives.

The physio-chemical changes could be recorded by various means, one of them being variations in the heavy to the light isotopic distribution pattern of certain low mass elements, such as hydrogen, carbon, oxygen, nitrogen, etc. The changes in heavy to light isotopic distribution, the so-called *isotope fractionation* process, both in biogenic and abiogenic materials, are governed by temperature and precipitation changes, pH variability, and isotope composition of the ambient environment (de Villiers et al., 1995). The fractionation processes have been extensively studied in biogenic and abiogenic carbonates and employed to reconstruct past atmospheric conditions and biomineralization processes (McConnaughey, 1989). The isotopic ratio is denoted in δ notation; see Box 7.1 for definition. Some of the natural archives that rely on the isotopic distribution characteristics are discussed below.

7.1.2 Speleothem

The speleothems are inorganic carbonate deposits formed in caves when the environmental conditions are conducive. The basic premise is that rainwater

Box 7.1 Isotopic Proxies

Various kinds of proxies are used to study the past climate depending on their sensitivity to environmental conditions. Isotopic ratios of a few low mass elements (H, C, N, O, S) are widely used for this purpose. Since the relative difference in isotope ratios can be measured more precisely than the absolute isotopic ratios, the concept of δ notation was introduced to report the isotopic data. For example, in the case of the oxygen isotopic ratio, the formulation is shown below:

$$\delta^{18}\mathrm{O} = \left[\frac{\left(^{18}\mathrm{O}/^{16}\mathrm{O}\right)_{\text{sample}} - \left(^{18}\mathrm{O}/^{16}\mathrm{O}\right)_{\text{reference}}}{\left(^{18}\mathrm{O}/^{16}\mathrm{O}\right)_{\text{reference}}} \right] \times 1000‰$$

where the numerator on the right-hand side is the difference between the ($^{18}O/^{16}O$) ratio of a sample and that of reference material; for oxygen or hydrogen, typically the VSMOW (Vienna Standard Mean Ocean Water) is used as a reference material (Criss, 1999).

percolating through the bedrock carries the isotopic signature of rainfall and is preserved in the speleothem calcium carbonate matrix. They record changes in the heavy to light isotopes of H and O in the rain owing to differences in precipitation amount and moisture sources (Fairchild et al., 2006; Lachinet, 2009). The rainwater, which percolates through the bedrock, integrates several years (up to 10 years) of climate information (Fairchild et al., 2006; Berkelhammer et al., 2014). As a result, the speleothem records act as a low-pass filter yielding low-frequency information better than the high-frequency variability (Berkelhammer et al., 2014). However, a near-continuous flow of groundwater in cave systems, in principle, enables us to retrieve climatic information nearly on an annual scale (Fairchild and Baker, 2012). This is aided by advancement in analytical techniques that offer high-resolution speleothem sampling and hence improved climatic information (Affolter et al., 2014). In the Indian context, however, contrasting patterns of subdecadal to decadal-scale Indian summer monsoon (ISM) variability (strong versus weak monsoon) have been better-studied (Sinha et al., 2007; Kathayat et al., 2017) than the near-annual scale variability (Sinha et al., 2011; Sinha et al., 2018).

7.1.3 Tree rings

In the continental environment, analysis of tree ring width and their isotopic ratios ($^{18}O/^{16}O$, $^{2}H/^{1}H$, $^{15}N/^{14}N$) offers a reliable means for studying the high-resolution records of past precipitation variability (Roden et al., 2000; Zhang et al., 2020). The tree ring width is usually susceptible to ambient environmental conditions mostly linked to temperature and precipitation changes (Yadav et al., 2011; Borgaonkar et al., 2018). As such, normal tree-ring growth may be impeded under climate-stressed conditions, such as insufficient water availability due to declining rainfall under drought-like conditions. Such kinds of environmental changes are reliably recorded in tree rings, which manifest in the form of varying tree ring widths. The annual changes in the tree ring width dominantly controlled by ambient environmental conditions have been reliably used to reconstruct past Indian monsoonal shifts (Yadav, 2013) and El Niño induced drought conditions (Cook et al., 2010; Borgaonkar et al., 2010; Zaw et al., 2020). As trees source their water from the root zone, the isotopic signature of soil water is believed to be recorded by the distribution of oxygen or hydrogen isotopes in the tree ring structure (Evans et al., 2006; Bose et al., 2014). Other isotopes, such as ^{13}C, ^{14}C, ^{15}N, that are sensitive to changes in CO_2 concentrations in the atmosphere have also been used (Chakraborty et al., 2008).

7.1.4 Marine sediments

The paleo-monsoonal shifts are also apparent from the biological response to the monsoonal activity preserved in the form of increased abundance of the

planktic foraminifera in the marine environments. For example, certain species, such as the *Globigerina bulloides,* reliably provided records of multidecadal to century-scale changes in the strength of the Indian summer monsoon (Gupta et al., 2003, 2005). During shell formation in foraminifera or corals, a relatively greater number of heavier isotopes are incorporated in the calcium carbonate matrix during cooler sea surface conditions. This process provides an effective means to quantify changes in the thermal and physical behavior of the surface ocean conditions (Cobb et al., 2003; Abram et al., 2008; Chakraborty, 2006, 2020), including surface and deep-ocean circulation (Chakraborty et al., 1994; Goldstein et al., 2001). Moreover, coralline oxygen isotopes are highly sensitive to thermal conditions; hence, changes in Sea Surface Temperature (SST) are reliably recorded in their oxygen isotopic distribution. Hence, the coralline archives are useful to study the ISM teleconnections with ENSO and IOD (Charles et al., 1997; Chakraborty et al., 2012; Chakraborty, 2015). Box 7.2 shows a schematic diagram illustrating how the tropical Pacific temperature anomalies set up a stationary wave response in the subtropics over Eurasia as well as zonal and meridional circulation in the Indian and Pacific region through the atmosphere-ocean interaction (also see Chapters 2–4). This perturbation, in turn, influences the north–south tropospheric temperature (TT) gradient and the circulation and convective activity associated with the monsoon, thereby controlling the spatial and temporal evolution of ISM rainfall (e.g., Kumar et al., 1999; Xavier et al., 2007).

7.1.5 Proxy's response to forcing mechanism

The climatic information retrieved from proxy records depends primarily on the sensitivity of the archives toward the changes in environmental conditions. This is because each climate archive and proxy has its own response for the same climatic perturbation. Paleo-climatologists have studied the above-mentioned proxy records and proposed several mechanisms that highlight the role of short- (multidecadal) and long-term (centennial to millennial) ocean-atmospheric forcing factors in modulating the monsoon variability (Agnihotri et al., 2002; Dutt et al., 2015). One significant aspect concerns the temporal relationship of the forcing mechanism between the multiproxy records. Interestingly, most of these proxy records highlight similar phase relationships and synchronous periodicities, suggesting a similar forcing mechanism (Menzel et al., 2014; Dutt et al., 2015; Gupta et al., 2019). Each of the proxy records suggests the role of independent and/or coupled forcing mechanism over land and ocean, allowing us to make robust inferences on coupled ocean-atmosphere-land dynamics. Because of these characteristics, the proxy-based paleoclimate reconstruction offers a reliable means to study the past monsoon variability modulated by external and internal factors occurring over multiple timescales. One such method involves reconstructing past monsoonal shifts in the Asian monsoon system and changes in the ISM (Gupta et al., 2005; Zhisheng et al., 2011; 2015; Saraswat et al.,

Box 7.2 How do the proxies record the teleconnections process?

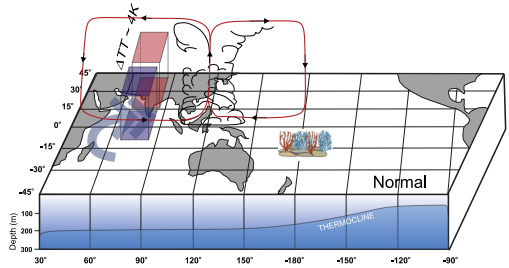

Tropical Pacific climatology during a normal year: the trade winds blow across the Pacific, and the air rises in the convergence zone over the warm SSTs in the west. At the upper level, it diverges and subsequently subsides over the Indian Ocean (IO) and the Pacific Ocean. The thick blue arrow shows the low-level southwest monsoon circulation

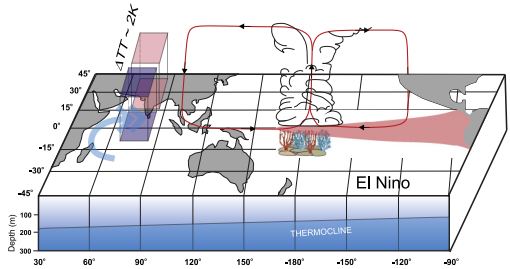

During an El Niño year, the equatorial Pacific warms considerably (as shown by reddish shading in the equatorial region). The Walker cell is shifted, as a result, anomalous convection takes place in the central equatorial Pacific. The heating anomaly is then transferred to the atmosphere, which in turn sets up a stationary wave response in the subtropics. This perturbation influences the TT anomalies over Eurasia, which subsequently modulates the north–south gradient of TT (denoted as ΔTT) over the Indian monsoon region and hence the Indian summer monsoon rainfall. The N-S gradient or ΔTT over the Indian region are calculated between the two vertical columns, as shown by two vertical boxes, red box (5°N–35°N, 40°E–100°E) and the blue box (15°S-5°N, 40°E-100°E; see details in Xavier et al., 2007). During a normal year, ΔTT is relatively high, approximately 4K (shown in the upper panel). But in an El Niño year, the north–south temperature gradient is decreased, and ΔTT is low (~2K). Corals growing in the equatorial Pacific can accurately record the SST anomaly in their oxygen isotopic composition (Cobb et al., 2003; Cole 2005). Since the anomaly in the SST is translated to a heating anomaly in the atmosphere through moist convection that drives the stationary wave and influences the ΔTT, the coralline oxygen isotopic ratios show a strong association with the TT gradient. This characteristic feature was used to quantify the past ISM rainfall variability (Chakraborty et al., 2012).

2011; Gill et al., 2017). More discussion in this aspect is provided in the later sections.

7.1.6 Proxy studies of Indian summer monsoon: scope of the work

The ISM undergoes a range of variability from intraseasonal to multimillennium timescales (e.g., Goswami et al., 2014). To study the natural modes of variability in the Indian summer monsoon system, various terrestrial and marine proxy records are used by paleo-climatologists (Ramesh et al., 2010).

In this chapter, we discuss how the proxy-based paleo-monsoon records have been used to study the nature and pattern of the *teleconnections mechanism* aimed at understanding the past ISM variabilities, approximately for the Holocene. Though we will rely on the proxy-based ISM reconstructions, a detailed review of the literature, however, is beyond the scope of this work. Recent studies have already presented the proxy-based reconstruction of the Indian summer monsoon system on millennium (Dixit and Tandon, 2016) and multimillennium times scales (Staubwasser, 2006; Banerji et al., 2020). Fig. 7.1 provides a schematic

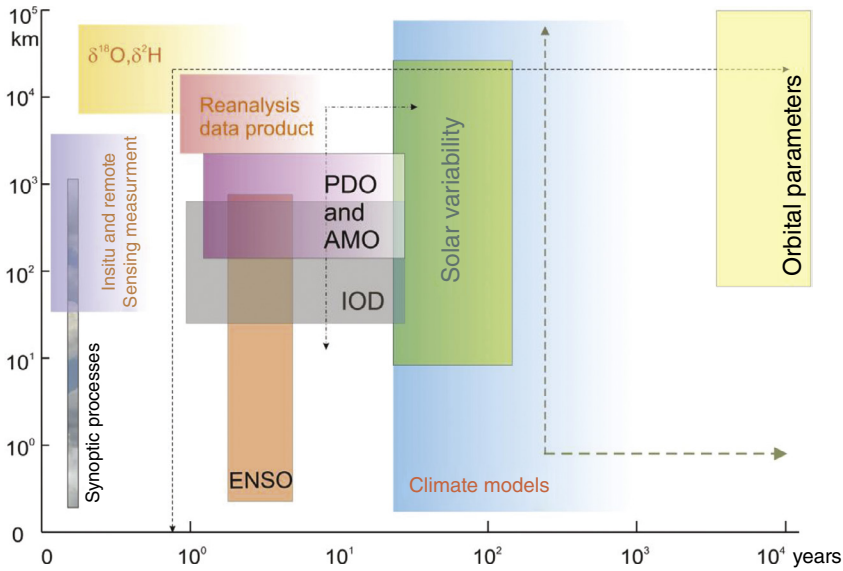

FIG. 7.1 A schematic representation of the processes controls the Indian summer monsoon variability at various temporal and spatial scales. The processes are shown as vertical boxes with black labels; their effect on monsoon covering the temporal and spatial scales is approximately shown by x- and y-axes. The intertropical convergence zone (*ITCZ*), which strongly modulates the monsoon dynamics both in seasonal and millennium timescales, is not shown here. Similarly, the greenhouse gas and volcanic forcing are not represented. The methods and tools of studying the monsoon processes are shown as boxes with varying shades and labeled in orange color (processes are indicative only).

representation of the processes that control monsoon variability across spatial and temporal scales. The analytical and observational methods used to study the monsoon system are shown in the shaded boxes (orange-colored labels).

Paleo-climatic information is largely retrieved by studying the isotopic composition of carbonate systems. These carbonate systems inherit their isotopic signature either through rainfall (i.e., speleothems) or through the ambient water environment (i.e., foraminifera, corals, gastropods, etc.). The isotopic characteristics of precipitation reliably record the atmospheric convective systems, which are transferred through the climate proxies (i.e., speleothems). Hence, it is important to understand how the 'atmospheric information' is passed on to the climate archives.

To provide a comprehensive review of the short and long-term forcing factors on the Indian monsoonal variability, we have divided this chapter into two sections. Firstly, we present a summary of the water isotope and an associated case study to explain how the rainfall information is recorded by land-based speleothem archives. The second part will discuss the proxy-based reconstruction of ISM variability on decadal to multimillennial time scales and its possible global teleconnections; this part is based on the available literature.

7.2 Precipitation isotopes: a proxy for large-scale moisture source signature

On a daily and monthly time scales, the stable oxygen isotope variations in precipitation are widely used to study the regional hydrology and short-term monsoonal variations (Araguas and Araguas et al., 1998; Rahul et al., 2016 Chakraborty et al., 2016, 2018; Midhun et al., 2018; Sinha et al., 2019; Lone et al., 2020; Sengupta et al., 2020). During this process, the evaporation from the sea surface preferentially removes the lighter isotopes (^{16}O, ^{1}H). As a result, the proportion of heavier isotopes (^{18}O, ^{2}H) is reduced in the vapor phase causing isotopic fractionation. Moreover, the initial composition of water vapor formed from evaporation over the ocean and land surface is subsequently modified by rainout and cloud microphysical processes, moisture recycling, advective mixing, raindrop evaporation, rain-vapor interaction, etc. (Dar and Ghosh, 2017; Rahul et al., 2018; Sinha and Chakraborty, 2020).

One pertinent question is how the isotopic signature of rainfall is transferred to individual geological deposits (i.e., speleothem) that enables us to estimate the past monsoon variability? A consequential matter is that how does an individual natural archive (considered as a point source) provide rainfall information over a vast region? To discuss this issue, one should understand that there is a fundamental difference in the dynamical properties of precipitation and its isotopic values. For example, in principle, rainfall is an episodic phenomenon having a limited spatial and temporal domain. However, its isotopic composition reflects the overall status of the water vapor reservoir at the time of precipitation formation (Rozanski 2005). Further, this means the isotopic values of

precipitation carry the signature of the water vapor, which is characterized by a much larger spatial domain than the individual rainfall events. To demonstrate this behavior, precipitation isotopic values on a point scale may be compared with rainfall data at different spatial scales. We present the isotopic records of precipitation from the Andaman Island, Bay of Bengal. The reason for choosing this region is that the island contains a variety of speleothems, which are known to provide past monsoonal information (Laskar et al., 2013). Secondly, being an island, the moisture comes predominantly from the ocean; hence the terrestrial controls on the precipitation isotopic variability are negligible. Fig. 7.2 shows oxygen isotope values of rainfall at Port Blair, situated in the southern part of this island. Isotopic time profiles (black line) of four years (2012, 2014, 2016, and 2018) are plotted on an intraseasonal time scale (May–Oct.). The rain gauge data representing point-scale rainfall variability are shown as red bars.

On the other hand, Tropical Rainfall Measuring Mission satellite-derived rainfall data averaged over a larger area (10°N–12°N, 90°E–92°E) has been examined to infer the impact of large-scale rainfall variability on the isotopic values. Rainfall anomaly was calculated by subtracting rainfall climatology of 20 years (1998–2018) over the above-mentioned grid box. The plot clearly shows that the depleted (enriched) isotopic values are mostly associated with high positive (negative) rainfall anomalies. Only for a few cases, heavy rainfall

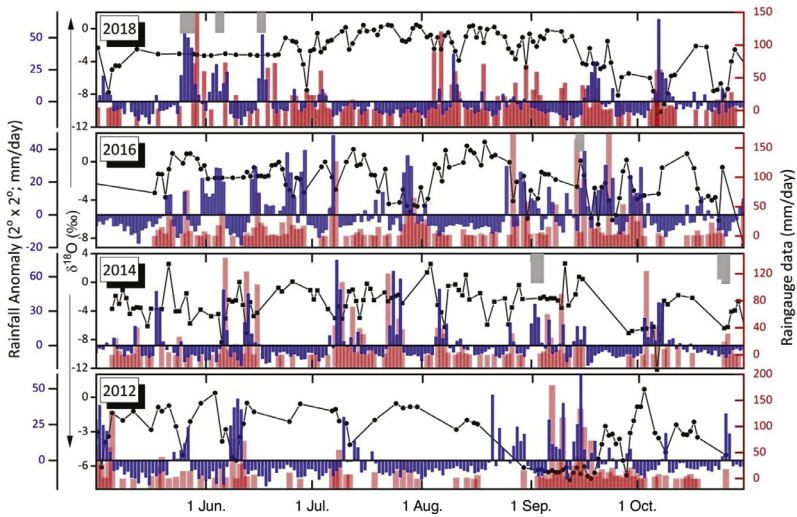

FIG. 7.2 Association of precipitation $\delta^{18}O$ (at Port Blair, Andaman Islands, Bay of Bengal) and the rainfall variability on two different spatial scales. The isotopic variability (black line) has been plotted on an intraseasonal timescale. The rain gauge data are shown as red bars. The satellite-derived rainfall anomaly (averaged over a 2° × 2° grid box) are shown as blue bars. Large isotopic depletions are mostly associated with high positive rainfall anomaly, except in a few cases (indicated as *grey bars*) when they deviate from the expected behavior.

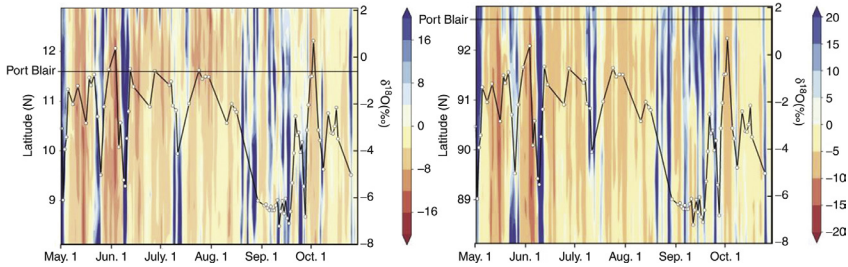

FIG. 7.3 Precipitation isotopes response to large scale rainfall anomaly: (left panel) time latitude Hovmoller diagram showing the rainfall anomaly averaged over a large area (88°E –93°E, 8°N–13°N) over the Bay of Bengal. Superimposed is the precipitation $\delta^{18}O$ record observed at Port Blair for the year 2012. (right panel) same as before but the time longitude Hovemoller diagram and the precipitation isotopes covariability are shown. Large isotopic depletions almost always coincided with the high positive rainfall anomaly represented by blue shading in both cases. The horizontal black lines show the position of Port Blair.

events did not produce large isotopic depletions (shown as grey bars). The graphical presentation of the result indeed demonstrates that isotopic values of rainfall, even on a point scale, could capture the signature of rainfall variability over a large spatial scale. We have also examined the behavior of the precipitation isotope records yet on a larger spatial scale, covering approximately an area of 250,000 km^2 over the Bay of Bengal (8°N –13°N, 88°E –93°E). Fig. 7.3 left panel (right panel) shows the time-latitude (time-longitude) Hovmoller diagram of rainfall anomaly calculated over the above-mentioned grid box. The precipitation isotope record of Port Blair-2012 has been superposed onto this diagram to observe the covariability. The data reveal a strong association of depleted isotopic values and the positive rainfall anomalies, both in zonal and meridional dimensions. It is apparent that the rainfall-isotope antiphase relationship improves when studied on a larger spatial scale. The records demonstrate that the isotopic signature of rainfall over a large region could be captured even by a climate archive having a short spatial extent. Intraseasonal variability of rainfall information may also be retrieved from a fast-growing biological proxy (Ghosh et al., 2017).

7.3 Proxy evidence of multiple-scale oscillation in Indian summer monsoon

7.3.1 Marine records

Paleoclimatic investigations highlight the occurrence of persistent variability in the monsoonal rainfall throughout the Holocene that was closely related to millennial-scale climate events suggesting a mechanistic link (Overpeck et al., 1996; Neff et al., 2001; Gupta et al., 2003, 2005; Fleitmann et al., 2007). The records retrieved from various geo-archives have suggested that monsoonal

variability is very sensitive to relatively small changes in the natural forcing (0.25% change in solar output, or a 2°C change in SST; Shindell et al., 2001). Gupta et al. (2003, 2005) postulated a solar-monsoon link, which suggests that ISM winds were stronger (high solar activity) during the early Holocene that steadily weakened over time. Similarly, the Medieval Warm Period (MWP; CE 800-1200; Kamae et al., 2017) also witnessed higher solar activity, but the Little Ice Age (LIA; CE 1400-1800) experienced low solar activity resulting in enhanced and weakened monsoonal intensity, respectively. In this context, the role of Tibetan Plateau (TP) was also discussed. According to Overpeck et al. (1996), reduced glacial boundary conditions triggered strong warming of the TP and generated a stronger pressure gradient to produce an intensified monsoon during the early Holocene period. These findings have prompted climate scientists to investigate the role of heating of the Eurasian continent and, more specifically, the role of TP (an indicator of surface heating) in modulating the Asian monsoon system (Liu and Yanai, 2002). An improved record of understanding the role of TP in linking ISM variations has confirmed that during the last two millennia, epochs of cool (warm) temperatures in the TP coincided with weak (strong) monsoon conditions (Feng and Hu, 2005). This study further confirms that the monotonic rise of the TP surface temperature had a dominant influence on the ISM variations in contrast to the Eurasian continent during the last ~350 years. However, some investigators (Neff et al., 2001; Zorzi et al., 2015) have put forward alternative hypotheses and opine that solar output might have played only an indirect role in modulating the monsoon intensity on a millennium timescale. Zorzi et al. (2015) suggested that direct insolation changes only control the long-term trends in the Indian summer monsoon precipitation. Whereas the ocean-atmospheric-land teleconnections dominantly modulate its millennial-scale intensity and variability with the partial role of solar activity. These studies suggest that minor variations over smaller timescales are unlikely to have directly caused significant differences in the sensible heating of the TP. Hence, it is argued that solar output may not have a direct impact on the ISM rainfall variability; instead, it leads to oceanic circulation changes (Neff et al., 2001).

7.3.2 Speleothem records

Previous studies using marine proxy records from the Arabian Sea have reliably reconstructed variations in the ISM and highlighted significant changes in the wind intensity, river discharge, and extent of upwelling (Anderson et al., 2002; Gupta et al., 2003). One of the fundamental limitations of these studies is that they do not directly reflect the precipitation changes, which is integral for assessing the actual monsoon precipitation behavior (Berkelhammer et al., 2010). Hence, appropriate proxy records from reliable archives such as speleothem, corals, tree rings, etc., are required to quantify the monsoon rainfall variability.

Speleothems (cave carbonate deposits) occurring in wide geographic regions such as the monsoon core zone (MCZ; approximately a box encompassing an

area of 18°N–28°N, and 65°N–88°E in central India, defined in Rajeevan et al., 2010) and the Himalayan region, form an ideal climate archive to reconstruct past changes in the Indian monsoon (Yadava and Ramesh, 2005; Sinha et al., 2007; 2011; Dutt et al., 2015; Kathayat et al., 2017; Kaushal et al., 2018; Kotlia et al., 2015; Gautam et al., 2019). These studies highlighted that variations in speleothem oxygen isotopic composition are primarily governed by changes in the precipitation/moisture sources and hence provide direct evidence of past monsoonal variability. Speleothem proxy records from Northeast India (Berkelhammer et al., 2012; Dutt et al., 2015) reveal significant changes in the ISM during the late Pleistocene and a prominent weakening during the mid-Holocene (the 4.2 ka event). Apart from inferring the monsoonal precipitation variations, these proxy records suggest a coupled relation of the ISM shifts to ocean-atmospheric processes (Gautam et al., 2019); Northern Hemisphere temperature changes (Kathayat et al., 2017), and changing moisture transport pathways (Kotlia et al., 2015). Moreover, speleothem oxygen isotope records of Central and Northeast India reveal that the frequency distribution of active-break periods in ISM varies on centennial timescales and suggests a significant role of internal dynamics in governing the ISM response to slowly evolving changes in the external boundary conditions (Sinha et al., 2011). Additionally, Berkelhammer et al. (2010) studied annually resolved and absolute dated speleothem oxygen isotopic records from the MCZ, the Dandak cave, (19°N and 82°E at 400 m). In their study, the robustness of the extracted climatic information was ascertained by comparing its isotopic profile with a Chinese speleothem record approximately 3000 km away (Wanxiang cave; Zhang et al., 2008) and observed three contemporaneous maxima occurring around AD 900, AD 1050, and AD 1375. Moreover, a high correlation coefficient (0.8) was obtained between these records during AD 880–1420, asserting a common forcing mechanism for the Asian monsoon system.

7.3.3 Pacific teleconnections with Indian summer monsoon

Several regional proxy records have revealed that periodic changes in natural forcing factors such as solar activity influence the monsoonal conditions on centennial to millennial time scales. For example, spectral analysis of the $\delta^{18}O$ record shows a single statistically significant peak centered around 90 years/cycle, commonly referred to as the Gleissberg solar cycle (Berkelhammer et al., 2010). However, this periodicity was restricted only during the MWP, which prompted these authors to suggest either varying ENSO dynamics and/or changing frequency, including the amplitude of IOD events intermittently amplify or neutralize the ENSO impact on monsoon circulation. Hence, the authors hypothesize that changes in the ocean-atmospheric system, specifically in the ENSO domain, may have operated to disrupt or enhance the solar output–monsoon relationship. This implies that the dynamical mechanism linking ISM variability and solar production is modulated by external boundary conditions, in which ENSO plays a critical role. According to this hypothesis, sustained

change in ENSO dynamics during the MWP could have provided the conditions necessary for a consistent solar flux variability–monsoon relationship.

To investigate further the coupling of the ISM with the ENSO and the North Atlantic climate variability, Berkelhammer et al. (2014) analyzed additional speleothem records from the MCZ of India. A composite time series of speleothem oxygen isotopes (~1400 years) was created using Jhumar cave (19°N, 82°E; AD 1075–2007) and Dandak cave (AD 625–1562) isotopic records. Additionally, coral and tree ring-based ENSO indices were also used to study the dynamical behavior of ENSO and monsoon.

Using a suite of proxy records, Berkelhammer et al. (2014) focused on two windows of the time spectrum. One is a high-frequency band that can capture all the power in the 5–15 years window, which provides insight into the long-term stability of the known dynamical connection between the ISM and ENSO during the instrumental period (Kumar et al., 1999). The other one is a low-frequency band that can extract the power in the 30–90 years window, aimed at providing information on the effect of the multidecadal climate variability on the ISM. This study further investigated the ENSO–ISM teleconnections mechanism by examining the coherency and phase angle between the two systems (ENSO and ISM) using multiple combinations of the proxy records (e.g., coral ENSO vs speleothem ISM, tree ring ENSO vs tree ring ISM, speleothem ISM vs composite ENSO). This study highlighted that in the high-frequency domain (5–15 years), periods of positive ENSO amplitude were associated with reduced ISM rainfall. However, no statistically significant phase relationship was found between ENSO amplitude and the speleothem-based ISM reconstruction in the low-frequency (30–90 years) domain. The result may appear inconsistent with the conventional wisdom as it shows a more active ENSO state coinciding with an intensified monsoon rainfall regime. Therefore, the authors suggest two hypotheses to explain this apparent inconsistency: (1) changes in ENSO variance are being driven by an increase in La Niña events, (2) in the low-frequency domain; the two systems are phase-locked through a common forcing mechanism, which leads to both an increase (decrease) in ENSO variance and a strengthened (weakened) ISM. In this context, it may be noted that Tejavath et al. (2019) performed a multimodel simulation of ISM for the last millennium and highlighted that majority of the models consistently simulated more strong El Niño events during the MWP as compared to the number of intense El Niño events during the LIA. On the other hand, most of the models consistently simulated more robust La Niña events during the LIA than the number of strong La Niña events during the MWP. Considering this, the second hypothesis proposed by Berkelhammer et al. (2014) seems to offer a more realistic mechanism within the last millennium timeframe. Accordingly, shared multidecadal power between these systems comes through periodic variability in the North Atlantic SSTs. In this case, positive (negative) SST anomaly in the North Atlantic would lead to both an increase (decrease) in ISM rainfall and ENSO variance. Berkelhammer et al. (2014) further argued

for a dominant role of dynamics internal to the Indian Ocean (IO) in producing multidecadal hydroclimate variability across the IO basin. This implies the presence of a relationship between IO dynamics and the ENSO system. If basin-wide shifts in the IO are influencing changes in ENSO variance, then the results here suggest that the IO's direct influence on the monsoon is more substantial than from the teleconnections that affect the ISM through ENSO. The results suggest that a continuous trend of increased variance in the ENSO system during the late 20th century will lead to a weakened monsoon. If this coupling between the systems remains stable in the future, the opposite trend, i.e., an increase in ISM rainfall, would be more likely. However, there is one caveat in this ISM projection by Berkelhammer et al. (2014). The antiphasing nature of ENSO–monsoon relation on the high-frequency domain, derived from the proxy records is characterized by high confidence. But the observed similar phasing on the multi-decadal time scale (30–90 years) is characterized by low confidence.

7.3.4 Atlantic Teleconnections with Indian summer monsoon

Recent studies have also suggested a significant influence of North Atlantic SST variations and AMO on the ISM conditions at various timescales (Gupta et al., 2003; Goswami et al., 2006; also see Chapter 18). More recently, multiple studies were proposed to establish the mechanism of this link. The records reveal that warm (cold) phases of AMO correspond to abundant (deficit) ISM rainfall conditions (Saraswat et al., 2011). The AMO is thought to influence the ISM rainfall by altering the temperature and heat source in the TP and thereby the Meridional Temperature Gradient (MTG) between TP and the tropical IO before the onset of the ISM season. The rising surface at TP causes increased MTG and strengthens the south-westerly monsoonal wind circulation, and contributes to extended wet ISM season. To further substantiate this hypothesis, Feng and Hu (2005) suggested that periods of weak TP heat sources concurred with phases of weak monsoon, and to confirm whether these phases also correspond to cooler North Atlantic SST, these authors examined the link between North Atlantic SST, TP, and MTG variations. A comparison of these variations with that of TP surface temperature and the proxy records of the ISM suggests a persistent impact of AMO variability on the ISM intensity. One of the strongest links between the North Atlantic SST and ISM was documented by Dixit et al. (2014a). Around 8200 years ago, the North Atlantic SST fell sharply (ca 3.3±1.1°C) due to glacial outbursts resulting in a massive amount of freshwater influx (the 8.2 ka event). The resulting decrease in ocean heat transport forced the Intertropical Convergence Zone to move southward and, in turn, caused a weakening of the ISM intensity (Haug et al., 2001; Mukherjee et al., 2016). Feng and Hu (2005) consider that the impact of AMO on ISM is less likely through the North Atlantic Oscillation related atmospheric circulation changes and views TP heat source as an essential mechanism that transitions

the AMO–ISM coupling. However, a comparison of the ISM rainfall records with instrumental records shows that AMO–ISMR link has weakened during the last decade, suggesting that the teleconnections between these two may not be stable (Sankar et al., 2016).

Another notable monsoonal shift was observed around 4200 years BP. The so-called "4.2 ka BP event" has been detected in several paleoclimate archives across the globe, and a concurrent decrease in ISM strength was reported in the Indian context (Berkelhammer et al., 2012; Dixit et al., 2014b). Different mechanisms were proposed to explain the nature and cause of this event. For example, Staubwasser et al. (2003) attributed solar variability, while Berkelhammer et al. (2012) invoked that changes in the mid-latitude circulation pattern led to this event. A weakened mid-latitude westerly system provided dry extratropical air into the ISM system, which suppressed the ISM. Dixit et al. (2014b) speculated that a coupled mechanism of negative IOD and an enhanced ENSO caused such a reduction in ISM at 4.2 ka BP. However, most of these descriptions are not supported by concrete evidence, and a consistent explanation of teleconnections mechanism is still lacking.

Proxy-based evidence suggests continuous drying of the ISM during the mid to late Holocene epoch (Gupta et al., 2003; Staubwasser et al., 2006; Misra et al., 2019). Although there have been various factors that caused this aridification, the predominantly cited records suggest that decreased solar insolation during the middle and later part of Holocene caused reduced land-ocean temperature gradient and reduced monsoonal wetness. According to these studies, the enhanced land surface temperature would contribute to more significant monsoonal precipitation, specifically over the Indian region. However, instrumental and simulation records generated over the Indian region have suggested a dramatic rise in the surface temperature corresponding to below-average rainfall (Krishnan et al., 2020). This apparent inconsistency in the proxy-based and instrumental records signifies that other processes besides solar insolation might be affecting the ISM dynamics.

The biological proxy-based work of past monsoonal circulation reconstruction (Gupta et al., 2003) and its characteristic variation over the Holocene was further strengthened by several other investigators. For example, Gill et al. (2017) analyzed a large pool of SST-based proxy records across the equatorial Pacific. Using a multiproxy reduced dimension methodology, these authors demonstrated that the Arabian Sea summer wind stress curl was higher by 30%–50%, and ISM rainfall was up to 60% higher in certain parts of India at 10 ka compared to recent times. The precipitation pattern across most Indian landmass, excluding the Western Ghats and Northeast India, experienced a declining trend throughout the Holocene. However, unlike Gupta et al. (2003), solar-monsoon linking mechanism and the land-ocean temperature gradient hypothesis, Gill et al. (2017) emphasized the role of ENSO in modulating the rainfall pattern. According to them, ENSO teleconnections during an early to mid-Holocene, La Niña state contributed an intensified rainfall in

north-western parts of India. This hypothesis agrees with the observation of Moy et al. (2002), who demonstrated a weak state of El Niño during the early phase of Holocene (see Fig. 7.4A). However, the weakening of the ISM intensity since the mid-Holocene was attributed to the orbital parameters (Cretat et al. 2020). Simulation of the monsoon seasonality during the mid-Holocene was found to be stronger than the modern times by these authors, which led them to invoke the ISM response to the orbital parameters. Interestingly, fossil coral records demonstrated that the mid-Holocene (ca. 6500 years BP) was characterized by low interannual variance in ENSO compared to modern conditions (Cole, 2005). Several studies reported that ENSO variance was significantly reduced during the mid-Holocene compared to today (see a review by Emile-Geay et al., 2021).

Fig. 7.4 provides an overview of the ISM variability and its association with the global climate variability for the past 10,000 years. A speleothem oxygen isotopic record (red line with a 51-year smoothing) from the Oman coast is considered to be a proxy for wind strength over the Arabian Sea, and ISM precipitation over India indicates a progressively declining trend (Fleitmann et al. 2007). A concurrent southward movement of the Intertropical Convergence Zone is illustrated by titanium concentration records from Cariaco Basin in Venezuela (Haug et al., 2001). Moy et al. (2002) documented the frequency of El Niño events through the Holocene, shown in this figure as grey shading. It clearly shows that the early Holocene experienced weak El Niño events but progressively intensified through the later part of the Holocene. The middle panel shows the reduced ENSO variance during the mid-Holocene (Cole, 2005), as evident from a fossil coral record (purple color) compared to a modern coral record (red color). The lower panel shows a north Indian cave (Sahiya cave) isotopic record (Kathyat et al., 2017) representing the ISM variability for the past two millennia. Since intense rainfall reduces the salinity and hence the isotopic composition of seawater, reconstruction of sea surface $\delta^{18}O$ is also used as a proxy for ISM variability. One such record from the western coastal region of the Bay of Bengal (Naidu et al., 2020) has also been shown. It is noteworthy that these two records show a good match as far as the long-term trend in ISM is concerned.

The records mentioned above highlight that variations in the ISM conditions are influenced by a set of variable factors acting either in association or independently. These factors include solar insolation, atmospheric circulation, elevation, altitude, SST, land-sea temperature gradient, ice/snow area, etc. Changes in these factors yielded substantial variations in the regional intensity and amount of ISM rainfall over orbital and millennial/decadal timescales. However, whether the variations in these factors influence the monsoonal precipitation directly (external forcing only) or more indirectly (internal processes playing a significant role) is still debated. On longer time (orbital) scales, ISM variations are known to follow the solar insolation forcing, whereas, on centennial to decadal timescales, solar output changes perhaps played a partial role in

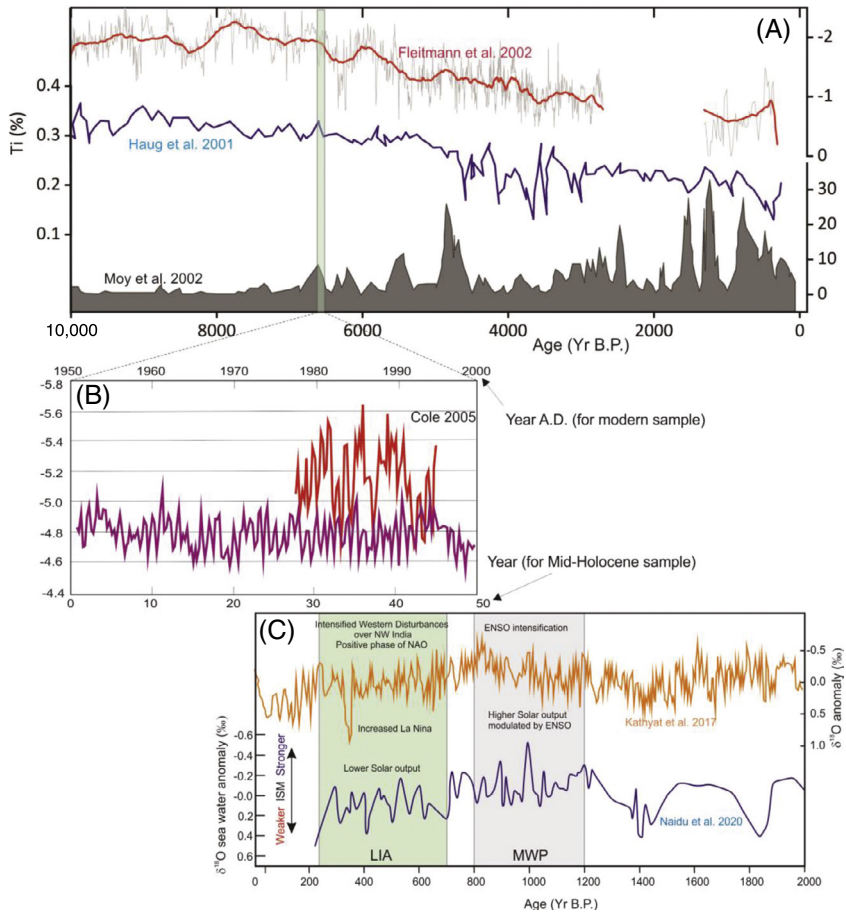

FIG. 7.4 Proxy records of the ISM variability and its association with global climate variables for the last 10,000 years. (A) Speleothem $\delta^{18}O$ record from Oman coast representing the circulation over the Arabian Sea (Fleitmann et al. 2007); *blue line* is the variation of titanium in the Carriaco Basin representing the movement of the ITCZ (Haug et al. 2001); the *grey shading* depicts the frequency of El Niño events during this timeframe (Moy et al. 2002). The middle panel (B) shows the coral oxygen isotopic records on a paleo (approximately 6500 years BP) scale (*purple color*) and a modern scale (*red color*; site: Houn Peninsula, Papua Guinea; Tudhope et al., 2001; Cole, 2005). Lower panel (C): the orange line shows the oxygen isotopic record of the Sahiya Cave speleothem from North India (Kathyat et al. 2017). The *blue line* depicts the seawater oxygen isotopic variability of the western coastal region of the Bay of Bengal (Naidu et al., 2020). *ISM*, Indian summer monsoon; *ITCZ*, intertropical convergence zone.

modulating the ISM intensity. This is because small changes (0.09%) in the total solar irradiance are not adequate to directly modulate the ISM oscillations via the radiation effects alone.

Apparent inconsistencies are found in explaining these mechanisms at different timescales. For example, the early Holocene is believed to have

experienced more (little) La Niña (El Niño) type episodes but intensified ISM (Gill et al., 2017). On the other hand, the LIA also experienced increased La Niña type events but was characterized by significantly reduced ISM (Tejavath et al., 2019). Furthermore, there seems an apparent inconsistency between the proxy and instrumental records generated over the Indian region to reconstruct past and modern fluctuations in the monsoonal precipitation and the controlling factors. Although, the proxy records show that much of the variations in the ISM rainfall are attributed to climate teleconnections processes, but the exact control is demonstrated by the type of process that dominantly controls the monsoon-teleconnections mechanism. Therefore, it is necessary to identify and quantify the role of predominant teleconnections processes that characterize the ISM variations at different timescales. A unified mechanism needs to be developed that can satisfactorily address the ISM variability at all timescales. Furthermore, most of these records suggest an ocean-atmosphere-land teleconnections link that characterizes changes in the ISM rainfall over different timescales. Yet, few of the studies consider that solar output drives the ISM oscillation directly. Hence, the role of solar insolation in modulating the ISM circulation directly or indirectly remains a crucial question and needs to be thoroughly studied.

7.4 Summary and recommendations

The Indian summer monsoon has undergone significant variability in its intensity and pattern over the Holocene epoch. Several proxy records revealed a significant rise in the monsoon precipitation during the early Holocene; simultaneously, it was characterized by substantial spatial heterogeneity. Subsequently, the ISM intensity weakened, believed to be caused by a decrease in the solar insolation. However, proxy records also indicated a rise in La Niña events during this time, resulting in relatively enhanced rainfall than the late Holocene. An abrupt reduction in ISM intensity was observed at ~8.2 ka, believed to be caused by a sharp cooling in the North Atlantic, indicating a strong connection between ISM and North Atlantic climate. If global warming forces the Arctic ice sheets to melt at an accelerated pace, the resulting freshening of the North Atlantic may adversely affect the ISM intensity in the foreseeable future.

The mid-Holocene experienced ISM intensification, which is believed to have been modulated by the tropical Pacific SST variability. Afterward, a progressive weakening of the ISM intensity was documented by various proxy records and climate model simulations. At the beginning of the last millennium, a moderate intensification of ISM activity was witnessed owing to increased solar activity. However, during the latter part of this millennium, proxy records indicated a significant reduction in ISM intensity owing to increased ENSO episodes.

Though the proxy records have made a significant contribution in enhancing our understanding of the ISM teleconnections to the global climate variables,

they, however, suffer from some limitations. The proxies are not uniformly distributed, and the data are too sparse to capture the broad spectrum of the climate variability. An accurate chronology of the records is imperative to decipher the lead-lag characteristics of the climatic events. However, analytical uncertainties exert a limit in this endeavor. Although several proxy records have been generated with some success to reconstruct past shifts in the Indian summer monsoon; however, climate records established from individual proxy materials are inadequate and represent a smoothed signal owing to poor sample resolution and inability to decipher short-term variations (Staubwasser, 2006). Individual proxies are unlikely to capture the diverse aspects of a natural event. Emile-Geay et al. (2021) opine that single sites provide only local-scale information; in order to capture the diversity of ENSO's spatial footprint, multiple records must be analyzed to understand its full range of variability. Another issue is that any given site may not be adequately *teleconnected* to a particular event. In the Indian context, collection of speleothem samples are preferred from the monsoon core zone with a perception that this area would be most sensitive to external processes such as ENSO. But an objective analysis of the ISM and ENSO teleconnections (Mahendra et al., 2021) shows that the northern parts of central India (approximately an area covering 74°N – 84°N, 26°E – 32°E) is more sensitive to ENSO processes. Hence, careful selection of sample collection sites is a prerequisite to capture signals of the teleconnected processes. Similarly, they will help in identifying and quantifying the dominant processes controlling ISM variability, which will guide future paleo-monsoon research. High-resolution multiproxy records with well-constrained chronology integrated over the immense ocean and continental provinces coupled with global climate model simulations would likely provide a better understanding in this endeavor.

Acknowledgments

IITM is fully funded by the Ministry of Earth Sciences, Government of India. We thank Amey Datye and Charuta Murkute for preparing the graphics. Comments and suggestions provided by two anonymous reviewers helped improve the presentation. This work is part of a project work of the International Atomic Energy Agency, CRP F31006.

References

Abram, N.J., Gagan, M.K., Cole, J.E., et al., 2008. Recent intensification of tropical climate variability in the Indian Ocean. Nature Geosci. 1, 849–853.

Agnihotri, R., Dutta, K., Bhushan, R., Somayajulu, B.L.K., 2002. Evidence for solar forcing on the Indian monsoon during the last millennium. Earth Planet. Sci. Lett. 198, 521–527.

Affolter, S., Fleitmann, D., Leuenberger, M., 2014. New-on-line method for water isotope analysis of speleothem fluid inclusions using laser absorption spectroscopy (WS-CRDS). Clim. Past 10, 1291–1304.

Anderson, D.M., Overpeck, J.T., Gupta, A.K., 2002. Increase in the Asian southwest monsoon during the past four centuries. Science 297, 596–599.

Araguas-Araguas, L., Froehlich, K, 1998. Stable isotope composition of precipitation over southeast Asia. J. Geophys. Res. 103, 28721–28742.

Ashok, K., Guan, Z., et al., 2001. Impact of the Indian Ocean Dipole in the relationship between the Indian monsoon rainfall and ENSO. Geophys. Res. Lett. 28, 4499–4502.

Banerji, U., Arulbalaji, P., Padmala, D., 2020. Holocene climate variability and Indian Summer monsoon: an overview. Holocene. doi:10.1177/0959683619895577.

Berkelhammer, M., Sinha, A., et al., 2010. Persistent multi-decadal power of the Indian summer monsoon. Earth Planet. Sci. Lett. 290, 166–172.

Berkelhammer, M., Sinha, A., Stott, L., Cheng, H., Pausata, F.S.R., Yoshimura, K, 2012. An Abrupt Shift in the Indian monsoon 4000 years ago. Geophys. Monogr. Ser. 198. doi:10.1029/2012GM001207.

Berkelhammer, M., Sinha, A., et al., 2014. On the low frequency component of the ENSO-Indian monsoon relationship: a paired proxy perspective. Clim. Past. 10, 733–744.

Bolton, C.T., Chang, L., Clemens, S.C., Kodama, K., Ikehara, M., MedinaElizalde, M., Yamamoto, Y., 2013. A 500,000 year record of Indian summer monsoon dynamics recorded by eastern equatorial Indian Ocean upper water-column structure. Quat. Sci. Rev. 77, 167–180.

Borgaonkar, H., Sikder, A., et al., 2010. El Niño and related monsoon drought signals in 523 year long ring width records of teak (Tectona grandis) trees from South India. Paleogr. Paleoclimtol. Paleoecol. 285, 74–84.

Borgaonkar, H.P., Gandhi, Naveen, Ram, Somaru, Krishnan, R., 2018. Tree-ring reconstruction of late summer temperatures in northern Sikkim (eastern Himalayas). Palaeogeogr., Palaeoclimatol., Palaeoecol. 504, 125–135.

Bose, T., Chakraborty, S., Borgaonkar, H.P., Sengupta, S., Ramesh, R., 2014. Estimation of past atmospheric carbon dioxide levels using tree-ring cellulose $\delta^{13}C$. Curr. Sci. 107 (6), 971–982.

Chakraborty, S., Ramesh, R., Krishnaswami, S., 1994. Air-sea exchange of CO2 in the Gulf of Kutch based on bomb carbon in corals and tree rings. Procd. Ind. Acad. Sci. (Earth Palnet. Sci.) 103, 329–340.

Chakraborty, S., 2006. Coral records from the Northern Indian Ocean: understanding the monsoon variability. J. Geological. Soc. India 68, 395–405.

Chakraborty, S., Dutta, K., Bhattacharyya, A., Nigam, M., Schuur, E.A.G., Shah, S., 2008. Atmospheric ^{14}C variability recorded in tree rings from Peninsular India: implications for fossil fuel CO_2 emission and atmospheric transport. Radiocarbon 50 (3), 321–330.

Chakraborty, S., Goswami, B.N., Dutta, K., 2012. Pacific coral oxygen isotope and the tropospheric temperature gradient over Asian monsoon region: a tool to reconstruct past Indian summer monsoon rainfall. J. Quat. Sci. 27 (3), 269–278. doi:10.1002/jqs.1541.

Chakraborty, S., 2015. Interannual climate variabilities of the tropical Indian Ocean and coral isotopic records. Gond. Geol. Mag. 29 (1 & 2), 61–66.

Chakraborty, S., Sinha, N., Chattopadhyay, R., Sengupta, S., Mohan, P.M., Datye, A., 2016. Atmospheric controls on the precipitation isotopes over the Andaman Islands, Bay Bengal. Sci. Rep. 6, 19555. https://doi.org/10.1038/srep19555.

Chakraborty, S., Belekar, A.R., Datye, A., Sinha, N., 2018. Isotopic study of intra-seasonal variations of plant transpiration: an alternative means to characterise the dry phases of monsoon. Sci. Rep. 8, 8647. https://doi.org/10.1038/s41598-018-26965-6.

Chakraborty, S., 2020. Potential of reef building corals to study the past Indian monsoon rainfall variability. Curr. Sci. 119 (2), 273–281. doi:10.18520/cs/v119/i2/273-281.

Charles, C.D., Hunter, D.E., Fairbanks, R.G., 1997. Interaction between the ENSO and the Asian monsoon in a coral record of tropical climate. Science 277, 925–928.

Cobb, K., Charles, C.D., Cheng, H., Edwards, L., 2003. El Niño/Southern Oscillation and tropical Pacific climate during the last millennium. Nature 424, 271–276.

Consortium, PAGES 2k, 2013. Continental scale temperature variability during the past two millennia. Nat. Geosci. doi:10.1038/NGEO1797.

Cook, E.R., Anchukaitis, K.J., Buckley, B.M., D'Arrigo, R.D., Jacoby, G.C., Wright, W.E., 2010. Asian monsoon failure and megadrought during the last millennium. Science 328, 486–489.

Cole, J.E., et al., 2005. Holocene coral records: windows on tropical climate variability. In: Mackay, A. et al (Ed.), Global Change in the Holocene. Hodder Arnold, New York, NY, p. 528.

Criss, R.E., 1999. Principles of Stable Isotope Distributions. Oxford University Press, New York, NY, p. 254.

Crétat, J., Braconnot, P., Terray, P., et al., 2020. Mid-Holocene to present-day evolution of the Indian monsoon in transient global simulations. Clim. Dyn. 55, 2761–2784. https://doi.org/10.1007/s00382-020-05418-9.

Dahl, K.A., Oppo, D.W., 2006. Sea surface temperature pattern reconstructions in the Arabian Sea. Paleoceanography 21 (1).

Dar, S.S., Ghosh, P., 2017. Estimates of land and sea moisture contributions to the monsoonal rain over Kolkata, deduced based on isotopic analysis of rainwater. https://doi.org/10.5194/esd-8-313-2017.

deVilliers, S., Nelson, B.K., Chivas, A.R., 1995. Biological controls on coral Sr/Ca and δ18O reconstructions of sea surface temperatures. Science 269, 1247–1249.

DiNezio, P.N., Puy, M., Thirumalai, K., Jin, F., Tierney, J.R., 2020. Emergence of an equatorial mode of climate variability in the Indian Ocean. Sci. Adv. 6, eaay7684.

Dixit, Y., Tandon, S.K., 2016. Hydroclimate variability on the Indian subcontinent in the past millennium: review and assessment. Earth Planet. Sci. Lett. 161, 1–15.

Dixit, Y., Hodell, D.A., Sinha, R., et al., 2014a. Abrupt weakening of the Indian summer monsoon at 8.2 kyr B.P. Earth. Planet. Lett. 391, 16–23.

Dixit, Y., Hodell, D.A., Petrie, C.A., 2014b. Abrupt weakening of the summer monsoon in northwest India∼ 4100 yr ago. Geology 42 (4), 339–342.

Doose-Rolinski, H., Rogalla, U., Scheeder, G., Lückge, A., von Rad, U., 2001. High-resolution temperature and evaporation changes during the Late Holocene in the northeastern Arabian Sea. Paleoceanography 16, 358–367.

Dutt, S., Gupta, A.K., Clemens, S.C., Cheng, H., Singh, R.K., Kathayat, G., Edwards, R.L., 2015. Abrupt changes in Indian summer monsoon strength during 33,800 to 5500 years BP. Geophys. Res. Lett. 42 (13), 5526–5532.

Emile-Geay, J., Cobb, K.M., Cole, J.C., Elliot, M., Zhu, F., 2021. Past ENSO variability: reconstructions, models, and implications, in: El Nino southern oscillation in a changing climate. In: McPhaden, M.J., Santoso, A., Cai, W. (Eds.). Geophysical Monograph, 253. AGU, Wiley, p. 506.

Evans, M.N., Reichert, B.K., Kaplan, A., Anchukaitis, K.J., Vaganov, E.A., Hughes, M.K., Cane, M.A., 2006. A forward modeling approach to paleoclimatic interpretation of tree-ring data. J. Geophys. Res. 111, G03008. doi:10.1029/2006JG000166.

Fairchild, I.J., Smith, C.L., Baker, A., Fuller, L., Spotl, C., Mattey, D., McDermott, F., 2006. Modification and preservation of environmental signals in speleothems. Earth-Sci. Rev. 75, 105–153.

Fairchild, I.J., Baker, A., 2012. Speleothem Science: From Process to Past Environments. John Wiley & Sons.

Feng, S., Qi, Hu, 2005. Regulation of Tibetan Plateau heating on variation of Indian summer monsoon in the last two millennia. Geophys. Res. Lett. 32. doi:10.1092/2004GL021246.

Fleitmann, D., Burns, S.J., Mangini, A., Mudelsee, M., Kramers, J., Villa, I., Neff, U., Al-Subbary, A.A., Buettner, A., Hippler, D., Matter, A., 2007. Holocene ITCZ and Indian monsoon dynamics recorded in stalagmites from Oman and Yemen (Socotra). Quat. Sci. Rev. 26, 170–188.

Gadgil, S., 2003. The Indian monsoon and its variability. Ann. Rev. Earth. Planet. Sci. 31, 429–467.
Gautam, P.K., Narayana, A.C., Band, S.T., Yadava, M.G., Ramesh, R., Wu, C.C., Shen, C.C., 2019. High-resolution reconstruction of Indian summer monsoon during the Bølling-Allerød from a central Indian stalagmite. Palaeogeogr. Palaeoclimatol. Palaeoecol. 514, 567–576.
Ghosh, P., Rangarajan, R., Thirumalai, K., Naggs, F., 2017. Extreme monsoon rainfall signatures preserved in the invasive terrestrial gastropod Lissachatina fulica. Geochem. Geophys. Geosyst. 18, 3758–3770. https://doi.org/10.1002/.
Gill, E.C., et al., 2017. Reconstruction of Indian summer monsoon winds and precipitation over the past 10,000 years using equatorial pacific SST proxy records. Paleoceanogr. Paleoclimatol. 32, 195–216.
Goldstein, S., Lea, D., et al., 2001. Uranium series and radiocarbon geochronology of deep-sea corals: implications for Southern Ocean ventillation rates and the oceanic carbon cycle. Earth Planet. Sci. Lett. 193, 167–182.
Goswami, B.N., Kripalani, R.H., Borgaonkar, H.P., Preethi, B., 2014. Multi-decadal variability in Indian summer monsoon rainfall using proxy data. In: Chang, C.P. (Ed.), Climate Change: Multi Decadal and Beyond. World Scientific, p. 376.
Goswami, B.N., Venugopal, V., et al., 2006. Increasing trend of extreme rain events over India in a warming environment. Science 314, 1442–1446.
Gupta, A.K., Dutt, S., Cheng, H., Singh, R.K., 2019. Abrupt changes in Indian summer monsoon strength during the last∼ 900 years and their linkages to socio-economic conditions in the Indian subcontinent. Palaeogeogr. Palaeoclimatol. Palaeoecol. 536, 109347.
Gupta, A.K., Anderson, D.M., Overpeck, J., 2003. Abrupt changes in the Asian southwest monsoon during the Holocene and their links to the North Atlantic Ocean. Nature 421, 354–357.
Gupta, A.K., Das, M., Anderson, D.M., 2005. Solar influence on the Indian summer monsoon during the Holocene. Geophys. Res. Lett. 32, L17703. doi:10.1029/2005GL022685.
Haug, G.H., Hughen, K.A., et al., 2001. Southward migration of the Intertropical Convergence Zone through the Holocene. Science 293, 1304–1308.
Jalihal, C., Srinivasan, J., Chakraborty, A., 2020. Different precipitation response over land and ocean to orbital and greenhouse gas forcing. Sci. Rep. 10, 11891. https://doi.org/10.1038/s41598-020-68346-y.
Jasechko, S., et al., 2015. Late-glacial to late-Holocene shifts in global precipitation $\delta^{18}O$. Climate Past 11 (11), 1375–1393.
Kamae, Y., Kawana, T., Oshiro, M., Ueda, H., 2017. Seasonal modulation of the Asian summer monsoon between the Medieval Warm Period and Little Ice Age: a multi model study. Progr. Earth Planet. Sci. 4 (1), 1–13.
Kathayat, G., Cheng, H., et al., 2017. The Indian monsoon variability and civilization changes in the Indian subcontinent. Sci. Adv. 3, e17001296.
Kaushal, N., Breitenbach, Sebastian F.M., Lechleitner, F.A., Sinha, A., Tewari, V.C., Ahmad, S.M., Berkelhammer, M., et al., 2018. The Indian summer monsoon from a Speleothem $\delta^{18}O$ perspective—a review. Quaternary 1 (3), 29.
Knudsen, M., Seidenkrantz, M., Jacobsen, B., et al., 2011. Tracking the Atlantic multidecadal oscillation through the last 8,000 years. Nat. Commun. 2, 178.
Kotlia, B.S., Singh, A.K., Joshi, L.M., Dhaila, B.S., 2015. Precipitation variability in the Indian Central Himalaya during last ca. 4,000 years inferred from a speleothem record: Impact of Indian Summer Monsoon (ISM) and Westerlies. Quat. Int. 371, 244–253.
Krishnan, R., Sanjay, J., Gnanaseelan, C., Mujumdar, M., Kulkarni, A., Chakraborty, S., 2020. Assessment of Climate Change over the Indian Region: A Report of the Ministry of Earth Sciences (MoES), Government of India. Springer, Singapore.

Kumar, K., Rajagopalan, B., et al., 1999. On the weakening relationship between the Indian monsoon and ENSO. Science 284, 2156–2160.

Lachinet, 2009. Climatic and environmental controls on speleothem oxygen-isotope values. Quat. Sci.Rev. 28, 412–432.

Laskar, A., Yadava, M., Ramesh, R., et al., 2013. A 4 kyr stalagmite oxygen isotopic record of the past Indian summer monsoon in the Andaman Islands. Geochem., Geophys., Geosyst 14 (9). doi:10.1002/ggge.20203.

Liu, X., Yanai, M., 2002. Influence of Eurasian spring snow cover on Asian summer rainfall. Int. J. Climatol. 22 (9), 1075–1089.

Lone, A.M., Achyuthan, H., Chakraborty, S., et al., 2020. Controls on the isotopic composition of daily precipitation characterized by dual moisture transport pathways at the monsoonal margin region of North-Western India. J. Hydrol. https://doi.org/10.1016/j.jhydrol.2020.125106.

Mahendra, N., Chowdary, J.S., Darshana, P., Sunitha, P., Parekh, A, Gnanaseelan, C., 2021. Interdecadal modulation of interannual ENSO-Indian summer monsoon rainfall teleconnections and CMIP6 models: Regional patterns. Int. J. Climatol. doi:10.1002/joc.6973.

McConnaughey, T.A., 1989. ^{13}C and ^{18}O isotopic disequilibrium in biological carbonates: I patterns. Geochim. Cosmochim. Acta 53, 151–162.

Mann, M.E, et al., 2008. Proxy-based reconstructions of hemispheric and global surface temperature variations over the past two millennia. Prod. Natl. Acad. Sci. 105, 13252–13257.

Menzel, P., Gaye, B., Mishra, P.K., Anoop, A., Basavaiah, N., Marwan, N., Plessen, B., et al., 2014. Linking Holocene drying trends from Lonar Lake in monsoonal central India to North Atlantic cooling events. Palaeogeogr., Palaeoclimatol. Palaeoecol. 410, 164–178.

Midhun, M., Lekshmy, P.R., Ramesh, et al., 2018. The effect of monsoon circulation on the stable isotopic composition of rainfall. J. Geophys. Res. Atmos. 123, 5205–5221. https://doi.org/10.1029/2017JD027427.

Misra, P., Tandon, S.K., Sinha, R., 2019. Holocene climate records from lake sediments in India: assessment of coherence across climate zones. Earth-Sci. Rev. 190, 370–397.

Moy, C.M., Seltzer, G.O., Rodbell, D.T., Anderson, D.M., 2002. Variability of El Nino/Southern oscillation activity at millennial timescales during the Holocene epoch. Nature 420, 162–165.

Mukherjee, P., Sinha, N., Chakraborty, S., 2016. Investigating the dynamical behavior of the Intertropical Convergence Zone since the last glacial maximum based on terrestrial and marine sedimentary records. Quat. Int. doi:10.1016/j.quaint.2016.08.030.

Naidu, P., Ganeshram, R., et al., 2020. Coherent response of the Indian monsoon rainfall to Atlantic multi-decadal variability over the last 2000 year. Sci. Rep. doi:10.1038/s41598-020-58265-3.

Neff, U., Burns, J., et al., 2001. Strong coherence between solar variability and the monsoon in Oman between 9 and 6 kyr ago. Nature 411, 290–293.

Newman, M., et al., 2016. The Pacific decadal oscillation, revisited. J. Climate 29, 4399–4427. https://doi.org/10.1175/JCLI-D-15-0508.1.

Overpeck, J., Anderson, D., Trumbore, S., Prell, W., 1996. The southwest Indian monsoon over the last 18,000 years. Clim. Dyn. 12, 213–225.

Polanski, S., Fallah, B., Befort, D.J., Prasad, S., Cubasch, U., 2014. Regional moisture change over India during the past Millennium: a comparison of multi-proxy reconstructions and climate model simulations. Global Planet. Change 122, 176–185.

Rahul, P., Ghosh, P., Bhattacharya, S.K, 2016. Rainouts over the Arabian Sea and Western Ghats during moisture advection and recycling explain the isotopic composition of Bangalore summer rains. J. Geophys. Res. (Atmos.) 121, 6148–6163.

Rahul, P., Prasanna, K., Ghosh, P., Anilkumar, N., Yoshimura, K, 2018. Stable isotopes in water vapor and rainwater over Indian sector of Southern Ocean and estimation of fraction of recycled moisture. Sci. Rep. 8, 7552. https://doi.org/10.1038/s41598-018-25522-5.

Rajeevan, M., Gadgil, S., Bhate, J., 2010. Active and break spells of the Indian summer monsoon. J Earth Syst. Sci. 119 (3), 229–247.

Ramesh, R., Tiwari, M., Chakraborty, S., Managave, S.R., Yadava, M.G., Sinha, D.K., 2010. Retrieval of South Asian monsoon variation during the Holocene from climate natural archives. Curr. Sci. 99, 1770–1786.

Roden, S.L., James, G., Ehleringer, R., 2000. A mechanistic model for interpretation of hydrogen and oxygen isotope ratios in tree-ring cellulose. Geochimica et Cosmochimica Acta 64 (1), 21–35.

Rozanski, K., 2005. Isotopes in atmospheric moisture. In: Aggarwal, P.K., Gat, J.R., Froehlich, K.F. (Eds.), Isotopes in the Water Cycle. Springer, Dordrecht. https://doi.org/10.1007/1-4020-3023-1_18.

Saraswat, R., Lea, D., Nigam, R, et al., 2011. Deglaciation in the tropical Indian Ocean driven by interplay between the regional monsoon and global teleconnection. Earth Planet. Sci. Lett. 375, 166–175.

Sengupta, S., Bhattacharya, S.K., Parekh, A., et al., 2020. Signatures of monsoon intra-seasonal oscillation and stratiform process in rain isotope variability in northern Bay of Bengal and their simulation by isotope enabled general circulation model. Clim. Dyn. doi:10.1007/s00382-020-05344-w.

Shindell, D.T., Schmidt, G.A., Mann, M.E., Rind, D., Waple, A., 2001. Solar forcing of regional climate change during the Maunder Minimum. science 294 (5549), 2149–2152.

Sinha, N., Chakraborty, S., 2020. Isotopic interaction and source moisture control on the isotopic composition of rainfall over the Bay of Bengal. Atmos. Res. 35, 104760. doi:10.1016/j.atmosres.2019.104760.

Sinha, N., Chakraborty, S., Chattopadhyay, R., et al., 2019. Isotopic investigation of the moisture transport processes over the Bay of Bengal. J. Hydrol. X. doi:10.1016/j.hydroa.2019.100021.

Sinha, A., Berkelhammer, M., Stott, L., Mudelsee, M., Cheng, H., Biswas, J., 2011. The leading mode of Indian summer monsoon precipitation variability during the last millennium. Geophys. Res. Lett. 38 (15). doi:10.1029/2011GL047713.

Sinha, A., Cannariato, K.G., Stott, L.D., Cheng, H., Lawrence Edwards, R., Yadava, M.G., Ramesh, R., Singh, I.B., 2007. A 900-year (600 to 1500 AD) record of the Indian summer monsoon precipitation from the core monsoon zone of India. Geophys. Res. Lett. 34 (16).

Sinha, N., Gandhi, N., Chakraborty, S., Krishnan, R., Yadava, M.G., Ramesh, R., 2018. Abrupt climate change at ∼ 2800 Yr BP evidenced by high-resolution oxygen isotopic record of a Stalagmite from Peninsular India. The Holocene 28 (11), 1720–1730. https://doi.org/10.1177/0959683618788647.

Singh, M., Krishnan, R., Goswami, B., Choudhury, A.D., Swapna, P., Vellore, R., Prajeesh, A.G., Sandeep, N., Venkataraman, C., Donner, R.V., Marwan, N., Kurths, J., 2020. Fingerprint of volcanic forcing on the ENSO–Indian monsoon coupling. Sci. Adv. 6, eaba8164. doi:10.1126/sciadv.aba8164.

Staubwasser, M, 2006. An overview of Holocene South Asian monsoon records–monsoon domains and regional contrasts. J. Geol. Soc. India. 68, 433–446.

Staubwasser, M., Sirocko, F., Grootes, P.M., Segl, M., 2003. Climate change at the 4.2 ka BP termination of the Indus valley civilization and Holocene south Asian monsoon variability. Geophys. Res. Lett. 30 (8).

Sankar S., L. Svendsen, et al. (2016) The relationship between Indian summer monsoon rainfall and Atlantic multidecadal variability over the last 500 years, Tellus A: Dyn. Meteorol. Oceanogr., 68:1, 31717, DOI: 10.3402/tellusa.v68.31717.

Tejavath, C., Ashok, K., Chakraborty, S., Ramesh, R., 2019. A PMIP3 narrative of modulation of ENSO teleconnections to the Indian summer monsoon by background changes in the Last Millennium. Clim. Dyn. doi:10.1007/s00382-019-04718-z.

Tiwari, M., Nagoji, S.S., Ganeshram, R.S., 2015. Multi-centennial scale SST and Indian summer monsoon precipitation variability since the mid-Holocene and its nonlinear response to solar activity. Holocene. doi:10.1177/0959683615585840.

Tudhope, A.W., et al., 2001. Variability in the El Nino: southern oscillation through a glacial–interglacial cycle. Science 291, 1511–1517.

Xavier, P.K., Marzina, C., Goswami, B.N., 2007. An objective definition of the Indian summer monsoon season and a new perspective on the ENSO–monsoon relationship. Q. J. R. Meteorol. Soc. 133, 749–764. doi:10.1002/qj.45.

Yadav, R.R., Braeuning, A., Singh, J., 2011. Tree ring inferred summer temperature variations over the last millennium in western Himalaya, India. Clim. Dyn. 36 (7-8), 1545–1554.

Yadav, R., 2013. Tree ring–based seven-century drought records for the Western Himalaya, India. J. Geophys. Res. (Atmos.) 118 (10). doi:10.1002/jgrd.50265.

Yadava, M.G., Ramesh, R., 2005. Monsoon reconstruction from radiocarbon dated tropical Indian speleothems. Holocene 15 (1), 48–59.

Zaw, Z., et al., 2020. Drought Reconstruction Over the Past Two Centuries in Southern Myanmar Using Teak Tree-Rings: Linkages to the Pacific and Indian Oceans. Geophys. Res. Lett. 47. https://doi.org/10.1029/2020GL087627.

Zhang, L., Delworth, T.L., 2016. Simulated response of the Pacific Decadal oscillation to climate change. J. Clim. 29, 5999–6018. https://doi.org/10.1175/JCLI-D-15-0690.1.

Zhang, P., Cheng, H., Edwards, L., et al., 2008. A test of climate, sun, and culture relationships from an 1810-year Chinese cave record. Science 322, 940–942.

Zhang, P., Jee-Hoon, Jeong, Yoon, Jin-Ho, et al., 2020. Abrupt shift to hotter and drier climate over inner East Asia beyond the tipping point. Science 370, 1095–1099.

Zhisheng, A., Clemens, S.C., Shen, J., et al., 2011. Glacial-Interglacial Indian summer monsoon dynamics. Science 333, 719–723.

Zhisheng, A., Clemens, S.C., Shen, J., et al., 2015. Indian monsoon variations during three contrasting climatic periods: The Holocene, Heinrich Stadial 2 and the last interglacial-glacial transition. Quat. Sci. Rev. doi:10.1016/j.quascirev.2015.06.009.

Zorzi, C., Krishnamurthy, A, et al., 2015. Indian monsoon variations during three contrasting climatic periods: The Holocene, Heinrich Stadial 2 and the last interglacial-glacial transition. Quat. Sci. Rev. doi:10.1016/j.quascirev.2015.06.009.